ABSTRACT

Title of Dissertation: CHANGES IN AMAZON FOREST STRUCTURE FROM LAND-USE FIRES: INTEGRATING SATELLITE REMOTE SENSING AND ECOSYSTEM MODELING

Douglas C. Morton, Ph.D., 2008

Directed By: Professor Ruth S. DeFries
Department of Geography

Fire is the dominant method of deforestation and agricultural maintenance in Amazonia, and these land-use fires frequently escape their intended boundaries and burn into adjacent forests. Initial understory fires may increase forest flammability, thereby creating a positive fire feedback and the potential for long-term changes in Amazon forest structure. The four studies in this dissertation describe the development and integration of satellite remote sensing and ecosystem modeling approaches to characterize land-use fires and their consequences in southern Amazon forests. The dissertation contributes three new methods: use of the local frequency of satellite-based active fire detections to distinguish between deforestation and maintenance fires, use of satellite data time series to identify canopy damage from understory fires, and development of a height-structured fire sub-model in Ecosystem Demography, an advanced ecosystem model, to evaluate the impacts of a positive fire feedback on forest structure and composition. Conclusions from the dissertation

demonstrate that the expansion of mechanized agricultural production in southern Amazonia increased the frequency and duration of fire use compared to less intensive methods of deforestation for pasture. Based on this increase in the frequency of land-use fires, fire emissions from current deforestation may be higher than estimated for previous decades. Canopy damage from understory fires was widespread in both dry and wet years, suggesting that drought conditions may not be necessary to burn extensive areas of southern Amazon forests. Understory fires were five times more common in previously-burned than unburned forest, providing satellite-based evidence for a positive fire feedback in southern Amazonia. The impact of this positive fire feedback on forest structure and composition was assessed using the Ecosystem Demography model. Scenarios of continued understory fires under current climate conditions show the potential to trap forests in a fire-prone structure dominated by early-successional trees, similar to secondary forests, reducing net carbon storage by 20-46% within 100 years. In summary, satellite and model-based results from the dissertation demonstrate that fire-damaged forests are an extensive and long-term component of the frontier landscape in southern Amazonia and suggest that a positive fire feedback could maintain long-term changes in forest structure and composition in the region.

CHANGES IN AMAZON FOREST STRUCTURE FROM LAND-USE FIRES: INTEGRATING SATELLITE REMOTE SENSING AND ECOSYSTEM MODELING

By

Douglas C. Morton

Dissertation submitted to the Faculty of the Graduate School of the
University of Maryland, College Park, in partial fulfillment
of the requirements for the degree of
Doctor of Philosophy
2008

Advisory Committee:
Professor Ruth S. DeFries, Chair
Professor Ralph Dubayah
Professor George C. Hurtt
Professor Eric S. Kasischke
Professor Ning Zeng

Acknowledgements

First and foremost, I thank Ruth DeFries for her steadfast support of my doctoral work. Ruth has been an outstanding mentor, thoughtfully guiding and challenging me during my development as an independent researcher. Ruth's intellectual curiosity is infectious, and I am grateful for her constant reminders to remember the big picture. I would also like to thank the members of my dissertation committee, Ralph Dubayah, George Hurtt, Eric Kasischke, and Ning Zeng for generously sharing their expertise and encouragement during the course of this project.

Many technical conversations with colleagues about this project were invaluable. Wilfrid Schroeder and Louis Giglio have been indispensable resources for my endless questions about remote sensing of fire. I also thank Guido van der Werf, Jim Randerson, Jim Collatz, Jennifer Balch, Jyothy Nagol, Ivan Csiszar, and Jeff Morisette for their thoughtful and timely feedback throughout this project. In addition, the members of Ruth DeFries' lab, Jan Dempewolf, Victor Gutierrez, Marcia Macedo, and Karl Wurster have been constant sources of support and inspiration.

I am grateful for the guidance and support of many Brazilian colleagues during the countless hours spent stomping through burned Amazon forests and processing satellite imagery. In particular, I thank Yosio Shimabukuro, Carlos Souza, Liana Anderson, Fernando del Bon Espírito-Santo, André Lima, and Egidio Arai for their support of this work.

Finally, I would never have come this far without the gracious and unwavering support of my family and friends. A thousand thanks to my loving wife, Lindsay, and daughter, Eleanor, for their patience through the long hours and the inspiration they provide me every day.

Table of Contents

Acknowledgements ii

Table of Contents iv

List of Tables vii

List of Figures ix

Chapter 1: Introduction 1

1.1 Background 1
1.2 Land-use Fires in Amazonia 4
1.3 Understory Forest Fires in Amazonia 6
1.4 Global Context of Land-use Fires in Amazonia 8
1.5 Priority Questions Regarding Land-use Fires in Amazonia 11
1.6 Objectives 12
1.7 The Dissertation and its Organization 13

Chapter 2: Agricultural Intensification Increases Deforestation Fire Activity in Amazonia 16

2.1 Summary 16
2.2 Introduction 17
2.3 Methods 20
2.3.1 Data 20
2.3.2 Identifying High-Frequency Fires 23
2.3.3 Fire Types in Amazonia 24
2.3.4 Basin-Wide Analysis 27
2.4 Results 27
2.4.1 Deforestation Fires 27
2.4.2 Patterns of Fire Use Stratified by Post-Clearing Land Use 32
2.5 Discussion 37
2.5.1 Deforestation Fires in Amazonia 37
2.5.2 Spatial and Temporal Dynamics of Fire Activity 42
2.5.3 Uncertainties 44
2.6 Conclusions 45

Chapter 3: A Time Series Approach to Map Canopy Damage from Understory Fires in Amazon Forests 47

3.1 Summary 47
3.2 Introduction 48
3.3 Methods 51
3.3.1 Study Area 51
3.3.2 Satellite-Based Measures of Fire Effects in Amazon Forests 52
3.3.3 Data 54
3.3.4 Burn Damage and Recovery (BDR) Algorithm 57

3.3.5 Validation 63
3.4 Results 67
3.4.1 Validation: Omission 67
3.4.2 Validation: Commission 69
3.4.3 Interannual Variation in Fire-Damaged Forest, 1997-2002 72
3.4.4 Burn Scar Sizes 73
3.5 Discussion 74
3.6 Uncertainties 80
3.7 Conclusions 81

Chapter 4: A Positive Fire Feedback in Southern Amazon Forests 83

4.1 Summary 83
4.2 Introduction 84
4.3 Methods 87
4.3.1 Study Area 87
4.3.2 Precipitation Data 89
4.3.3 MODIS Time Series 2000-2007 90
4.3.4 Mapping Canopy Damage from Fire with the Burn Damage and Recovery Algorithm 91
4.3.5 Deforestation 92
4.3.6 Validation Data 92
4.3.7 Statistical Analyses 94
4.4 Results 95
4.4.1 Validation 95
4.4.2 Interannual Variation in Burned Forest 97
4.4.3 Recurrent Forest Fires 100
4.4.4 Deforestation of Burned Forests 103
4.5 Discussion 105
4.5.1 Interannual Variation in Burned Forest 106
4.5.2 Impact of Recurrent Fires on Amazon Forests 108
4.5.3 Study Limitations and Uncertainties 111
4.6 Conclusions 113

Chapter 5: Modeling Long-Term Changes in Amazon forest Structure from Repeated Exposure to Land-Use Fires 115

5.1 Summary 115
5.2 Introduction 116
5.3 Methods 120
5.3.1 Ecosystem Demography (ED) 120
5.3.2 Fuels 121
5.3.3 Height-Structured Fire Sub-Model 122
5.3.4 Fire Spread 126
5.3.5 Study Area 128
5.3.6 Calibration: Current Rates of Logging and Understory Fires 128
5.3.7 Land-Use Scenarios 130
5.3.8 Biomass Validation 131
5.4 Results 132

5.4.1 Xingu Biomass 132
5.4.2 Century Scenarios 133
5.4.3 Decade Scenarios 137
5.5 Discussion 140
5.6 Conclusions 146

Chapter 6: Conclusions and Policy Implications from the Dissertation and Directions for Future Research 148

6.1 Summary 148
6.2 Dissertation Summary and Conclusions Related to Priority Research Areas 148
6.3 Additional Conclusions from the Dissertation 152
6.4 Policy-Relevant Implications of Dissertation Conclusions 155
6.4.1 Lessons for Managing Land-Use Fires in Southern Amazonia 155
6.4.2 Satellite-Based Monitoring of Deforestation and Degradation 156
6.5 Future Research Directions 158

Appendix: List of Abbreviations 161

Bibliography 162

List of Tables

Table 2-1: Combined MODIS Terra and Aqua fire detections associated with deforestation, indigenous reserves, agricultural maintenance, and small properties in government settlement areas in the Brazilian State of Mato Grosso and sugarcane production in São Paulo state according to the number of days with fire detections in the same year. Fire frequency for 2004 and 2005 deforestation events is calculated for the year of deforestation detection, and clearings >25 ha are classified based on post-clearing land use as cropland, pasture, or not in production (NIP)..... 28

Table 2-2: Number of high-confidence MODIS Terra and Aqua fire detections (1-km pixels) for the nine states of the Brazilian Legal Amazon during 2003-2007 as a function of fire frequency. States are listed in decreasing order of fire activity..... 30

Table 2-3: Number of high-confidence MODIS Terra and Aqua fire detections (1-km pixels) within the Amazon Basin during 2003-2006, summarized at the national level according to the frequency of fire detections. Countries are listed in decreasing order of fire activity..... 31

Table 3-1: Data sources for calibration and validation of fire-damaged forest area derived from the BDR algorithm. 56

Table 3-2: Detection of field and image-derived validation forest burn scars with results from the BDR algorithm applied to time series of Landsat and MODIS data. 68

Table 3-3: Overlap between Landsat-based selective logging from Asner et al. (2005) and fire-damaged forest for all BDR results (Total) and high-confidence burn scars (HC) from Landsat and MODIS time series. Total high confidence fire-damaged forest area (HC Area) and the percentage of HC Area that overlapped with selective logging are also shown..... 69

Table 3-4: Overlap between fire-damaged forest (2000-2002) and PRODES deforestation (2001-2003) (INPE, 2007) for all BDR results (Total) and high-confidence burn scars (HC). Total overlap with PRODES deforestation is further divided by size and post-clearing land use (Morton et al., 2006). Total high confidence fire-damaged forest area (HC Area) and the percentage of HC Area that overlapped with deforestation are also shown. 70

Table 3-5: Fire-damaged forest area detected by the BDR algorithm using Landsat and MODIS time series for all forest burn scars (Total) and high-confidence burn scars (HC). Coincident detections at both high and moderate resolution (overlap) were derived from high-confidence burn scars..... 71

Table 4-1: Field observations of forest that burned during 1999-2005 in the upper Xingu River study area. 93

Table 4-2: Detection of field validation burned forest perimeters as a function of burn scar size using the BDR algorithm applied to the time series of MODIS data..... 96

Table 4-3: Percentage of field validation data detected by the BDR algorithm for areas burned multiple times. 96

Table 4-4: Detection of field-observed deforestation according to clearing size in 2004 and 2005 using the MODIS time-series approach. 97

Table 4-5: Fire-damaged forest area (FDFA) during 1999-2005 and the contribution from first, second, and third fires to FDFA in each year. Interactions between burned forest and deforestation (Defor.) are shown separately for fire-damaged forest that was subsequently deforested, FDFA adjacent to new deforestation (2002-2006), and total deforestation identified in the MODIS time series during 2001-2006. All areas are shown in km^2..... 98

Table 5-1: ED model results in year 200 for the Xingu study area from Forest Control and land-use scenarios. Values for total biomass, fraction of biomass in early-successional (ES) trees, and basal area in year 200 were calculated as forest area-weighted means from all 1° x 1° grid cells in the Xingu study area. Values for mean canopy height and age since last disturbance were only calculated at the Sinop site for each scenario. 133

Table 5-2: ED model results for the Sinop study site from Forest Control, Logging, and Decade land-use scenarios in year 110. 139

List of Figures

Figure 1-1: Six countries administer portions of the Amazon Basin in South America. The Brazilian Legal Amazon extends beyond the Amazon Basin to include the historic range of contiguous tropical forest in Brazilian territory. Dense tropical forests appear dark green and savanna or Cerrado regions appear light green in the 2000 percent tree cover data layer from the MODIS Vegetation Continuous Fields (VCF) product (Hansen *et al.*, 2002). The names of Brazilian states in the Legal Amazon are abbreviated using postal codes: RR: Roraima, PA: Pará, AP: Amapá, MA: Maranhão, TO: Tocantins, MT: Mato Grosso, RO: Rondônia, AC: Acre, and AM: Amazonas. 2

Figure 1-2: A photo series of fire types in Amazonia. Deforestation fires (a) are set after cutting trees and understory vegetation to permit agricultural use. Maintenance fires (b) such as this pasture fire are set to reduce woody encroachment. Understory forest fires (c) are typically the result of deforestation or maintenance fires that escape their intended boundary and burn into adjacent forest areas. 5

Figure 1-3: Changes in forest structure from initial fire exposure may increase forest flammability, leading to a positive fire feedback in Amazon forests (Cochrane & Schulze, 1999; Nepstad *et al.*, 1999a). Selective logging, drought, or edge effects from forest fragmentation may also increase forest flammability. Anthropogenic ignitions are critical to initiate and continue the feedback mechanism, as land-use fires burn into flammable forest to create understory fires. The feedback ends when land-use fires cease or forest flammability declines due to forest regrowth or decomposition of surface fuels (Cochrane, 2003). 7

Figure 2-1: Total high-confidence fire detections across the Amazon Basin (upper) and percentage of all fires detected on two or more days during the same dry season (lower) summarized at 0.25° resolution. North of the equator, the fire year is July-June (July 2003-June 2004, July 2004-June 2005); south of the equator, the fire year is January-December (2004, 2005). Outlines show country borders (gray), Brazilian state boundaries (blue), and the extent of the Amazon Basin (black). In clockwise order, letter codes for Brazilian states are: AP: Amapá, PA: Pará, MA: Maranhão, TO: Tocantins, MT: Mato Grosso, RO: Rondônia, AC: Acre, AM: Amazonas, RR: Roraima. 21

Figure 2-2: Intensity of fire use for 2004 deforestation events >25 ha in Mato Grosso state according to post-clearing land use (cropland, pasture, and not in production-NIP), measured as the maximum fire frequency in each deforested area during 2004. 33

Figure 2-3: Seasonality of fire activity during 2003-2005 for pasture and cropland deforestation events >25 ha in Mato Grosso state from 2004. 35

Figure 2-4: Years of high-frequency fire activity for three different land uses following deforestation in Mato Grosso state. The typical duration of high-frequency fire activity (>2 fire days per year) is shown as a percentage of deforestation events during 2003-2005 for each land use. Fire activity was examined for the year prior to deforestation mapping until 2006. 36

Figure 2-5: The duration of deforestation fire activity following forest clearing highlights the contribution of multiple years of deforestation to fire in any year. Average fire frequency and total deforested area in polygons >25 ha in size for 2002-2005 are shown separately for cropland (top), pasture (middle), and areas not in agricultural production (NIP, bottom). Deforested area for each post-clearing land use is taken from Morton *et al.* (2006, 2007). Fire data for 2002 are derived only from Terra-MODIS observations. 38

Figure 2-6: Percent of initial forest biomass remaining following repeated deforestation fire activity. The range of combustion completeness for each fire is shown as low (19.5%, Carvalho *et al.*, 2001), average of published figures for Amazonia (40.6%, (Fearnside *et al.*, 1993; Kauffman *et al.*, 1995; Carvalho *et al.*, 1998; Guild *et al.*, 1998; Araujo *et al.*, 1999; Carvalho *et al.*, 2001), and high (61.5%, Carvalho *et al.*, 2001). Curves end once initial forest biomass drops below 1% (5-22 fires). Vertical lines show the mean number of fire days for 2004 deforestation in Mato Grosso for pasture and cropland in 2004 (year 1) and during 2003-2006 (total). 40

Figure 3-1: MODIS mean dry-season NDVI (mNDVI) in 2000 for the upper Xingu River watershed (blue) and Landsat study area (black) in the Brazilian state of Mato Grosso (inset, white). Forested areas are shown in green, grasslands and Cerrado in shades of yellow, and bare soils typical of cropland in dry-season months appear red. 52

Figure 3-2: Time series of annual mean ± 1 S.D. MODIS mean dry-season NDVI (mNDVI, top) and Landsat shade-normalized green vegetation fraction (GVs, bottom) for calibration data on intact, logged, and burned forest and deforestation for pasture and cropland during 2002. 58

Figure 3-3: The BDR algorithm has three main processing steps: 1) MODIS (top) and Landsat (bottom) time series trajectories are used to identify candidate core areas of canopy damage from fire (black) and growth regions (gray). Dashed lines show the range of values for 2-year recovery in growth regions. See table (bottom) for pre-burn, drop, burn, and recovery parameter ranges for each BDR trajectory. 2) Large core areas (white) are joined to adjacent growth areas (red) to generate forest burn scars. 3) Individual burn scars are classified as low and high confidence based on

spatial and spectral metrics. Small or linear burn scars are removed from consideration; high-confidence burn detections are large and non-linear, with burn values intermediate between damages from deforestation and logging. 60

Figure 3-4: Landsat and MODIS 1999 forest burn scar results classified according to high and low confidence based on spatial and spectral metrics for a subset of the study area (inset). The background image shows the shade-normalized green vegetation fraction (GVs) for 2000. 62

Figure 3-5: Flow diagram of data processing and analysis for annual maps of fire-damaged forest area from the BDR algorithm applied to time series of MODIS and Landsat data. We compared low and high-confidence burn scars to validation data on burned forest, selective logging, and deforestation, but only high-confidence burn scars were used to examine interannual variability in burn scar size and total fire-damaged forest area. 63

Figure 3-6: Number of burn scars (bars) and cumulative contribution to total validation fire-damaged forest area (◊) by size class for 145 validation burn scars from 1999 identified in Landsat imagery 65

Figure 3-7: Total Landsat high confidence fire-damaged forest area during 1997-2002 (white) impacted 10% of the forested area in 1997. Forested regions appear gray and deforested areas appear black in the background image of the study area (2003 shade-normalized green vegetation fraction, GVs). 72

Figure 3-8: Percent contribution from burn scars of different sizes to annual high-confidence fire-damaged forest area for the BDR algorithm applied to time series of Landsat (top) and MODIS (bottom). 75

Figure 4-1: MODIS mean dry-season NDVI (mNDVI) in 2000 for the upper Xingu River watershed (blue) in the Brazilian state of Mato Grosso (inset, white). The Xingu Indigenous Park (black outline) occupies the center of the study area. Forested areas are shown in green, grasslands and Cerrado in shades of yellow, and bare soils typical of cropland in dry-season months appear red. Within the Xingu River watershed, Cerrado and inundated vegetation along river courses that were excluded from the analysis are masked in light-gray tones 88

Figure 4-2: Relationship between the annual extent of burned forest (a) and mean annual precipitation anomalies ± 1 S.D. during 1998-2005 of accumulated rainfall in the year (June-May) before burning (b) and dry season rainfall (June-August) in the year of forest fire damages (c). 99

Figure 4-3: Forests burned one, two, or three times during 1999-2005 within the upper Xingu River watershed (blue) in eastern Mato Grosso State (inset, white). The Xingu Indigenous Park (black outline) occupies the center of the study area. 101

Figure 4-4: Effect of multiple burns on burn (upper) and recovery mNDVI values (lower). Symbols signify the level of statistical significance between mean mNDVI values in each year for first and second burns (stars) and second and third burns (squares) using t-tests: *** p<0.0001, ** p<0.001, * p<0.01, ns = not significant. Sample sizes for burned forest area in each year as a function of burn number can be found in Table 4-4. Note that results for the third burn in 2003 are based on substantially smaller burned forest area (10.8 km^2) than any other estimate. 102

Figure 4-5: Understory forest fires in 1999-2005 (red) and deforestation during 2001-2006 (blue) damaged 30.7% of the forested area in 2000 outside of the Xingu Indigenous Park (black outline) in the upper Xingu River basin (blue outline). Burned forests that were later deforested are shown in black. 104

Figure 5-1: Fuel amount (●, kg C/m^2) in the oldest forest patch from model initiation to 40 years. Fuel amount is calculated as the sum of fast soil carbon (Δ) and a fraction of the biomass in short vegetation (■). Maximum height (X) in the patch is shown on the secondary y-axis. 123

Figure 5-2: Fire disturbance rate (λ_F) from the new height-structured fire sub-model for two patches, the oldest patch (created at time = 0) and a patch resulting from selective logging at time = 148 years..... 125

Figure 5-3: Forested areas in 2000 (gray) and 1° x 1° ED model grid cells within the Xingu River basin (black) in the Brazilian state of Mato Grosso (inset, white). Detailed modeling runs were conducted for a single model cell near Sinop, Mato Grosso (11.5° S, 54.5° W, dark black outline). 127

Figure 5-4: Comparison of mean (± 1 S.D.) above-ground live biomass (AGLB) from ED to satellite-based estimates of AGLB from Saatchi *et al.* (2007) for all 1° x 1° grid cells in the Xingu study region. 132

Figure 5-5: Annual total above-ground biomass (TAGB, top) and the fraction of TAGB in pioneer (early-successional trees) (bottom) for the Sinop site from the forest Control scenario and five 'Business as Usual' land use scenarios calibrated based on current rates of logging and understory fire damage. 134

Figure 5-6: Distribution of patch age since last disturbance in year 200 for Century scenarios at the Sinop study site. 135

Figure 5-7: Total above-ground biomass (TAGB) at the Sinop study site under the Century Spread scenario with land use beginning in year 1, 25, 50, 100, and 200. . 136

Figure 5-8: Total above-ground biomass (TAGB, top) and net ecosystem production (NEP, bottom) for Control and Decade scenarios of land use with and without fire spread at the Sinop study site..... 138

Chapter 1: Introduction

1.1 Background

The Amazon basin contains more than one-third of the world's remaining humid tropical forests (4×10^6 km^2) and provides a range of important ecosystem services such as climate regulation, carbon sequestration, and maintenance of biodiversity (Millennium Ecosystem Assessment, 2005; Hansen *et al.*, 2008). Although six countries share administrative control of forest resources in Amazonia, the majority (60%) of the Amazon basin is under Brazilian jurisdiction (Figure 1-1). The Brazilian "Legal Amazon" designation also includes the full extents of Amapá, Mato Grosso, and Tocantins states and Maranhão state west of 44° W longitude.

The 'arc of deforestation' along the southern and eastern extent of the Brazilian Amazon is the most active land-use frontier in the world in terms of total forest loss (FAO, 2006) and deforestation rates during 2000-2005 (Hansen *et al.*, 2008) (Figure 1-1). Numerous studies have documented the economic and political incentives driving phases of frontier expansion and deforestation in the Brazilian Amazon (e.g., Sawyer, 1984; Schmink & Wood, 1992; Margulis, 2004). Historically, variations in forest clearing rates have been linked with changes in access to the region; thus, road construction and migration were critical precursors to forest losses. During the 1980s and 1990s, large-scale colonization projects, credit incentives, and steady investment in the region led to annual forest losses of 1-3 million ha in the Brazilian Amazon (INPE, 2008). Planned investments to upgrade roads and build

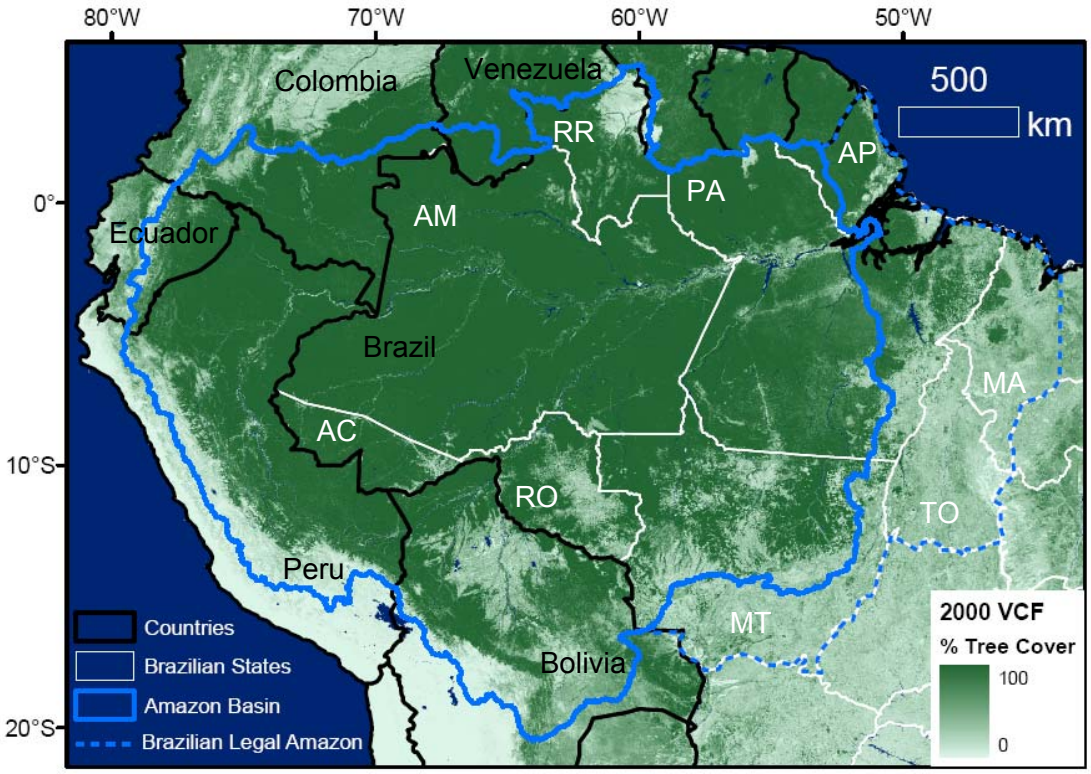

Figure 1-1: Six countries administer portions of the Amazon Basin in South America. The Brazilian Legal Amazon extends beyond the Amazon Basin to include the historic range of contiguous tropical forest in Brazilian territory. Dense tropical forests appear dark green and savanna or Cerrado regions appear light green in the 2000 percent tree cover data layer from the MODIS Vegetation Continuous Fields (VCF) product (Hansen *et al.*, 2002). The names of Brazilian states in the Legal Amazon are abbreviated using postal codes: RR: Roraima, PA: Pará, AP: Amapá, MA: Maranhão, TO: Tocantins, MT: Mato Grosso, RO: Rondônia, AC: Acre, and AM: Amazonas.

dams to extend navigable waterways may therefore accelerate forest losses in regions that currently have limited transportation infrastructure (Nepstad *et al.*, 2001; Kirby *et al.*, 2006; Soares-Filho *et al.*, 2006).

In recent years, economic forces within and beyond Amazonia have exerted stronger control over deforestation rates and post-clearing land uses, including domestic and global demand for beef, soybeans, and wood products (Fearnside, 2001;

Chomitz & Thomas, 2003; Margulis, 2004; Asner *et al.*, 2005; Naylor *et al.*, 2005; Morton *et al.*, 2006; Nepstad *et al.*, 2006b). Current deforestation dynamics in the Brazilian Amazon represent a new paradigm of intensive agricultural production driven by industrial-scale operators (Morton *et al.*, 2006; Hansen *et al.*, 2008). The combination of larger clearings for mechanized agriculture and lower rates of land abandonment alters the patterns of forest fragmentation and increases net carbon emissions from deforestation in Amazonia compared to previous decades (Alves *et al.*, in press).

The state of Mato Grosso is a focal region in the discussion of changing land use dynamics in Amazonia due to high rates of recent deforestation and a strong seasonal climate (Figure 1-1). Mato Grosso contributed 40% of the estimated deforestation and nearly 100% of the growth in mechanized cropland in the Brazilian Amazon during 2000-2005 (Morton *et al.*, 2006; INPE, 2007). Forest degradation from selective logging was also widespread in Mato Grosso during 1999-2002, accounting for more than 60% of satellite-based estimates of logging activity in the Brazilian Legal Amazon during this period (Asner *et al.*, 2005). Mato Grosso experiences a 3-5 month dry season which facilitates the use of fire for land clearing and management compared to less seasonal Amazon regions (Nepstad *et al.*, 2004; Giglio *et al.*, 2006a). Low dry-season cloud cover and large-scale deforestation activity in Mato Grosso also aids satellite-based remote sensing of changes in forest cover and land-use fires (Asner, 2001; Morton *et al.*, 2005; INPE, 2006; Schroeder *et al.*, 2008a). Nevertheless, the fragmented and rapidly-changing landscape in Mato

Grosso complicates efforts to isolate the individual contributions from selective logging, deforestation, and fires to canopy damage identified in satellite data.

1.2 Land-use Fires in Amazonia

Land-use fires are the dominant source of ignitions in Amazonia (Sanford *et al.*, 1985; Goldammer, 1990) and the primary method of both deforestation and agricultural maintenance (Cochrane, 2003; Schroeder *et al.*, 2005; Schroeder *et al.*, 2008b). Fires are in deforested areas set to burn trunks, stumps, and woody roots following clear-felling of forest vegetation in preparation for cattle ranching or crop production (Figure 1-2). These fires may also be described as "conversion fires" since burning is part of a land cover conversion. Maintenance fires include burning for routine management of cattle pastures to reduce woody encroachment or to eliminate crop residues in agricultural fields (Figure 1-2). Land-use fires in Amazonia are most common during the end of the dry season because extended rainless periods reduce fuel moisture and the nutrient-rich ash layer enhances agricultural productivity at the onset of the rainy season (Schroeder *et al.*, 2005).

Satellite observations are the only reasonable way to monitor land-use fire activity over large regions such as Amazonia (e.g., Setzer & Pereira, 1991; Schroeder *et al.*, 2005; Giglio *et al.*, 2006a; Schroeder *et al.*, in press). A range of data products exist for detection of active fires from satellites (e.g., Setzer & Pereira, 1991; Prins & Menzel, 1992; Giglio *et al.*, 2003; Giglio *et al.*, in press). Despite limitations regarding spatial and temporal coverage of satellite observations (Cardoso *et al.*, 2005; Schroeder *et al.*, 2005; Schroeder *et al.*, 2008b), satellite-based time series of

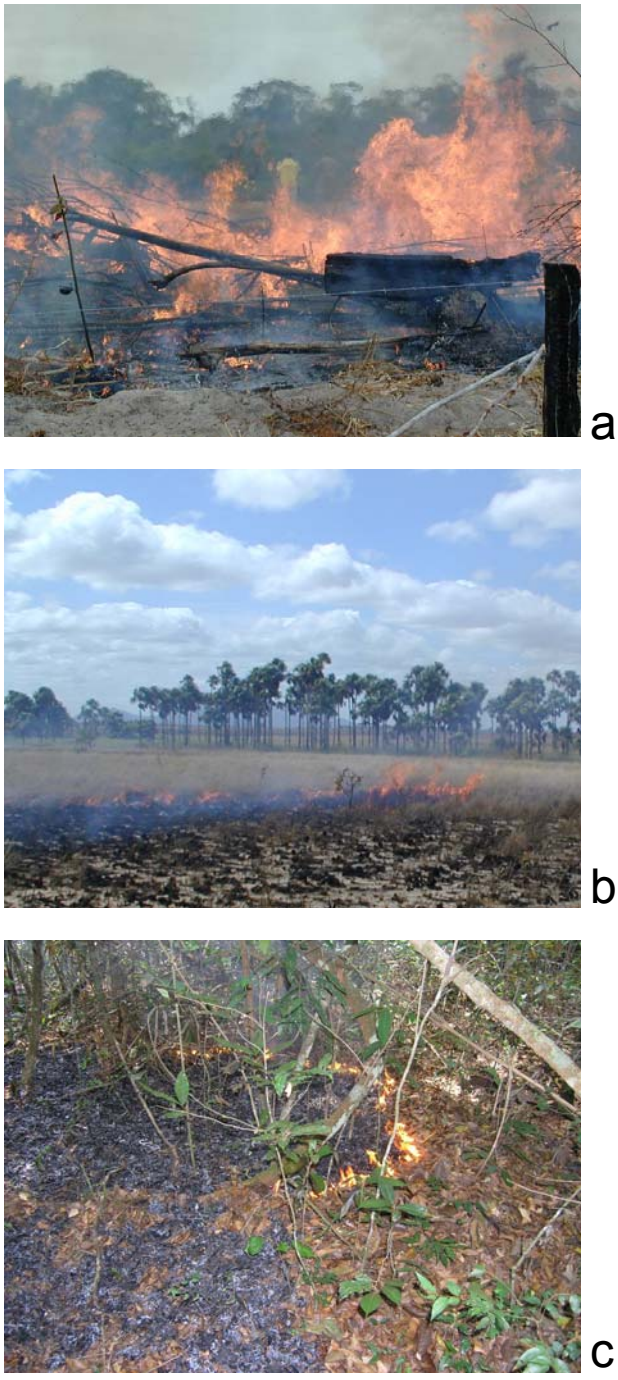

Figure 1-2: A photo series of fire types in Amazonia. Deforestation fires (a) are set after cutting trees and understory vegetation to permit agricultural use. Maintenance fires (b) such as this pasture fire are set to reduce woody encroachment. Understory forest fires (c) are typically the result of deforestation or maintenance fires that escape their intended boundary and burn into adjacent forest areas.

fire activity have defined distinct diurnal, seasonal, and spatial patterns of land-use fires in Amazonia (e.g., Schroeder *et al.*, 2005; Giglio *et al.*, 2006a; Giglio, 2007; Schroeder *et al.*, in press). However, the relative contributions from land-use fires for deforestation and agricultural maintenance to satellite-based fire detections remain uncertain, due in part to the difference in spatial resolution between satellite data and landscape heterogeneity.

1.3 Understory Forest Fires in Amazonia

Land-use fires for deforestation and agricultural maintenance in Amazonia frequently escape their intended boundaries and burn into adjacent forests (Figure 1-2). The resulting understory forest fires are low-intensity surface fires that burn leaf litter and fine fuels on the forest floor (Cochrane *et al.*, 1999). However, damage to cambial tissue from these slow-moving understory fires may cause high rates of canopy-tree mortality because few Amazon tree species have fire-adapted traits (Uhl & Kauffman, 1990; Holdsworth & Uhl, 1997; Cochrane & Schulze, 1999). Selective logging increases the risk of understory fires in Amazon forests because canopy gaps permit greater penetration of sunlight to the forest floor and slash from logging increases fuel loads (Holdsworth & Uhl, 1997; Nepstad *et al.*, 1999b). Once burned, forests become more susceptible to future burning based on changes in canopy structure and the proliferation of short vegetation in canopy-tree gaps (Cochrane & Schulze, 1999; Barlow *et al.*, 2003). Figure 1-3 diagrams this positive fire feedback from land-use fires in Amazon forests. Recurrent fire damage in previously-burned forest is one potential mechanism for large-scale changes in Amazon forest structure

from land-use fires (Cochrane & Schulze, 1999). Conversion of Amazon forests into fire-adapted grasslands or woodlands from repeated exposure to land-use fires, a process referred to as "savannization," would have dramatic consequences for carbon storage and biodiversity (Cochrane & Schulze, 1999; Cochrane, 2003).

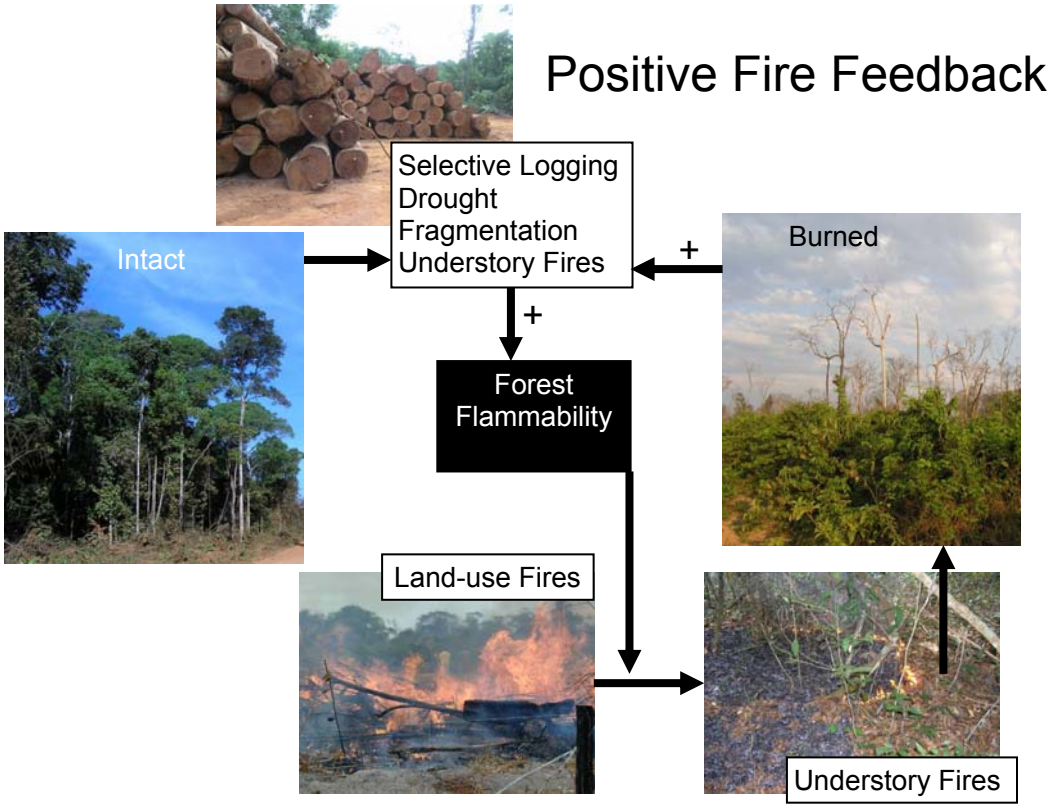

Figure 1-3: Changes in forest structure from initial fire exposure may increase forest flammability, leading to a positive fire feedback in Amazon forests (Cochrane & Schulze, 1999; Nepstad *et al.*, 1999a). Selective logging, drought, or edge effects from forest fragmentation may also increase forest flammability. Anthropogenic ignitions are critical to initiate and continue the feedback mechanism, as land-use fires burn into flammable forest to create understory fires. The feedback ends when land-use fires cease or forest flammability declines due to forest regrowth or decomposition of surface fuels (Cochrane, 2003).

Understory forest fires represent a challenge for satellite-based active fire detection and burn scar mapping since canopy trees may obscure evidence of fire energy and ash, respectively (Giglio *et al.*, 2003; Giglio, 2007; Roy *et al.*, 2008). Recent studies have mapped understory fires in Amazonia using nighttime active fire detections (Elvidge *et al.*, 2001), high-resolution optical sensors such as Landsat (e.g., Cochrane & Souza, 1998; Cochrane & Laurence, 2002; Phulpin *et al.*, 2002; Alencar *et al.*, 2006), and field surveys (Nepstad *et al.*, 1999b; Alencar *et al.*, 2004). However, none of these approaches have been implemented over large regions to evaluate the annual or cumulative forest degradation from understory fires in Amazonia. As a result, the total impact from land-use fires on Amazon forests, including degradation of habitats and loss of biodiversity, may be significantly underestimated (Peres *et al.*, 2006).

1.4 Global Context of Land-use Fires in Amazonia

Globally, tropical deforestation accounted for an estimated 13-25% (0.9 – 2.2 Pg C) of annual atmospheric CO_2 emissions from anthropogenic activities in recent decades (Houghton *et al.*, 2000; Achard *et al.*, 2002; DeFries *et al.*, 2002; Houghton, 2003; Canadell *et al.*, 2007). Fire emissions contribute to the total carbon loss from deforestation, although the fraction of forest biomass that is lost from combustion versus decomposition remains uncertain (e.g., Fearnside *et al.*, 1993; Carvalho Jr. *et al.*, 2001; Morton *et al.*, 2006). In tropical forest nations such as Brazil, carbon emissions from deforestation also constitute a large fraction of the total greenhouse gas emissions from anthropogenic activities (MCT, 2004). Reducing emissions from

Deforestation and Degradation (REDD) in tropical forest regions has therefore emerged as a priority for the next global agreement to regulate anthropogenic greenhouse gas emissions (e.g., Santilli *et al.*, 2005; Gullison *et al.*, 2007). Improving and implementing satellite-based methods to monitor deforestation and degradation is a central aspect of REDD (DeFries *et al.*, 2007). However, technical preparations for REDD have largely focused on existing methods for identifying deforestation and logging (e.g., Asner *et al.*, 2005; Souza Jr. *et al.*, 2005a; Oliveira *et al.*, 2007; INPE, 2008) because satellite-based approaches to detect forest degradation from understory fire are not yet available (GOFC-GOLD, 2008).

Understory fires in Amazon forests are potentially a large source of atmospheric carbon emissions, particularly during drought conditions associated with El Niño Southern Oscillation (ENSO) phenomena (Nepstad *et al.*, 1999b; van der Werf *et al.*, 2004; Randerson *et al.*, 2005; Alencar *et al.*, 2006). Alencar *et al.* (2006) estimated a gross committed flux of 0.05-0.33 Pg C for respiration of fire-killed trees from the 1997-1998 ENSO, but the net contribution of forest burning to carbon emissions from Amazonia remains uncertain. Improving estimates of the long-term carbon consequences of understory fires will require time series of satellite observations or ecosystem models to evaluate the net impact from forest regrowth and future disturbances in burned forests. Additionally, long-term carbon losses from a positive fire feedback in Amazon forests may depend on future climate variability; a return of drought conditions during 2005 in western Amazonia resulted in widespread forest fire activity (Brown *et al.*, 2006; Aragão *et al.*, 2007; Zeng *et al.*, 2008),

highlighting the role of rainfall anomalies for understory fires in regions where land use is concentrated.

Modeling studies of current (Oyama & Nobre, 2003) and future climate (Cox *et al.*, 2004) show the potential for Amazon "dieback" through climate-induced forest loss. However, the mechanisms of forest dieback in these studies, vegetation and carbon-cycle feedbacks with regional and global climate, respectively, do not include the direct influence of land use on Amazon forest structure or extent. Continued deforestation and understory fires in Amazon forests could also lead to large changes in carbon storage in Amazonia in the absence of climate-related feedbacks (Soares-Filho *et al.*, 2006).

Synergistic effects between land-use fires and changing climate could potentially accelerate forest losses in Amazonia. Reductions in precipitation over the Amazon region from climate change may exacerbate future fire risk in Amazon forests (Hoffmann *et al.*, 2003), similar to conditions during recent drought events (Nepstad *et al.*, 2004; Malhi *et al.*, 2008; Zeng *et al.*, 2008). Climate projections for the 21st century suggest that the strongest reduction in dry-season precipitation may occur in southern Amazonia (Meehl *et al.*, 2007; Malhi *et al.*, 2008) where land-use fires are currently most concentrated (Giglio *et al.*, 2006a). Forest burning could also feed back on climate, further increasing fire risk; changes in forest structure from fire damage could strengthen rainfall reductions by altering local convective activity (Werth & Avissar, 2002) or enhancing global climate forcing through carbon-cycle feedbacks (Cox *et al.*, 2004; Friedlingstein *et al.*, 2006). Characterizing the extent of canopy damage from understory fires in Amazonia under current climate conditions,

in addition to climate anomalies that increase forest fire activity, is therefore an important research priority.

1.5 Priority Questions Regarding Land-use Fires in Amazonia

Reducing uncertainties regarding carbon emissions from deforestation and degradation and the long-term impacts on Amazon forests of a positive feedback from land-use fires remain critical areas for additional research using satellite remote sensing and ecosystem models. Several priority research questions regarding land-use fires in Amazonia include:

- How has the trend towards intensification of agricultural production in southern Amazonia altered the use of fire for deforestation? Characterizing the spatial and temporal patterns of fire activity for different land uses in Amazonia is critical to estimate carbon emissions and their atmospheric transport (e.g., Freitas *et al.*, 2006; van der Werf *et al.*, 2006) and the risk of understory fires in adjacent forest areas (Alencar *et al.*, 2004).
- What is the extent and frequency of forest damages from understory fires in southern Amazonia? Satellite-based mapping and real-time monitoring of deforestation are well-established (INPE, 2006; INPE, 2007), and several recent studies have identified new approaches for automated detection of selective logging in Amazonia (Asner *et al.*, 2005; Matricardi *et al.*, 2005; Souza Jr. *et al.*, 2005a). However, a method for routine mapping of canopy damages from fire remains a research priority for both science and policy objectives (e.g., REDD).

- What are the long-term carbon consequences from changes in forest structure due to recurrent fires in Amazon forests? A positive fire feedback in Amazon forests that maintains changes in forest structure and species composition from initial fire damages could reduce long-term carbon storage in Amazonia relative to current conditions (Cochrane & Schulze, 1999; Cochrane, 2003; Barlow & Peres, 2008).

This dissertation integrates satellite remote sensing and ecosystem modeling approaches to specifically address the priority research areas outlined above. Individual studies in the dissertation focus on dynamics of land-use fires and evidence for a positive fire feedback in southern Amazon forests. The emphasis on this region is based on the collocation of rapid land use change (Morton *et al.*, 2006; Hansen *et al.*, 2008), seasonal climate (Vourlitis *et al.*, 2001; Nepstad *et al.*, 2004), and projections of dry-season precipitation reductions from climate change (e.g., Malhi *et al.*, 2008).

1.6 Objectives

The specific objectives of the dissertation were:

1. To characterize spatial and temporal trends in deforestation fires related to intensification of agricultural production in southern Amazonia.
2. To evaluate the interannual variability in fire-damaged forest in southern Amazonia in relation to fire ignitions, deforestation, selective logging, and regional precipitation anomalies.

3. To quantify the frequency of recurrent fires in previously-burned forests to assess the potential for changes in forest structure from a positive fire feedback in Amazonia.
4. To evaluate the carbon consequences and long-term changes in forest structure from repeated understory fires in Amazon forests by integrating satellite remote sensing and ecosystem modeling approaches.

1.7 The Dissertation and its Organization

Chapter 1 (this chapter) presents a brief overview of land-use fires in Amazonia for deforestation and land management, contemporary trends towards intensification of land use, and consequences of forest burning for carbon emissions and changes in Amazon forest structure that provide the context for the work presented in the dissertation.

Chapter 2 describes a new approach to estimate the contribution from deforestation to fire activity in Amazonia based on the local frequency of active fire detections from the Moderate Resolution Imaging Spectroradiometer (MODIS) sensors. Spatial and temporal trends in deforestation fire activity are presented for the entire Amazon region before considering the individual contributions from deforestation for cropland and pasture in the Brazilian state of Mato Grosso where active fire detections are most concentrated. Several applications of the new approach are presented including a new method for monitoring deforestation for

cropland in near-real time and direct interpretation of satellite-based fire detections for information regarding fire emissions.

Chapter 3 documents the development of an automated method to identify canopy damage from understory fires in time series of satellite data, the Burn Damage and Recovery (BDR) algorithm. This chapter focuses on fire-damaged forest in one Landsat scene in the Brazilian state of Mato Grosso, an area identified in Chapter 2 as having concentrated land-use fire activity, to compare field observations of understory fire damages to results from the BDR algorithm applied to time series of high and moderate-resolution satellite data. Isolating canopy damage from fire is a critical first step towards science and policy goals of mapping forest degradation in addition to deforestation for agricultural use.

The BDR algorithm is applied over a larger area using a longer time series of MODIS data in Chapter 4 to characterize the frequency and interannual variability in fire-damaged forest within the upper Xingu River watershed in the Brazilian state of Mato Grosso. This chapter directly addresses the savannization hypothesis by comparing vegetation greenness following repeated understory fires to identify evidence for changes in vegetation structure using optical satellite data.

Chapter 5 describes the development of a new height-structured fire sub-model to explore the impacts of repeated understory forest fires using Ecosystem Demography (ED), an advanced ecosystem model (Hurtt *et al.*, 1998; Moorcroft *et al.*, 2001). The model is calibrated using estimates of forest burning from Chapter 4 to evaluate the short and long-term consequences of land use on forest structure and species composition under current climate conditions.

Finally, Chapter 6 presents conclusions and policy implications of the results presented in previous chapters, focusing on the consequences of land-use fires in Amazonia for carbon emissions from deforestation, forest degradation, and changes in forest structure from a positive fire feedback. The dissertation concludes with a discussion of directions for future research.

Chapter 2: Agricultural Intensification Increases Deforestation Fire Activity in Amazonia[1]

2.1 Summary

Fire-driven deforestation is the major source of carbon emissions from Amazonia. Recent expansion of mechanized agriculture in forested regions of Amazonia has increased the average size of deforested areas, but related changes in fire dynamics remain poorly characterized. This study estimated the contribution of fires from the deforestation process to total fire activity based on the local frequency of active fire detections from the Moderate Resolution Imaging Spectroradiometer (MODIS) sensors. High-confidence fire detections at the same ground location on two or more days per year are most common in areas of active deforestation, where trunks, branches, and stumps can be piled and burned many times before woody fuels are depleted. Across Amazonia, high-frequency fires typical of deforestation accounted for more than 40% of MODIS fire detections during 2003-2007. Active deforestation frontiers in Bolivia and the Brazilian states of Mato Grosso, Pará, and Rondônia contributed 84% of these high-frequency fires during this period. Among deforested areas, the frequency and timing of fire activity varies according to post-clearing land use. Fire usage for expansion of mechanized crop production in Mato Grosso is more

[1] The material in Chapter 2 was previously published in Morton DC, DeFries RS, Randerson JT, Giglio L, Schroeder W, van der Werf GR (2008). Agricultural intensification increases deforestation fire activity in Amazonia. *Global Change Biology* **14**, 2262-2275.

intense and more evenly distributed throughout the dry season than forest clearing for cattle ranching (4.6 vs. 1.7 fire days per deforested area, respectively), even for clearings >200 ha in size. Fires for deforestation may continue for several years, increasing the combustion completeness of cropland deforestation to nearly 100% and pasture deforestation to 50-90% over 1-3 year timescales typical of forest conversion. The results from this study demonstrate that there is no uniform relation between satellite-based fire detections and carbon emissions. Improved understanding of deforestation carbon losses in Amazonia will require models that capture inter-annual variation in the deforested area that contributes to fire activity and variable combustion completeness of individual clearings as a function of fire frequency or other evidence of post-clearing land use.

2.2 Introduction

Agricultural expansion is the main cause of tropical deforestation (FAO, 2006), highlighting the tradeoffs among ecosystem services such as food production, carbon storage, and biodiversity preservation inherent in land cover change (Foley *et al.*, 2005). Expansion of intensive agricultural production in southern Amazonia, led by the development of specific crop varieties for tropical climates (Warnken, 1999) and international market demand (Naylor *et al.*, 2005), contributed one-third of the growth in Brazil's soybean output during 1996-2005 (IBGE, 2007). The introduction of cropland agriculture in forested regions of Amazonia also changed the nature of deforestation activities; forest clearings for mechanized crop production are larger, on average, than clearings for pasture, and the forest conversion process is often

completed in less than one year (Morton *et al.*, 2006). How this changing deforestation dynamic alters fire use and carbon emissions from deforestation in Amazonia is germane to studies of future land cover change (Soares-Filho *et al.*, 2006), carbon accounting in tropical ecosystems (Stephens *et al.*, 2007), and efforts to reduce emissions from tropical deforestation (Gullison *et al.*, 2007).

Fires for land clearing and management in Amazonia are a large anthropogenic source of carbon emissions to the atmosphere (Houghton *et al.*, 2000; DeFries *et al.*, 2002; van der Werf *et al.*, 2006; Gullison *et al.*, 2007). Deforestation fires largely determine net carbon losses (Guild *et al.*, 2004), since fuel loads for Amazon deforestation fires can exceed 200 Mg C/ha (e.g., Carvalho *et al.*, 1998). Reductions in forest biomass from selective logging prior to deforestation are small, averaging less than 10 Mg C/ha (Asner *et al.*, 2005). In contrast, typical grass biomass for Cerrado or pasture rarely exceeds 10 Mg C/ha (Ottmar *et al.*, 2001) and is rapidly recovered during the subsequent wet season (Santos *et al.*, 2003). Yet, the fraction of all fire activity associated with deforestation (Cardoso *et al.*, 2003; Eva & Fritz, 2003; Schroeder *et al.*, 2005) and combustion completeness of the deforestation process remain poorly quantified (Ramankutty *et al.*, 2007).

Satellite fire detections have provided a general indication of spatial and temporal variation in fire activity across Amazonia for several decades (e.g., Setzer & Pereira, 1991; Prins & Menzel, 1992; Elvidge *et al.*, 2001; Schroeder *et al.*, 2005; Giglio *et al.*, 2006a; Koren *et al.*, 2007). However, specific information regarding fire type or fire size can be difficult to estimate directly from active fire detections since satellites capture a snapshot of fire energy rather than a time-integrated measure

of fire activity (Giglio *et al.*, 2006a). Overlaying active fire detections on land cover maps provides a second approach to classify fire type. Evaluating fire detections over large regions of homogenous land cover can be instructive (e.g., Mollicone *et al.*, 2006; Aragão *et al.*, 2007), but geolocation errors and spurious fire detections may complicate these comparisons, especially in regions of active land cover change and high fire activity such as Amazonia (Eva & Fritz, 2003; Schroeder *et al.*, 2008b). Finally, post-fire detection of burn-scarred vegetation is the most data-intensive method to quantify carbon emissions from fires. Two recent approaches to map burn scars with Moderate Resolution Imaging Spectroradiometer (MODIS) data show great promise for identifying large-scale fires (Roy *et al.*, 2005; Giglio *et al.*, 2006b), yet neither algorithm is capable of identifying multiple burning events in the same ground location typical of deforestation activity in Amazonia. Deriving patterns of fire type, duration and intensity of fire use, and combustion completeness directly from satellite fire detections provides an efficient alternative to more data and labor-intensive methods to estimate carbon emissions from land cover change.

This chapter assesses the contribution of deforestation to fire activity in Amazonia based on the intensity of fire use during the forest conversion process, measured as the local frequency of MODIS active fire detections. High-confidence fire detections on two or more days in the same dry season are possible in areas of active deforestation, where trunks, branches, and other woody fuels can be piled and burned many times. Low-frequency fire detections are typical of fires in Cerrado woodland savannas and for agricultural maintenance, since grass and crop residues are fully consumed by a single fire. The frequency of fires at the same location, or

fire persistence, has been used previously to assess Amazon forest fire severity (Elvidge *et al.*, 2001), adjust burned area estimates in tropical forest ecosystems (Giglio *et al.*, 2006b), and scale combustion completeness estimates in a coarse-resolution fire emissions model (van der Werf *et al.*, 2006). This study builds on these approaches to characterize fire activity at multiple scales. First, the frequency of satellite fire detections over recently-deforested areas is compared to other land cover types. Next, an assessment is conducted of regional trends in the contribution of high-frequency fires typical of deforestation activity to the total satellite-based fire detections for Amazonia during 2003-2007. Finally, temporal patterns of fire usage are compared among individual deforested areas with different post-clearing land uses, based on recent work to separate pasture and cropland following forest conversion in the Brazilian state of Mato Grosso with vegetation phenology data (Morton *et al.*, 2006). The goals of this research are to 1) test whether fire frequency distinguishes between deforestation fires and other fire types and 2) characterize fire frequency as a function of post-clearing land use to enable direct interpretation of MODIS active fire data for relevant information on carbon emissions.

2.3 Methods

2.3.1 Data

This study analyzed active fire detections from the MODIS sensors aboard the Terra (2002-2007) and Aqua (2003-2007) satellite platforms to determine spatial and temporal patterns in satellite fire detections from deforestation in Amazonia during this period. Combined, the MODIS sensors provide two daytime (10:30/13:30 local

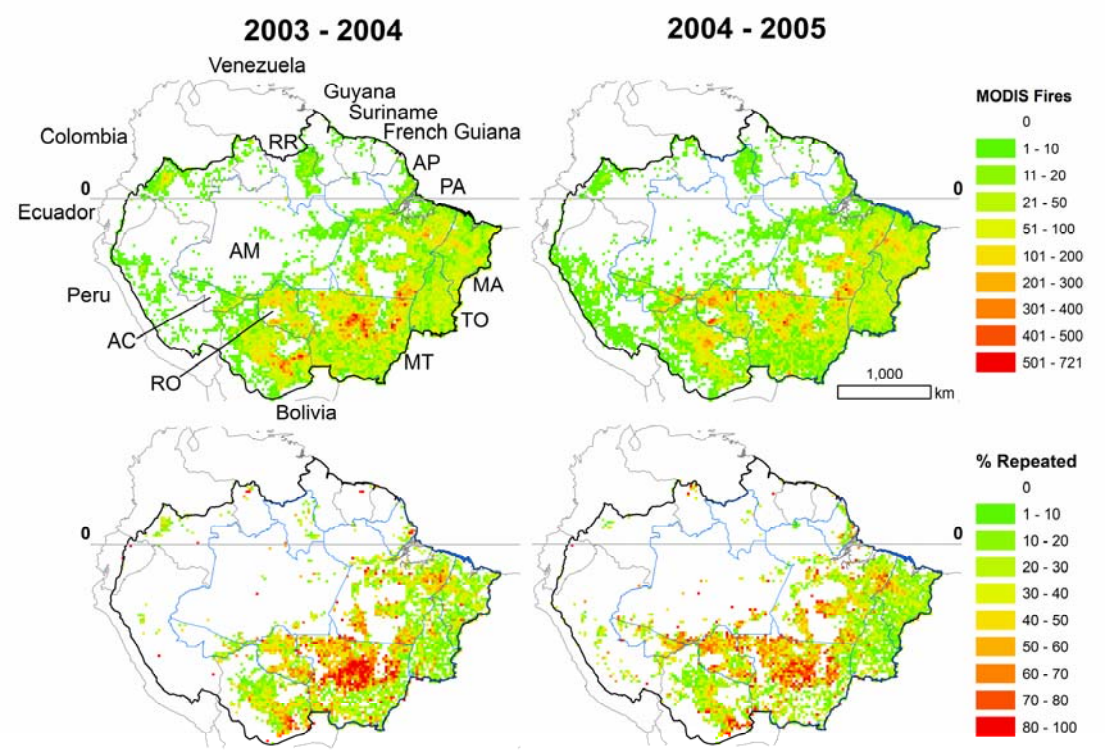

Figure 2-1: Total high-confidence fire detections across the Amazon Basin (upper) and percentage of all fires detected on two or more days during the same dry season (lower) summarized at 0.25° resolution. North of the equator, the fire year is July-June (July 2003-June 2004, July 2004-June 2005); south of the equator, the fire year is January-December (2004, 2005). Outlines show country borders (gray), Brazilian state boundaries (blue), and the extent of the Amazon Basin (black). In clockwise order, letter codes for Brazilian states are: AP: Amapá, PA: Pará, MA: Maranhão, TO: Tocantins, MT: Mato Grosso, RO: Rondônia, AC: Acre, AM: Amazonas, RR: Roraima.

time) and two nighttime (22:30/01:30 local time) observations of fire activity. Figure 2-1 shows the location of the study area and administrative boundaries of the nine countries that contain portions of the Amazon Basin. For data from 2002-2006, the date and center location of each MODIS active fire detection, satellite (Terra or Aqua), time of overpass, 4 micron brightness temperature (band 20/21), and

confidence score were extracted from the Collection 4 MODIS Thermal Anomalies/Fire 5-minute swath (Level 2) product at 1 km spatial resolution (MOD14/MYD14) (Justice *et al.*, 2006). Beginning in 2007, MODIS products were transitioned to Collection 5 algorithms. Data for 1 January - 1 November 2007 were provided by the Fire Information for Resource Management System (FIRMS) at the University of Maryland, College Park (http://maps.geog.umd.edu) based on the Collection 5 processing code. Seasonal differences in fire activity north and south of the equator related to precipitation (Schroeder *et al.*, 2005) were captured using different annual calculations. North of the equator, the fire year was July-June; south of the equator, the fire year was January-December.

This study considered a high-confidence subset of all MODIS fire detections to reduce the influence of false fire detections over small forest clearings in Amazonia (Schroeder *et al.*, 2008b). For daytime fires, only those 1-km fire pixels having >330 K brightness temperature in the 4 μm channel were considered. This threshold is set based on recent work to identify true and false MODIS fire detections with coincident high-resolution satellite imagery (Schroeder *et al.*, 2008b), comparisons with field data (D. Morton, unpublished data), and evidence of unrealistic MODIS fire detections over small historic forest clearings in Mato Grosso state with >20 days of fire detections (fire days) per year in 3 or more consecutive years, none of which exceeded 330 K during the day. Daytime fire detections >330 K correspond to a MOD14/MYD14 product confidence score of approximately 80/100. The subset of high-confidence fires includes all nighttime fire detections, regardless of brightness temperature. Differential surface heating between forested and cleared

areas during daylight hours that may contribute to false detections (Schroeder *et al.*, 2008b) should dissipate by the 22:30 or 01:30 local time overpasses for Terra and Aqua, respectively. Subsequent references to MODIS fire detections refer only to the high-confidence subset of all 1-km fire pixels described above.

2.3.2 Identifying High-Frequency Fires

This study proposes a simple method for separating deforestation and agricultural maintenance fires based on evidence for repeated burning at the same ground locations. The spatial resolution of the analysis is defined by the orbital and sensor specifications of the MODIS sensors and the 1 km resolution bands used for fire detection. The geolocation of MODIS products is highly accurate, and surface location errors are generally less than 70 m (Salomonson & Wolfe, 2004). However, due to the orbital characteristics of the Terra and Aqua satellite platforms, the ground locations of each 1 km pixel are not fixed. This study analyzed three static fire sources from gas (Urucu, Amazonas, Brazil: 65.3° W, 4.86° S), mining (Chuquicamata, Antofagasta, Chile: 68.89° W, 22.31° S), and steel production (CST, Espírito-Santo, Brazil: 40.43° W, 20.24° S) in South America to identify the spatial envelope for MODIS active fire detections referencing the same ground location. Over 98% of high-confidence 2004 MODIS active fire detections from Terra and Aqua for these static sources were within 1 km of the ground location of these facilities. Therefore, this empirically-derived search radius was used to identify repeated burning of forest vegetation during the conversion process. High-frequency fire activity was defined as fire detections on two or more days within a 1 km radius during the same fire year. The time interval between fire detections is not considered

in this analysis, such that fires on consecutive and non-consecutive days at the same ground location are treated equally. A 1 km radius is also consistent with fire spread rates of 200-5,000 m/hr (4.8-140 km/day) for grass, grass/shrub, and deforestation fuel types (Scott & Burgan, 2005), such that even slow-moving grassland fires would spread beyond the 1 km search limit on sequential days. Fires which burn on consecutive days at the same ground location can occur where fuel loads are very high, as is the case in deforestation fires when woody fuels that are piled together may smolder for several days.

The frequency of fire detections was calculated using a neighborhood search algorithm. Specifically, the variety of days on which fires were detected was determined for each cell of the standard MODIS 250 m grid using a search radius of 1 km to interpret the center locations of all high-confidence fire detections for each year. This gridded product of fire days was then used to select those fire detections contributing to high-frequency fire activity and characterize fire frequency for recent deforestation events.

2.3.3 Fire Types in Amazonia

To determine whether active fire detections associated with the conversion of forest to other land uses are unique in terms of fire frequency, this study compared active fire detections from recently-deforested areas to four additional types of fire management. This section describes the test datasets used to evaluate patterns in active fire detections for maintenance of cattle pastures, indigenous reserves in Cerrado savanna-woodland land cover, small properties associated with government settlement programs, and sugarcane production regions.

This study used data on recent deforestation and land use following deforestation to identify and characterize active fire detections associated with forest conversion. Data for the annual deforestation increment in the Brazilian Amazon were acquired from the Brazilian National Institute for Space Research (INPE) PRODES (Program for the estimation of deforestation in the Brazilian Amazon), available at http://www.obt.inpe.br/prodes. Deforestation was mapped using high-resolution Landsat Thematic Mapper or Chinese-Brazilian Environmental Research Satellite data from approximately August of each year 2001-2005 (INPE, 2007).

Data for Mato Grosso state were used to develop the approach for identifying deforestation fires. For individual deforestation events >25 ha in size, this study also evaluated differences in patterns of active fire detections for conversion of forest to pasture, forest to mechanized agriculture, and forest conversions not in agricultural production (NIP). The post-clearing land use for each deforestation event was identified previously using phenological information from time series of MODIS data at 250 m resolution (Morton *et al.*, 2006). Finally, this study examines fire activity in the year prior to deforestation detection by PRODES, year of forest clearing, and for as many years post-clearing as possible to characterize the nature of fire usage during the conversion process. These comparisons provide the timing, frequency, and degree of repeated burning detected by the MODIS sensors for forest conversion to different land uses. Annual deforestation from 2003-2005 was selected to utilize combined Terra and Aqua fire observations. Since few areas are deforested without the use of fire in Amazonia, deforestation events without any MODIS fire detections

provide a measure of the extent of omission due to satellite observation (e.g., orbital, sensor, and atmospheric) and fire characteristics (size, intensity, and timing).

This study utilized data on historic deforestation and recent land use changes to identify maintenance fires on agricultural lands in Mato Grosso state. The dataset is derived from areas that were deforested prior to the initial year of PRODES digital data (1997-2000 analysis), buffered by 1 km from remaining forest edges to exclude fires from new deforestation. Next, areas were removed that underwent conversion from pasture to cropland during 2001-2004 (Morton *et al.*, in press) or were identified as secondary forest in previously-cleared areas (Morton *et al.*, 2007a). The resulting dataset isolates old deforestation not associated with forest edges, secondary forest, or recent conversion to cropland.

To identify patterns of fire detections for extensive grassland fires in Cerrado regions, 18 indigenous reserves were selected in Mato Grosso and Tocantins states covering more than 42,000 km^2. Fire is used during the dry season on some indigenous reserves to facilitate hunting, but extensive land cover change is rare (Nepstad *et al.*, 2006a).

Small properties are an additional challenge for separating evidence of fire activity in the same location. To test the influence of property size on fire frequency, this study considered a subset of the demarcated Instituto Nacional de Colonização e Reforma Agrária (INCRA) land reform settlements in Mato Grosso without large deforestation events (>25 ha) in either 2004 or 2005 (N=127). The typical lot size in these settlements is 100 ha, of which 20-50 ha may be cleared for agricultural use.

Although some sugarcane is grown in the Amazon region, the majority of Brazil's sugarcane industry is located in the southern and northeastern regions of the country. São Paulo State had more than 3 million hectares planted in sugarcane in 2005. This study evaluated active fire detections in 31 municipalities in São Paulo state with >20,000 ha of sugarcane planted in 2005 (IBGE, 2007) to calculate the degree of high-frequency fire associated with sugarcane production.

2.3.4 Basin-Wide Analysis

This study analyzed the high-confidence subset of the MODIS active fire data record for the entire Amazon Basin to distinguish the contribution of deforestation and agricultural maintenance fires to overall fire activity during 2003-2007. Fire type statistics for each Amazon country and Brazilian state are provided. Finally, this study summarizes the ratio of high-frequency to low-frequency fires at 0.25° degree spatial resolution to evaluate inter-annual variations in deforestation fire activity across the basin.

2.4 Results

2.4.1 Deforestation Fires

High-frequency fire activity (more than two fire days per year) is common in areas of recent deforestation but rare for other fire types in Amazonia (Table 2-1). Deforestation in Mato Grosso state had more total fire detections than all other fire types in Table 2-1 combined and seven times the number of fires detected in the same location on two or more days during one year. High-frequency fire activity accounted

Table 2-1: Combined MODIS Terra and Aqua fire detections associated with deforestation, indigenous reserves, agricultural maintenance, and small properties in government settlement areas in the Brazilian State of Mato Grosso and sugarcane production in São Paulo state according to the number of days with fire detections in the same year. Fire frequency for 2004 and 2005 deforestation events is calculated for the year of deforestation detection, and clearings >25 ha are classified based on post-clearing land use as cropland, pasture, or not in production (NIP).

		2004 MODIS Fire Days					2005 MODIS Fire Days			
Fire Location	Area (km^2)	1 (%)	2 (%)	3+ (%)	Total	Area (km^2)	1 (%)	2 (%)	3+ (%)	Total
Deforestation	10,009	2,573 (19)	2,684 (20)	7,946 (60)	13,203	8,279	2,600 (33)	2,449 (31)	2,817 (36)	7,866
Cropland	1,807	374 (7)	468 (9)	4,192 (83)		658	259 (20)	172 (14)	836 (66)	
Pasture	6,159	1,892 (26)	1,970 (27)	3,491 (47)		5,297	1,823 (34)	1,744 (32)	1,804 (34)	
NIP	698	108 (41)	67 (25)	90 (34)		932	133 (39)	106 (31)	106 (31)	
Small (<25 ha)	1,345	199 (36)	179 (32)	173 (31)		1,392	264 (43)	200 (32)	155 (25)	
Indigenous	42,598	3,300 (84)	600 (15)	21 (1)	3,921	42,598	3,877 (82)	480 (16)	38 (2)	4,395
Maintenance	35,013	718 (73)	160 (16)	111 (12)	989	35,013	497 (76)	68 (16)	54 (8)	619
Small producers	7,598	328 (73)	68 (15)	54 (12)	450	7,598	230 (73)	55 (18)	29 (9)	314
São Paulo Sugarcane	24,219	782 (84)	138 (15)	10 (1)	930	24,219	799 (79)	182 (18)	30 (3)	1,011

for 27% of high-confidence MODIS detections associated with small producers in Mato Grosso 2004 and 2005, but the total number of detections was small (N=764), suggesting that property size is not a main component of the pattern of repeated fire usage associated with deforestation. Fires detected on two days at the same location are rare within indigenous reserves and agricultural areas of Mato Grosso state or sugarcane production municipalities in São Paulo state; fires on three or more days are almost exclusively linked to deforestation.

Mato Grosso had both the highest total fire activity and greatest fraction of high-frequency fire activity during 2003-2007 of any state in Brazilian Amazonia (Table 2-2). Combined with fires in neighboring Pará and Rondônia states, these three states contributed 83% of the fires that burn on two or more days and 74% of

the total fire activity in the Brazilian portion of the Amazon Basin during this period. Inter-annual variability in the total number of fires highlights drought conditions in Roraima state during 2003 and widespread drought in 2005 affecting Rondônia, Acre, and Amazonas states. The fraction of total fire activity from burning on two or more days also increased during drought years in these states. Fire detections were highest in 2005 for Pará and Amapá states, although these regions were less affected by drought conditions; the fraction of repeated fire activity did not increase in 2005 compared to other years. After a decrease in fire activity in Brazilian Amazonia during 2006, fires in 2007 returned to a similar level as seen in 2004 and 2005, led by increased fire activity in south-eastern Amazonia. Major contributions to this increase in 2007 were from low-frequency fires in Tocantins and Maranhão states and additional high frequency fires in Mato Grosso and Pará. Overall, fires on two or more days during the same dry season accounted for 36-47% of annual fire activity in Brazilian Amazonia during 2003-2007, with greater contributions from repeated fires in years with highest fire activity.

At the national scale, fire activity in Brazil (85%) and Bolivia (13%) accounted for 98% of all fire detections in the Amazon Basin during 2003-2007 (Table 2-3). High-frequency fires contribute a large fraction of MODIS detections in both countries, with peak repeated fire activity during 2004 in Brazil and 2007 in Bolivia. Small contributions to overall fire activity from other Amazon countries are primarily low-frequency fires, with the notable exceptions of 2004 and 2007 in Colombia, 2003 in Guyana and Suriname, and 2003 and 2007 in Venezuela.

Table 2-2: Number of high-confidence MODIS Terra and Aqua fire detections (1-km pixels) for the nine states of the Brazilian Legal Amazon during 2003-2007 as a function of fire frequency. States are listed in decreasing order of fire activity.

State	Fire Days	2003		2004		2005		2006		2007*	
Mato Grosso	1	27,036	43%	37,575	41%	33,711	51%	20,875	57%	39,592	50%
	2	12,938	21%	19,992	22%	16,848	25%	8,851	24%	22,434	28%
	3+	22,359	36%	33,979	37%	15,853	24%	7,078	19%	17,475	22%
	Total	62,333		91,546		66,412		36,804		79,501	
Para	1	18,501	69%	25,729	58%	28,439	59%	20,423	66%	21,068	54%
	2	6,072	23%	11,738	27%	13,182	27%	7,255	24%	11,821	30%
	3+	2,407	9%	6,626	15%	6,581	14%	3,140	10%	6,321	16%
	Total	26,980		44,093		48,202		30,818		39,210	
Maranhao	1	12,566	72%	12,954	73%	16,388	71%	8,397	80%	16,592	65%
	2	3,538	20%	3,425	19%	4,906	21%	1,528	15%	6,285	25%
	3+	1,378	8%	1,463	8%	1,784	8%	559	5%	2,760	11%
	Total	17,482		17,842		23,078		10,484		25,637	
Rondonia	1	8,018	62%	11,107	55%	12,523	47%	8,911	52%	7,227	51%
	2	3,394	26%	6,114	30%	8,427	32%	5,272	31%	4,435	32%
	3+	1,470	11%	2,886	14%	5,745	22%	2,791	16%	2,382	17%
	Total	12,882		20,107		26,695		16,974		14,044	
Tocantins	1	7,732	86%	11,139	81%	12,540	83%	6,140	86%	20,243	73%
	2	921	10%	1,987	14%	2,050	14%	807	11%	6,153	22%
	3+	306	3%	693	5%	526	3%	200	3%	1,288	5%
	Total	8,959		13,819		15,116		7,147		27,684	
Amazonas	1	2,253	68%	1,795	78%	4,068	55%	3,145	66%	2,089	65%
	2	727	22%	386	17%	1,874	25%	1,038	22%	665	21%
	3+	342	10%	121	5%	1,479	20%	573	12%	477	15%
	Total	3,322		2,302		7,421		4,756		3,231	
Acre	1	1,893	73%	1,159	76%	3,894	50%	1,274	87%	1,368	83%
	2	540	21%	249	16%	2,479	32%	169	12%	245	15%
	3+	174	7%	120	8%	1,340	17%	18	1%	43	3%
	Total	2,607		1,528		7,713		1,461		1,656	
Roraima	1	3,955	54%	1,075	91%	583	96%	811	93%	1,866	69%
	2	1,958	27%	82	7%	26	4%	49	6%	535	20%
	3+	1,427	19%	21	2%	1	0%	8	1%	313	12%
	Total	7,340		1,178		610		868		2,714	
Amapa	1	687	56%	828	65%	1,121	69%	492	69%	447	83%
	2	180	15%	251	20%	345	21%	113	16%	73	14%
	3+	355	29%	204	16%	152	9%	112	16%	19	4%
	Total	1,222		1,283		1,618		717		539	

* Data through 11-01-07

Table 2-3: Number of high-confidence MODIS Terra and Aqua fire detections (1-km pixels) within the Amazon Basin during 2003-2006, summarized at the national level according to the frequency of fire detections. Countries are listed in decreasing order of fire activity.

Country	Fire Days	2003		2004		2005		2006		2007*	
Brazil	1	82,641	58%	103,361	53%	113,267	58%	70,468	64%	110,492	57%
	2	30,268	21%	44,224	23%	50,137	25%	25,082	23%	52,646	27%
	3+	30,218	21%	46,113	24%	33,461	17%	14,479	13%	31,078	16%
	Total	143,127		193,698		196,865		110,029		194,216	
Bolivia	1	9,611	77%	23,368	65%	18,918	68%	13,143	64%	15,383	53%
	2	1,797	14%	8,343	23%	5,705	20%	3,885	19%	6,558	23%
	3+	1,029	8%	4,396	12%	3,287	12%	3,440	17%	7,094	24%
	Total	12,437		36,107		27,910		20,468		29,035	
Peru	1	1,418	92%	815	95%	2,453	87%	1,240	92%	1,800	79%
	2	107	7%	36	4%	319	11%	84	6%	360	16%
	3+	19	1%	6	1%	45	2%	21	2%	125	5%
	Total	1,544		857		2,817		1,345		2,285	
Colombia	1	958	95%	2,019	79%	486	96%	480	96%	2,784	72%
	2	54	5%	427	17%	20	4%	19	4%	818	21%
	3+	0	0%	107	4%	0	0%	0	0%	244	6%
	Total	1,012		2,553		506		499		3,846	
Venezuela	1	515	67%	323	79%	227	76%	179	87%	599	75%
	2	146	19%	50	12%	61	20%	13	6%	155	19%
	3+	107	14%	37	9%	10	3%	14	7%	43	5%
	Total	768		410		298		206		797	
Guyana	1	833	80%	198	96%	203	94%	228	88%	210	94%
	2	133	13%	8	4%	8	4%	28	11%	13	6%
	3+	80	8%	0	0%	4	2%	4	2%	0	0%
	Total	1,046		206		215		260		223	
Suriname	1	155	72%	67	86%	95	98%	14	100%	66	97%
	2	42	20%	11	14%	2	2%	0	0%	2	3%
	3+	18	8%	0	0%	0	0%	0	0%	0	0%
	Total	215		78		97		14		68	
French Guiana	1	33	94%	24	62%	67	70%	61	87%	35	71%
	2	2	6%	9	23%	7	7%	3	4%	7	14%
	3+	0	0%	6	15%	22	23%	6	9%	7	14%
	Total	35		39		96		70		49	
Ecuador	1	4	100%	20	40%	41	43%	8	73%	12	21%
	2	0	0%	4	8%	3	3%	3	27%	0	0%
	3+	0	0%	26	52%	51	54%	0	0%	46	79%
	Total	4		50		95		11		58	

* Data through 11-01-07

Spatial patterns of high-frequency fire activity in 2004 and 2005 highlight active deforestation frontiers in Mato Grosso, Rondônia, and Pará states in Brazil and in southeastern Bolivia (Figure 2-1). Isolated locations of high-frequency fire activity can also be seen across other portions of the Amazon Basin, but these areas have low total fire detections. Differences in the total fire activity and high-frequency fire detections between 2004 and 2005 highlight the influence of drought conditions in western Amazonia on fire frequency. Total fire detections in central Mato Grosso decreased slightly between 2004 and 2005, while fire detections in drought-stricken northern Rondônia, southern Amazonas, and eastern Acre states in Brazil show higher total fire activity in 2005 than in 2004. The number of 0.25° cells with >50% of fire activity occurring on 2 or more days is similar during 2004 (n=733) and 2005 (n=773), but the spatial distribution is broader in 2005 than 2004, as fires associated with deforestation activity in Mato Grosso, Pará, and southern Rondônia spread west into northern Rondônia, Acre, and southern Amazonas states. In addition to deforestation-linked fires, slow-moving forest fires and contagion of other accidental burning events may also have contributed to the higher fraction of repeated fire activity in these regions.

2.4.2 Patterns of Fire Use Stratified by Post-Clearing Land Use

Among deforested areas in Mato Grosso, the intensity of fire usage varies according to post-clearing land use (Figure 2-2). Forest conversion for cropland exhibits the most frequent fire usage; more than 50% of 2004 cropland deforestation events had fire detections on three or more days during the 2004 dry season and 14% burned on ten or more days. Over 70% of the forest clearings with fires on more than

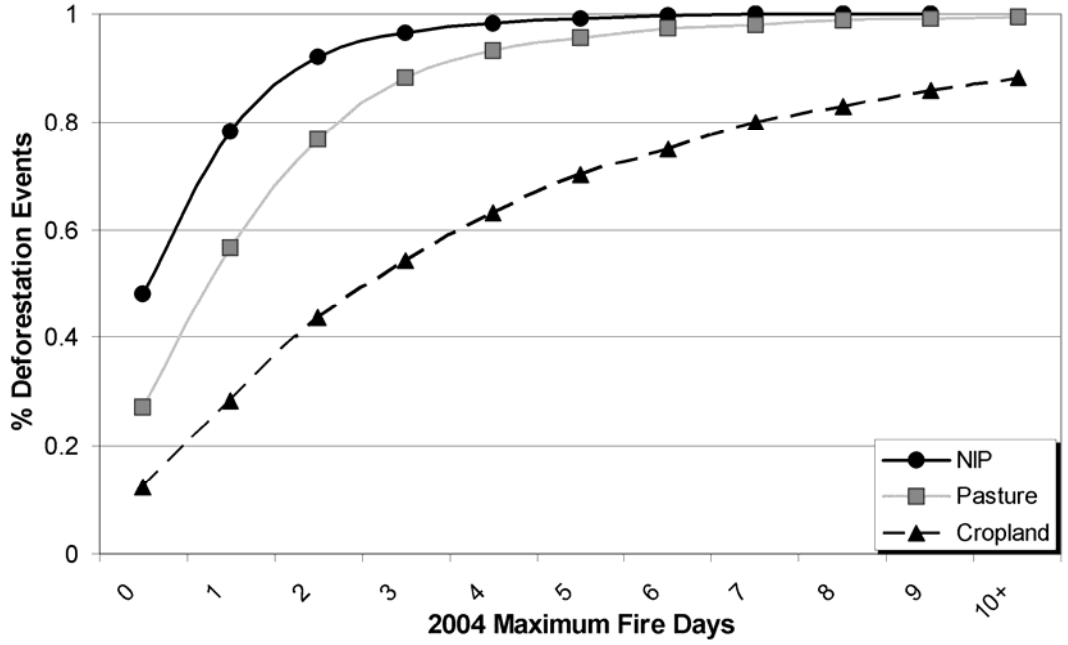

Figure 2-2: Intensity of fire use for 2004 deforestation events >25 ha in Mato Grosso state according to post-clearing land use (cropland, pasture, and not in production-NIP), measured as the maximum fire frequency in each deforested area during 2004.

five days were subsequently used for cropland. Due to more frequent fire usage in preparation for mechanized agriculture, few areas deforested for cropland in 2004 had no high-confidence fire detections during 2004 (12%).

Deforestation for pasture averaged less than half as many fire days as deforestation for cropland, measured as either the maximum (pasture = 1.7, cropland = 4.6) or mean (pasture = 1.15, cropland = 3.0) days of fire detection per clearing. Even among very large clearings (>200 ha), fire usage was significantly higher for cropland deforestation than forest clearing for pasture (Wilcoxon Rank Test, $p<0.0001$). Only 13% of all deforestation events for pasture >200 ha averaged three

or more fire days in any year, suggesting that mechanized forest clearing and high-frequency burning is more related to post-clearing land use than clearing size. For both pasture and cropland deforestation, polygons in which the conversion occurs within one year have a greater number of fire days in the year that the deforestation was detected than conversions occurring over two or more years (Wilcoxon Rank Test, $p<0.0001$), consistent with the expectation that higher fire frequency leads to higher combustion completeness.

For those areas that showed no clear pasture or cropland phenology in the years following deforestation, fire activity was minimal. Nearly 50% of the areas described as NIP showed no high-confidence fires in 2004, and only 22% of these deforestation events exhibited fires on two or more days typical of other deforestation events.

The timing of fire use during the dry season also differed for cropland and pasture deforestation (Figure 2-3). Deforestation fire activity may begin during the late dry season (September-November) in the year before the deforestation is mapped and continue for several years post-clearing as the initial forest biomass is gradually depleted to the desired conditions for cropland or pasture use. September was the most common month of fire activity for all types of deforestation in Mato Grosso in 2004. More than 70% of fires associated with 2004 deforestation for pasture during 2003-2005 occurred during the late dry season (August-October). In contrast, fire activity for conversion to cropland was more evenly distributed through the dry season, with 45% of fire detections occurring in May-July.

Burning activities initiated in the early dry season for both pasture and cropland deforestation continue to burn in subsequent months. The highest percentage of fires without detections on additional days (fire days = 1) occurred during the late dry season; approximately 30% of fires for conversion to pasture during September and October were the first fire detection for those deforestation events compared to 11% of all fires for cropland conversion during this period.

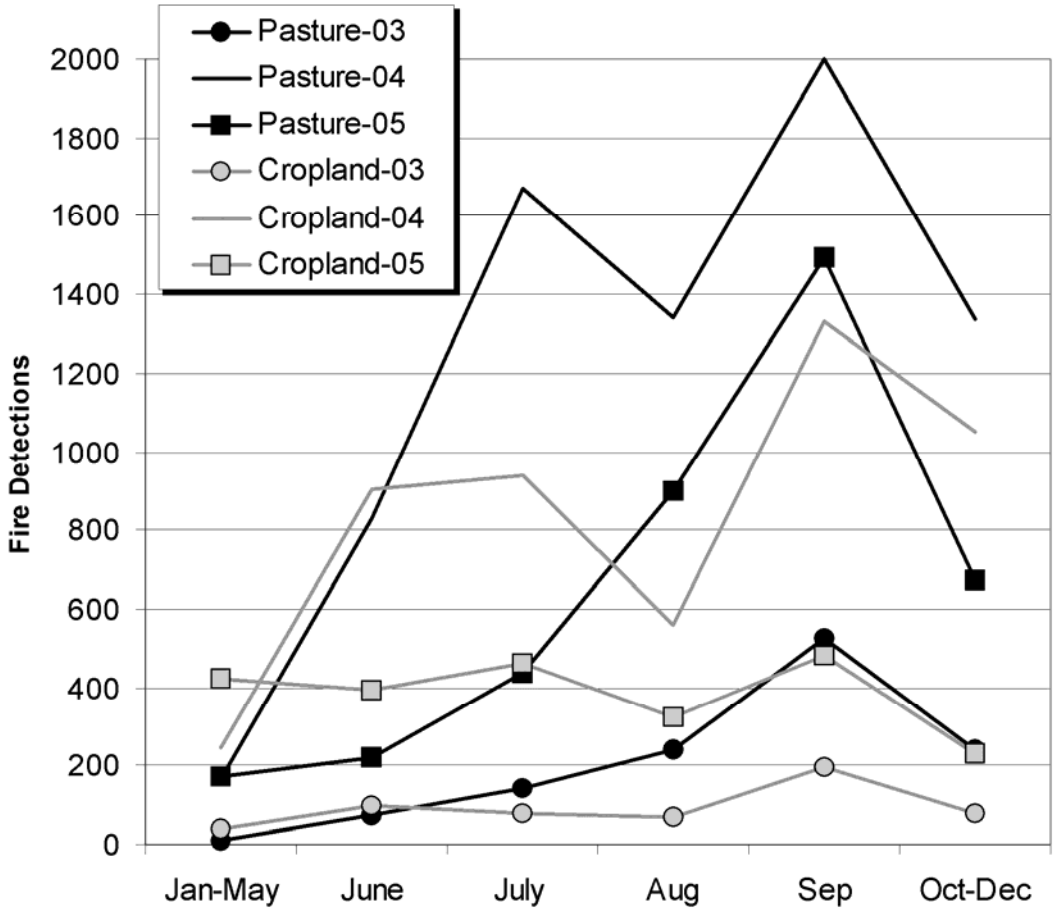

Figure 2-3: Seasonality of fire activity during 2003-2005 for pasture and cropland deforestation events >25 ha in Mato Grosso state from 2004.

High-frequency fire activity may last for several years following initial forest clearing, further increasing the expected combustion completeness of the deforestation process (Figure 2-4). Forty percent of the areas deforested for cropland during 2003-2005 had two or more years during 2002-2006 with 3+ fire days. The duration of clearing for pasture was more variable. Most areas cleared for pasture had 0-1 years of high-frequency fire usage, although a small portion (14%) had frequent fire detections over 2-3 years typical of mechanized forest clearing.

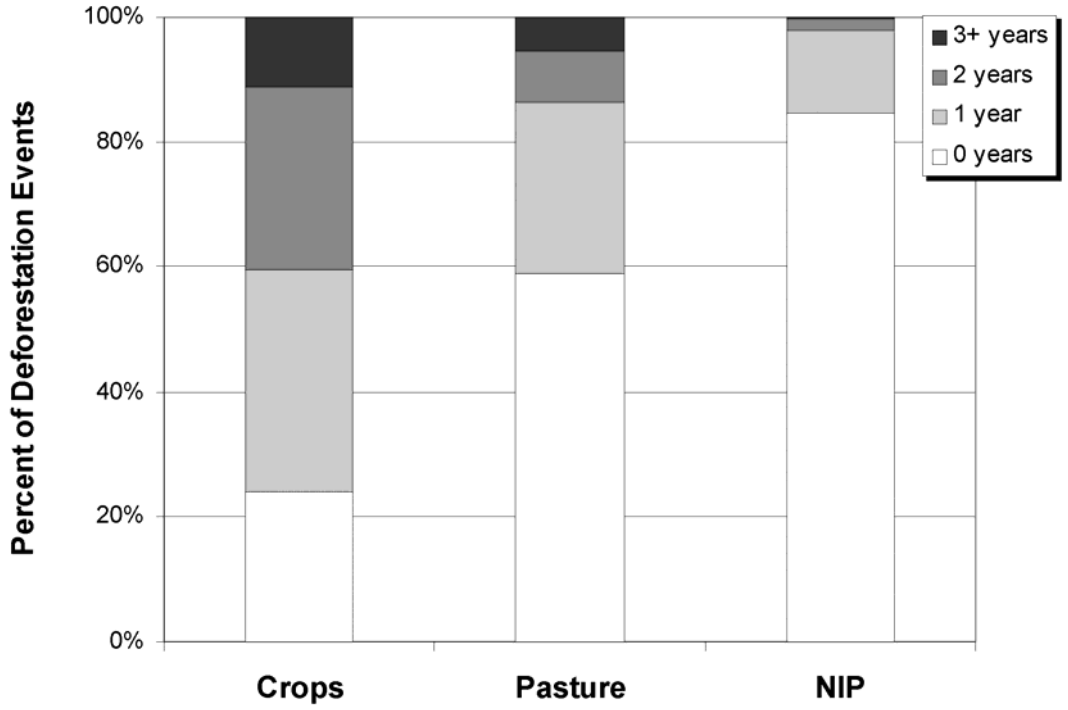

Figure 2-4: Years of high-frequency fire activity for three different land uses following deforestation in Mato Grosso state. The typical duration of high-frequency fire activity (>2 fire days per year) is shown as a percentage of deforestation events during 2003-2005 for each land use. Fire activity was examined for the year prior to deforestation mapping until 2006.

The carryover of fire activity from forest clearing into subsequent years is a cumulative process, such that total high-frequency fire activity in any year represents burning for multiple years of forest loss (Figure 2-5). For example, elevated fire activity during 2004 in Mato Grosso (Table 2-2) is the product of deforestation rates during 2002-2005 and high fire frequencies in 2004 for cropland and pasture deforestation. In general, fire frequency is highest for the year in which the deforestation was mapped. For cropland deforestation, fire frequency is similar in the year prior to (n-1) and following (n+1) deforestation mapping. For pasture deforestation, fire frequency is consistently higher in the year following deforestation mapping than the year prior to detection of deforestation. Deforestation NIP contributes little to the fire activity or deforested area during this period.

2.5 Discussion

2.5.1 Deforestation Fires in Amazonia

The number of days on which fires are detected at the same ground location is higher for areas undergoing deforestation than for other fire types in Amazonia, and fires on three or more days at the same ground location are almost exclusively linked with forest conversion. During 2003-2007, more than 40% of all high-confidence MODIS fire detections within Amazonia were associated with deforestation. Within this subset of repeated fire detections, variations in fire frequency suggest that carbon losses from deforestation vary with post-clearing land use. Deforestation for cropland

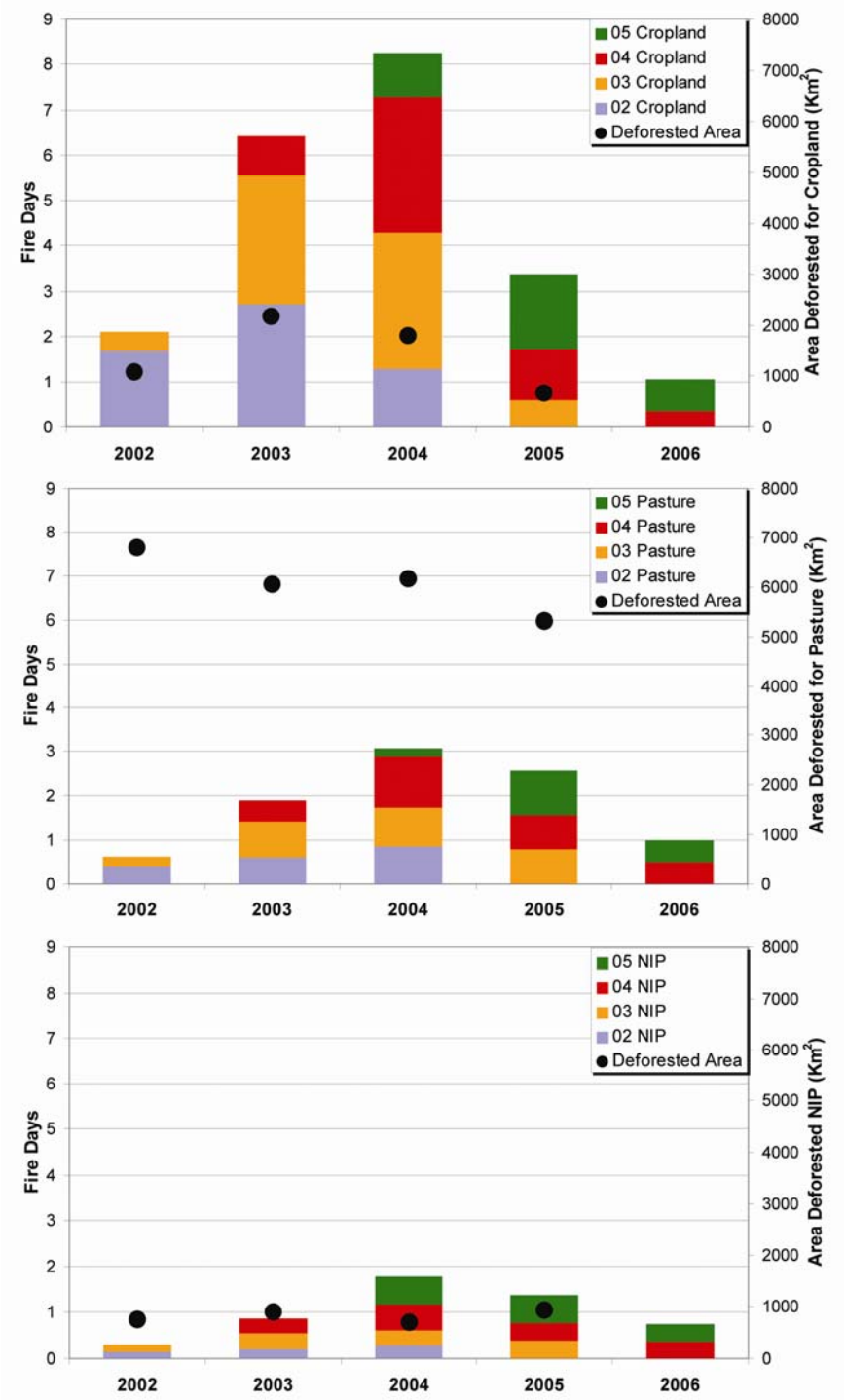

Figure 2-5: The duration of deforestation fire activity following forest clearing highlights the contribution of multiple years of deforestation to fire in any year. Average fire frequency and total deforested area in polygons >25 ha in size for 2002-2005 are shown separately for cropland (top), pasture (middle), and areas not in agricultural production (NIP, bottom). Deforested area for each post-clearing land use is taken from Morton *et al.* (2006, 2007). Fire data for 2002 are derived only from Terra-MODIS observations.

may involve burning on as many as 15 days during the same dry season as woody fuels are piled and re-burned to prepare the land for mechanized agricultural production. Forest conversion for pasture is characterized by fewer days of burning during the dry season, on average, and fewer years of high-frequency fire detections than conversion to cropland. Forests without evidence for cropland or pasture usage following deforestation detection have the lowest fire activity.

Higher fire frequency associated with mechanized deforestation suggests greater combustion completeness of the deforestation process compared to less intensive clearing methods. Whereas the first fire following deforestation may consume 20-62% of forest biomass depending on fuel moisture conditions (Fearnside *et al.*, 1993; Kauffman *et al.*, 1995; Carvalho *et al.*, 1998; Guild *et al.*, 1998; Araujo *et al.*, 1999; Carvalho *et al.*, 2001), piling and burning trunks, branches, and woody roots many times in the same dry season may increase the combustion completeness of the deforestation process to near 100% (Figure 2-6). Based on published combustion completeness estimates of 20% or 62% per fire, repeated burning during the deforestation process could eliminate initial forest biomass after 5-22 fire events.

Combustion completeness and fire emissions from recent deforestation may be higher than previous estimates for deforestation carbon losses. Mechanized equipment can remove stumps and woody roots in preparation for cropland (Morton *et al.*, 2006) such that both above and below-ground forest biomass are burned. Burning woody roots may increase the fire-affected biomass by as much as 20% (Houghton *et al.*, 2001). Fires that burn piled wood are likely to be at the high end of the published range for combustion completeness, given field measurements of high

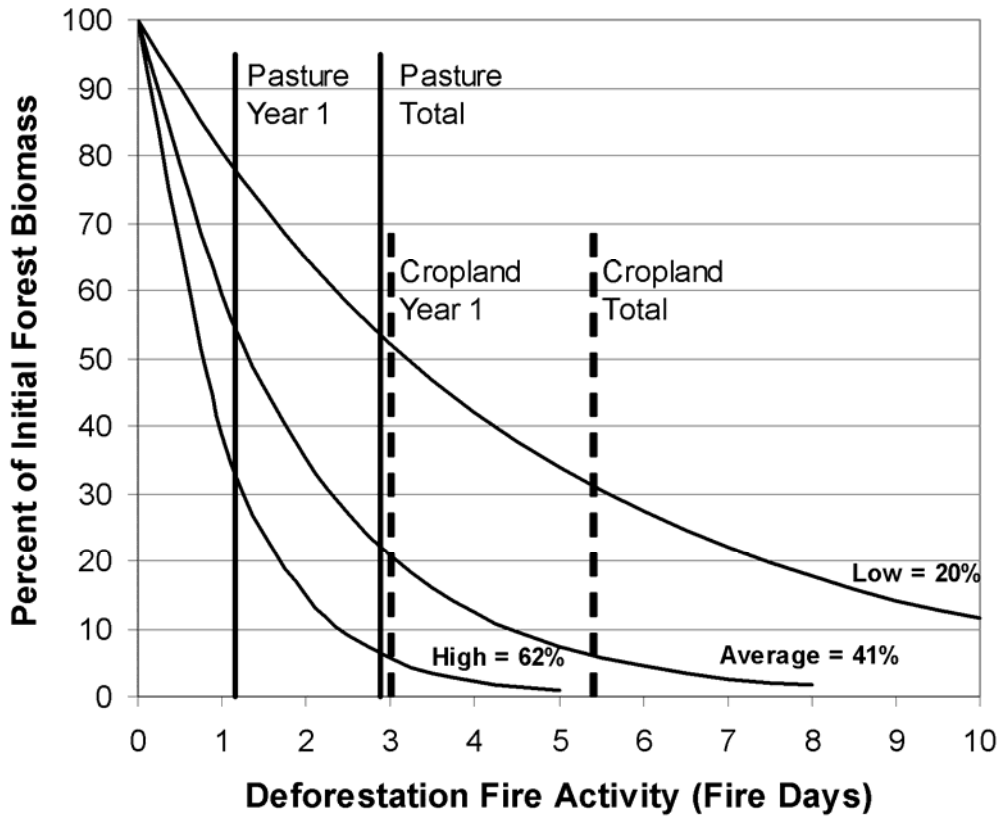

Figure 2-6: Percent of initial forest biomass remaining following repeated deforestation fire activity. The range of combustion completeness for each fire is shown as low (19.5%, Carvalho *et al.*, 2001), average of published figures for Amazonia (40.6%, (Fearnside *et al.*, 1993; Kauffman *et al.*, 1995; Carvalho *et al.*, 1998; Guild *et al.*, 1998; Araujo *et al.*, 1999; Carvalho *et al.*, 2001), and high (61.5%, Carvalho *et al.*, 2001). Curves end once initial forest biomass drops below 1% (5-22 fires). Vertical lines show the mean number of fire days for 2004 deforestation in Mato Grosso for pasture and cropland in 2004 (year 1) and during 2003-2006 (total).

fire temperature and longer duration of flaming and smoldering stages of combustion in piled fuels compared to pasture or initial deforestation fires (Schroeder *et al.*, 2008b). High fire frequency for recent deforestation also generates higher total fire emissions compared to previous estimates that assume a majority of carbon is lost as

CO_2 from heterotrophic respiration of unburned biomass (e.g., Houghton *et al.*, 2000).

These attributes of fire use for mechanized deforestation in Amazonia challenge the basic assumptions that monitoring deforested area and estimating above-ground biomass of tropical forests are sufficient to estimate carbon emissions from deforestation (DeFries *et al.*, 2007; Gullison *et al.*, 2007). Failure to consider the evolving roles of post-clearing land use on combustion completeness could introduce substantial uncertainty into calculated reductions in carbon emissions from declines in deforestation rates. Findings in this study suggest that average combustion completeness for recent deforestation may be 2-4 times greater than estimated for deforestation during 1989-1998 (Houghton *et al.*, 2000), increasing per-area gross fire emissions for the current decade by a similar magnitude in regions where mechanized deforestation is common. Deforestation for highly-capitalized, intensive agricultural production may also reduce the rates of land abandonment to secondary forest compared with previous periods of Amazon colonization, reducing the offset of gross fire emissions from regrowing forests (Ramankutty *et al.*, 2007). In addition to further field measurements, a detailed model representing variations in forest biomass, combustion completeness of new deforestation, and offset of fire emissions from regrowing vegetation is needed to more accurately quantify the influence of agricultural intensification on carbon emissions in the region.

The use of heavy equipment to manage forest biomass may also change the nature of trace-gas emissions from deforestation. Emissions factors for CO_2 are relatively similar for flaming and smoldering phase combustion, but emissions of

CH_4, CO, and some VOCs from the smoldering stage of deforestation fires are nearly double that during the flaming phase (Guild *et al.*, 2004). The balance between flaming and smoldering phase combustion for 2^{nd} - N^{th} fires during the forest conversion process is unknown. If emissions ratios do change during the course of the deforestation process as a function of the size or moisture content of woody fuels, the frequency of satellite-based fire detections provides one method to characterize time-varying trace gas emissions for Amazonia. Combining day and nighttime observations from multiple sensors may better characterize the duration of individual fires to allow more direct interpretation of satellite data for trace gas emissions.

2.5.2 Spatial and Temporal Dynamics of Fire Activity

Inter-annual differences in total and high-frequency fire activity highlight trends in both economic and climate conditions across Amazonia. Concentrated fire activity in Mato Grosso state during 2003-2004 is consistent with peak deforestation for cropland, driven, in part, by high prices for soybean exports (Morton *et al.*, 2006). Carryover of fire activity from previous years' deforestation also contributes to high fire detections during 2003-2005 in Mato Grosso. Thus, reductions in fire-intensive cropland deforestation during 2005 (Morton *et al.*, 2007b) do not result in a shift in fire intensity away from central Mato Grosso state until 2006.

Regional differences in concentrated fire activity also highlight the role of climate in mediating human-caused fires. Roraima, Acre, and Tocantins states in Brazil show dramatic differences in fire activity during 2003, 2005, and 2007. During drought periods in 2003 and 2005, Roraima and Acre had approximately 7 and 4 times as many fires as under normal climate conditions, respectively. The

fraction of high-frequency fires was also highest during these drought years, supporting the results from recent studies showing anomalous fire activity (Aragão *et al.*, 2007) and large areas of burned agricultural land and forest in drought-affected areas (Shimabukuro *et al.*, 2006). Future work to verify the detection of active forest burning by satellites is needed to quantify the contribution of forest fires to the regional patterns of high-frequency fire in drought years. In 2007, anomalous fire activity was driven primarily by low-frequency fires concentrated in south-eastern Amazonia and a return to 2004 levels of deforestation fire activity in southeastern Bolivia and the Brazilian states of Mato Grosso and Pará. These examples suggest that even localized drought conditions can spur anomalous fire activity in the presence of anthropogenic ignition sources for deforestation and agricultural land management with important consequences for gross fire emissions.

The timing of fires for forest conversion may influence the likelihood of fires escaping their intended boundaries and burning neighboring forest and Cerrado vegetation. Deforestation for pasture contributes more fires during the late dry season when forests in Mato Grosso state may be most flammable after 3-5 months with little rainfall. More even distribution of fires for cropland clearing throughout the dry season may reduce the risk of forest fires. Different timing for cropland and pasture deforestation fires is consistent with management practices for intensive agriculture; mechanized crop production with chemical fertilizers is less reliant on the ash layer from deforestation fires for soil fertility than cattle pasture or smallholder agriculture land uses. However, deforestation fires for both cropland and pasture in Mato Grosso state were common during July and August of 2003-2005 despite local regulations

prohibiting fires during these months to minimize the risk of unintended forest fires (Schroeder *et al.*, in press).

Because the most frequent fire detections are indicative of mechanized deforestation and post-clearing land use for intensive agricultural production, monitoring cumulative fire frequency could aid the rapid detection of mechanized forest clearing. Improved geolocation and fire detection capabilities of the MODIS sensors compared to previous satellite instruments enables a higher-resolution investigation of these patterns of repeated fire activity. Despite the moderate resolution of the MODIS sensors, information on fire frequency at 1 km resolution is commensurate with clearing sizes for mechanized crop production in Amazonia that average 3.3 km^2 (Morton *et al.*, 2006). Active fire information has not previously been merged with land cover change estimates for deforestation monitoring.

2.5.3 Uncertainties

The approach in this study to quantify the contribution of deforestation to satellite-based fire activity and characterize individual forest conversions in terms of fire frequency is intentionally conservative. Due to issues of both omission and commission of fires by the MODIS sensors, it is not possible to determine the exact timing or frequency of all fires for the conversion process. This study begins with a high-confidence subset of active fire detections to reduce data errors from spurious fire detections over tropical forest (Schroeder *et al.*, 2008b). Next, deforestation fire activity is linked to high-frequency fire detections, such that fires must be detected at the same ground location on two or more days, despite omission of fires from MODIS attributable to fire size (Cardoso *et al.*, 2005), orbital coverage (Schroeder *et*

al., 2005), and the diurnal cycle of fire activity (Giglio, 2007). Despite well-defined changes in land cover, 12% of cropland and 27% of pasture deforestation events in 2004 showed no fire activity in the high-confidence subset of fire detections. Therefore, low-frequency and omitted fires likely increase the fraction of total fire activity in Amazonia linked to deforestation. Due to omission of active fires by MODIS, a more robust method to estimate combustion completeness of the deforestation process may be to combine active fire detections from multiple sensors with other satellite data on deforestation or vegetation phenology to follow the fate of cleared areas over time.

2.6 Conclusions

The spatial and temporal patterns of fire activity in Amazonia characterize the differences in fire frequency for deforestation and agricultural maintenance. This chapter presents the fraction of MODIS fire detections associated with forest conversion, quantifying the disproportionate contribution of high-frequency burning for conversion of forest to mechanized cropland in satellite-based fire detections. Patterns of high-frequency fire use for deforestation compared to agricultural maintenance highlight the fact that post-clearing land use is more important than clearing size for determining the intensity of fire use during deforestation. Fire activity for both cropland and pasture deforestation may continue over multiple years, contributing to higher combustion completeness compared to previous estimates of carbon losses from deforestation. Since deforestation from multiple years may

contribute to fire activity in any given year, a decrease in deforestation may not reduce fire activity in that year.

The trend towards more intensive land management in Amazonia is clearly linked with an increase in the frequency of fire usage for deforestation. Proper characterization of related changes in fire emissions will therefore depend on the ability to separate fires from repeated burning of deforested areas from other fire types in Amazonia, as demonstrated here. In addition, combining the frequency of active fire detections with existing deforestation monitoring approaches could assist in the identification of mechanized forest clearing typical of intensive agricultural production.

Chapter 3: A Time Series Approach to Map Canopy Damage from Understory Fires in Amazon Forests

3.1 Summary

Understory fires in Amazon forests alter forest structure, species composition, and the likelihood of future disturbance. The annual extent of fire-damaged forest in Amazonia remains uncertain due to difficulties in separating burning from other forest damages in satellite data. This chapter documents the development of a new approach, the Burn Damage and Recovery (BDR) algorithm, to identify fire-related canopy damages in multi-year time series of satellite data. The BDR algorithm was applied to time series of Landsat (1997-2004) and MODIS (2000-2005) data covering one Landsat scene (path/row 226/68) in southern Amazonia and the results were compared to field and image-derived burn scars and independent data on selective logging and deforestation. Landsat resolution was essential for high-confidence detection of small burn scars (<50 ha). However, small burn scars contributed only 12% of all fire-damaged forest area during 1997-2002. MODIS data were suitable for mapping medium (50-500 ha) and large (>500 ha) burn scars which accounted for the majority of all fire-damaged forest in this study. Thus, moderate resolution satellite data may be suitable to provide estimates of fire-damaged Amazon forest at a regional scale. Similar overlap of Landsat and MODIS results with independent data on selective logging and deforestation was unexpected, given that high and moderate resolution satellite data typically generate different types of commission errors in studies of land cover change. Further resolution of the individual contributions from

fire, logging, and deforestation to annual forest damages in Amazonia may require an integrated time-series approach to classify multiple sources of canopy damage in an internally-consistent manner. In the study region, Landsat-based understory fire damages in 1999 (1508 km^2) were an order of magnitude higher than during the 1997-1998 El Niño (124 km^2 and 39 km^2, respectively), suggesting a different link between climate and understory fires compared to other Amazon regions. The results in this study illustrate the potential to address critical questions concerning climate and fire risk in Amazon forests when the BDR algorithm is applied over larger areas.

3.2 Introduction

Fire is an important cause of tropical forest degradation with myriad impacts on forest structure, biodiversity, and nutrient cycling (Goldammer, 1990; Cochrane, 2003). In Amazonia, forest fires occur when human ignitions for deforestation or land management escape their intended boundaries and burn into neighboring forest areas (e.g., Uhl & Buschbacher, 1985; Cochrane *et al.*, 1999). Damages from understory fires in tropical forests can be severe, reducing species richness by 30% and above-ground live biomass by up to 50% (Cochrane & Schulze, 1999). Even moderate-intensity understory fires can result in high canopy mortality, as few Amazon forest species have fire-adapted traits (Uhl & Kauffman, 1990). Widespread forest fire activity in Amazonia occurred during drought conditions associated with the El Niño Southern Oscillation (ENSO) in 1997-1998 (Barbosa & Fearnside, 1999; Elvidge *et al.*, 2001; Phulpin *et al.*, 2002; Alencar *et al.*, 2006), yet the interannual

variation in burned forest extent remains uncertain due to difficulties in separating fires from other forest damages using satellite data.

Fire, selective logging, and deforestation are related and often sequential processes in dynamic Amazon frontier landscapes (Uhl & Buschbacher, 1985; Nepstad *et al.*, 1999b; Alencar *et al.*, 2004; Souza Jr. *et al.*, 2005a; Asner *et al.*, 2006). Thus, isolating the unique contribution to forest degradation from fire requires reconciling the spatial and spectral similarities among disturbance types in satellite imagery. Previous methods to map understory forest fires in Amazonia have combined field data with high-resolution imagery from a single date to identify canopy damage from fire in near-real time (Elvidge *et al.*, 2001; Phulpin *et al.*, 2002; Brown *et al.*, 2006) or during the subsequent dry season (Pereira & Setzer, 1993; Cochrane & Souza, 1998; Alencar *et al.*, 2004; Souza Jr. *et al.*, 2005a). However, single-date methods are ill-equipped to separate fire-related canopy damage from conventional logging and deforestation that may be spectrally similar in any given year (e.g., Cochrane *et al.*, 1999; Souza Jr. *et al.*, 2005b). Changes in forest structure remain visible for several years following fire exposure (Cochrane & Souza, 1998; Souza Jr. *et al.*, 2005b), whereas canopy closure removes evidence of most logging within one year (Asner *et al.*, 2004; Souza Jr. *et al.*, 2005b) and deforestation for pasture or cropland remains cleared following forest conversion (Morton *et al.*, 2006), introducing the possibility that a time-series method with images over three or more years may aid the separation of disturbance types in Amazonia.

Time series of satellite imagery have been used to map burned forest at a range of spatial and temporal scales (e.g., Lopez Garcia & Caselles, 1991; Kasischke

& French, 1995; Viedma *et al.*, 1997; Barbosa *et al.*, 1999; Roy *et al.*, 2002; Giglio *et al.*, submitted). In most biomes, multiple images within a single season can accurately track the timing and extent of vegetation fires, but these approaches have lower performance in tropical forest regions due to persistent cloud cover and subtle changes in surface reflectance associated with sub-canopy burning (Eva & Lambin, 1998; Roy *et al.*, 2008; Giglio *et al.*, submitted). Evidence of forest disturbance and recovery in time series of annual or biannual Landsat imagery has been used to identify forest fires in northern Spain (Viedma *et al.*, 1997) and logging activity in North America (Kennedy *et al.*, 2007). Souza *et al.* (2005b) documented a similar trajectory of loss and recovery of green vegetation fraction over four years following fire in an Amazon forest. This study builds on these efforts to design a multi-year time-series approach to differentiate canopy damage related to understory fires from other forest damages.

This chapter describes the development of an automated approach, the Burn Damage and Recovery algorithm (BDR), to map the annual extent of canopy damage from understory fires in Amazonia based on the unique trajectory of disturbance and recovery for fire-damaged forests in time series of dry-season imagery. The BDR algorithm was applied to time series of Landsat and MODIS data to compare automated detection of forest fire damages across a range of spatial scales. Landsat data (30 m) are an important intermediary between field information and MODIS data because higher-resolution data permit detection of small forest disturbances. Advantages of 250 m MODIS data for time series processing and burn detection include reduced data volumes, consistent data quality (e.g., atmospheric correction,

georeferencing, cloud cover), and more homogenous depiction of canopy damage that facilitate automated detection of fire-damaged forests in regional-scale studies. The goals of this study were three-fold: 1) to evaluate the accuracy of the BDR approach for mapping fire-damaged forest with field validation data and independent, satellite-based measures of selective logging and deforestation, 2) to determine what size burned scars are appropriate for detection with moderate and high-resolution data, and 3) to quantify the interannual variability in fire-damaged forest area in ENSO and non-ENSO years during 1997-2002.

3.3 Methods

3.3.1 Study Area

This study mapped the annual extent of canopy damage from fire for the area covered by one Landsat scene (path/row 226/68) in central Mato Grosso state, Brazil (Figure 3-1). In the past decade, the region experienced high rates of deforestation for cattle ranching and soybean cultivation (Morton *et al.*, 2005; Morton *et al.*, 2006) and forest degradation from selective logging (Asner *et al.*, 2005; Matricardi *et al.*, 2005; Souza Jr. *et al.*, 2005b), but the unique contribution from fire to forest degradation has not been documented previously. The 29,275 km^2 study area was 77% forested in 1997 (>70% shade-normalized green vegetation fraction, following Souza *et al.*, 2005a) and lies predominantly within the Xingu River basin near the southern extent of Amazon forests. Prior to analysis, topographic data were used to exclude 1,450 km^2 of water and seasonally-inundated vegetation for three main tributaries of the Xingu River (Rio Manissuiá-Miçu, Rio Arraias, and Rio Ferro) in

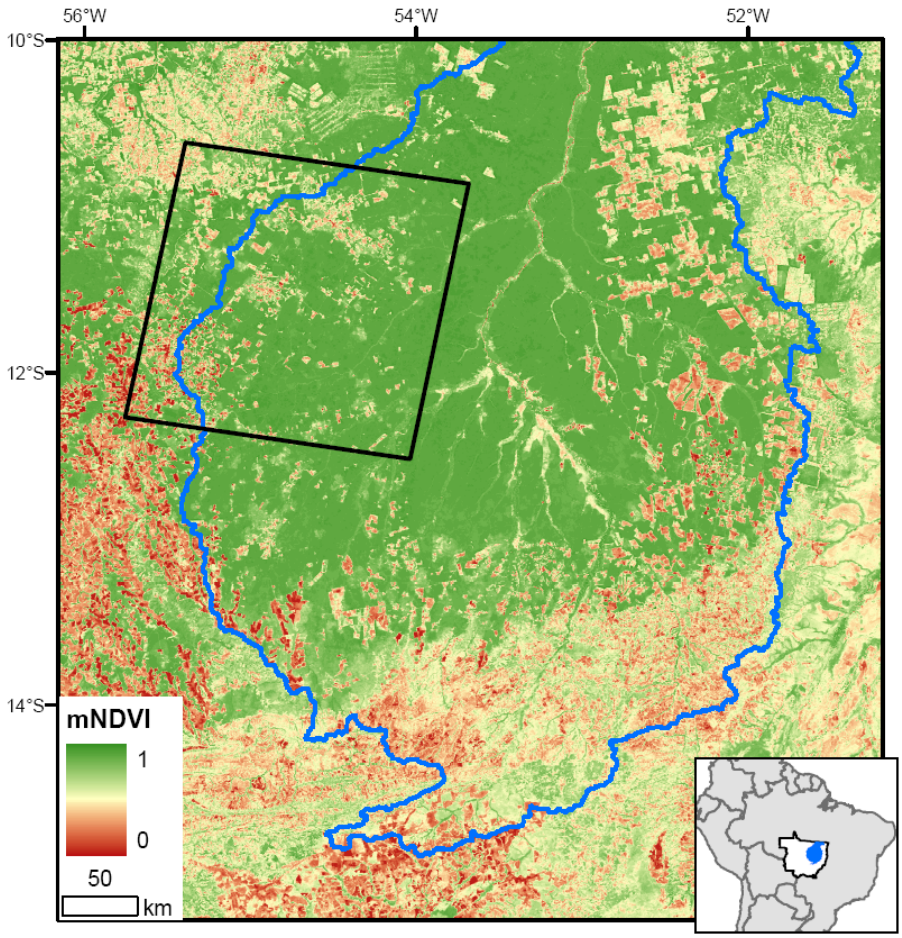

Figure 3-1: MODIS mean dry-season NDVI (mNDVI) in 2000 for the upper Xingu River watershed (blue) and Landsat study area (black) in the Brazilian state of Mato Grosso (inset, white). Forested areas are shown in green, grasslands and Cerrado in shades of yellow, and bare soils typical of cropland in dry-season months appear red.

order to avoid spurious errors associated with interannual changes in river levels or unreliable vegetation index values over water (SEPLAN-MT, 2004).

3.3.2 Satellite-Based Measures of Fire Effects in Amazon Forests

Canopy damage from understory fires in Amazon forests is highly variable. Field studies suggest that understory fires may kill 6-44% of trees >10 cm diameter at breast height, and canopy mortality is typically higher in logged forest than in un-

logged areas (Holdsworth & Uhl, 1997; Barbosa & Fearnside, 1999; Pinard *et al.*, 1999; Barlow *et al.*, 2003; Haugaasen *et al.*, 2003; Ivanauskas *et al.*, 2003; Balch *et al.*, 2008). Canopy mortality from understory fire also exhibits fine-scale spatial heterogeneity. Edaphic conditions and differential mortality among tree species may partially explain these patterns (Ivanauskas *et al.*, 2003), although the distribution of leaf litter and fine fuels may also be important for patterns of canopy mortality in more seasonal Amazon forests (Balch *et al.*, 2008). In the months following fire, the patchy distribution of high and low canopy damage areas from understory fires can be detected with high-resolution optical satellite data (e.g., Cochrane & Souza, 1998; Souza Jr. & Roberts, 2005).

This study derived two parameters of canopy damage from fire using high and moderate resolution satellite data. Because the BDR algorithm uses imagery from the early dry season to detect evidence of burning from the previous year, this study mapped post-fire effects on canopy trees and not burned area, *per se* (Lentile *et al.*, 2006). Therefore, the total fire-damaged forest area was calculated as the sum of all pixels within the study area with canopy damage from fire. Individual burn scars of different sizes were delineated from the map of fire-damaged forest area based on contiguous patches of canopy damage. Individual burn scars represent perimeters of contiguous canopy damage from fire at high and moderate resolution. Given the fine-scale spatial heterogeneity in canopy mortality from fire observed in field and satellite-based studies, burn scars derived from both high and moderate resolution satellite data may include some fraction of unburned forest at the sub-pixel level.

This study did not attempt to further classify canopy damage within the perimeter of individual burn scars into classes of burn severity (Lentile *et al.*, 2006).

3.3.3 Data

This study used a variety of data sources to build and test the BDR algorithm for mapping the extent of canopy damage from fire. The pre-processing steps to generate dry-season time series of Landsat and MODIS data and describe the satellite and field data used to calibrate the BDR algorithm are described below. Section 3.3.4 provides a detailed description of the BDR algorithm. Finally, Section 3.3.5 presents the approach for validation of the satellite-based maps of canopy damage from fire using field observations of burned forest and independent data products on selective logging and deforestation.

3.3.3.1 Landsat TM 1997-2004

This study used a recently-published Landsat TM/ETM+ dataset for the Mato Grosso study area to characterize patterns of disturbance and recovery from fire at high resolution (30 m) (Souza Jr. *et al.*, 2005b). Reflectance values in annual dry-season images from June-August of each year were normalized to one atmospherically-corrected scene, and a linear spectral mixture model with common endmembers for green vegetation (GV), non-photosynthetic vegetation (NPV), shade, and soil was used to derive annual fraction images and normalized difference fraction index (NDFI) data layers (Souza Jr. *et al.*, 2005a; Souza Jr. *et al.*, 2005b). Annual shade-normalized green vegetation fraction (GVs) data layers from 1997-2004 were analyzed in this study following the calculation presented by Souza *et al.*, (2005a):

$$GVs = \frac{GV}{(100 - Shade)} \quad (3\text{-}1)$$

Souza *et al.* (2005a) showed that the GV fraction was best for separating logged and burned forests, while the composite NDFI was best for separating logged and intact forest classes.

3.3.3.2 MODIS 250 m Dry-season Mean NDVI 2000-2005

An annual time series of MODIS dry-season mean normalized difference vegetation index (mNDVI) was constructed to identify evidence of forest disturbance and recovery from fire at moderate resolution (250 m). mNDVI data layers were produced by averaging dry-season NDVI values from the Collection 4 MOD13 Q1 Vegetation Indices (Huete *et al.*, 2002). Annual mNDVI data values for each 250 m pixel were derived from seven 16-day composite periods (day 129-225) in order to 1) limit interference from clouds or biomass burning aerosols typical of wet-season and late dry-season months, respectively, 2) eliminate artifacts from new forest burning that occurs during the late dry season, and 3) maintain consistent solar illumination conditions relative to the June solstice to minimize the impacts of seasonal changes in solar illumination on canopy reflectance. Remaining cloudy or other low-quality data values identified in the Quality Assurance data layer were replaced using a local spline function with high-quality data values in each pixel's time series prior to averaging for each annual mNDVI data layer for 2000-2005 (Morton *et al.*, 2006). Finally, in order to evaluate evidence of fire damage prior to the MODIS era, all regions were assigned a forested mNDVI value in 1999 (mNDVI = 0.85). Landsat-based maps of fire-damaged forest from 1998 and 1999 were used to quantify the

Table 3-1: Data sources for calibration and validation of fire-damaged forest area derived from the BDR algorithm.

	Calibration			Validation		
Class	**Source**	**Years***	**Area (km^2)**	**Source**	**Years***	**Area (km^2)**
Forest	Field Obs.	2005		NA		
Selective Logging	Souza *et al.* 2005*a*	2002	102.8	Asner *et al*., 2005	1999-2001	5932.3
Logged & Burned Forest**	Souza *et al.* 2005*a*	2002	105.2	Field Obs.; Image-derived; Inter-comparison	1999-2002; 1999; 1999-2002	144.7; 1767.9; ***
Deforestation	INPE, 2007; Morton *et al.,* 2006	2002	Pasture: 89.6; Cropland: 91.6	INPE, 2007; Morton *et al.,* 2006	2000-2002	1332.6

* Deforestation and selective logging between annual images are assigned to the end image date by INPE (2007) and Asner *et al.* (2005), respectively. Calibration and validation comparisons used forest damages identified in the same year; for consistency this study reports all comparisons according to the year of forest burning from the BDR approach (e.g., Year 1999 = 1999 fire damages and 2000 logging).
** Souza *et al.* (2005a) identified forest areas that were logged and subsequently burned. Field and image-derived forest burn scars used for validation were not necessarily logged prior to burning.
***Inter-comparison of annual high confidence fire-damaged forest area, total: Landsat (1879.8 km^2), MODIS (3040.1 km^2)

fraction of historic burning from these years that was visible in 2000 MODIS imagery.

3.3.3.3 Calibration Data

Algorithm calibration data for logged, burned, deforested, and intact forest areas were derived from Landsat data products and field observations (Table 3-1). Calibration data were used to characterize the trajectory of GVs and mNDVI over time for each forest disturbance class and the spatial attributes (size, shape) of selective logging and fire-damaged forest areas derived at high and moderate resolution to assign individual burn scars to low or high-confidence classes. Forest damages between 2002 and 2003 were selected for algorithm calibration based on overlap with the MODIS era. Logged forest and logged forests that subsequently

burned were identified using NDFI results from Souza *et al.* (2005a) and were visually inspected to eliminate areas that were later deforested using data from the PRODES (Monitoramento da Floresta Amazônica Brasileira por Satélite) annual Landsat-based deforestation assessments (INPE, 2007). Field observations of intact forest in 2005 were used to identify forest areas that were not logged, burned, or cleared during the combined Landsat and MODIS time series (1997-2005). Finally, large deforestation events (>25 ha) with post-clearing land use of either pasture or cropland were selected to compare time series trajectories among major classes of forest cover change within the study area (Morton *et al.*, 2006; INPE, 2007). Calibration data totaled approximately 100 km^2 for each class (Table 3-1).

3.3.4 Burn Damage and Recovery (BDR) Algorithm

The BDR algorithm is a time-series approach to distinguish fire-related canopy damage from selective logging and deforestation. The idealized BDR time series trajectory for fire-damaged forest has three components (Figure 3-2, Figure 3-3): 1) forested conditions in the year prior to burning, 2) intermediate change in post-burn vegetation greenness relative to either logging or deforestation (0.75 years post-fire), and 3) recovery of mNDVI or GVs values during subsequent years (1.75 and 2.75 years post-fire). Based on calibration data, minor canopy damages from logging and complete canopy removal during deforestation for agricultural use have different MODIS mNDVI and Landsat GVs trajectories over time compared to burned forest. Similar vegetation greenness values among forest disturbance classes in individual years highlights the value of a time series approach for isolating canopy damages from fire in Amazonia (Figure 3-2).

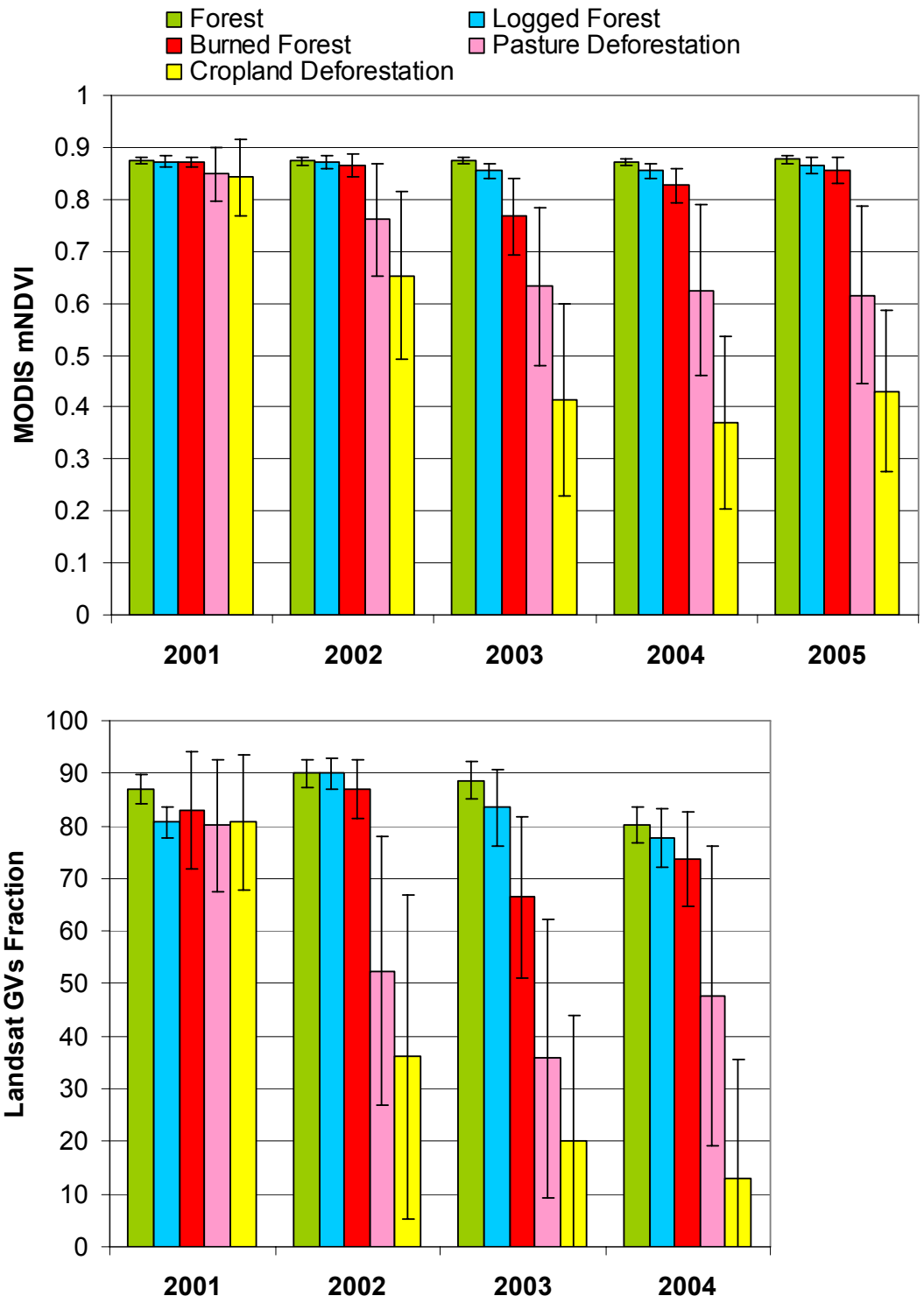

Figure 3-2: Time series of annual mean ± 1 S.D. MODIS mean dry-season NDVI (mNDVI, top) and Landsat shade-normalized green vegetation fraction (GVs, bottom) for calibration data on intact, logged, and burned forest and deforestation for pasture and cropland during 2002.

The automated BDR algorithm also uses spatial attributes to separate fire-damaged forest from logged forest and eliminate possible edge effects along class boundaries common at MODIS resolution. Consistent linear and point patterns from roads (skid trails) and log decks (patios) facilitate automated detection of selective logging in Amazonia using high resolution satellite data (Asner *et al.*, 2005; Matricardi *et al.*, 2005; Souza Jr. *et al.*, 2005a). To minimize confusion between canopy damage from fire and selective logging infrastructure, the BDR algorithm only identifies burn scars larger than individual log decks (0.4 ha) (Souza Jr. *et al.*, 2005a), and burn scars with linear or dendritic patterns are considered low confidence detections to reduce potential overlap with skid trails and logging roads.

3.3.4.1 BDR Processing

The BDR algorithm has three main processing steps to identify canopy damage from fire (Figure 3-3). The first step is to identify core areas of canopy damage from fire for each year based on the BDR time series trajectory. Clusters of pixels that satisfy all criteria for pre-burn, burn, and recovery elements of the BDR trajectory are considered core areas. Next, suitably-sized core areas are grown into larger regions by running a neighborhood search for adjacent pixels that meet BDR trajectory criteria for growth regions. Compared to core areas of canopy damage from fire, pixels that fit the growth region BDR trajectory have a wider range of pre and post-burn values and may have slower recovery of vegetation greenness over time. A similar, two-phase classification approach was used previously to map burned forest in Alaska with AVHRR data (Kasischke & French, 1995). The third step is to calculate spatial statistics for each burn scar: size, perimeter-area ratio, average greenness in the year of burn detection, and interior fraction. Interior fraction

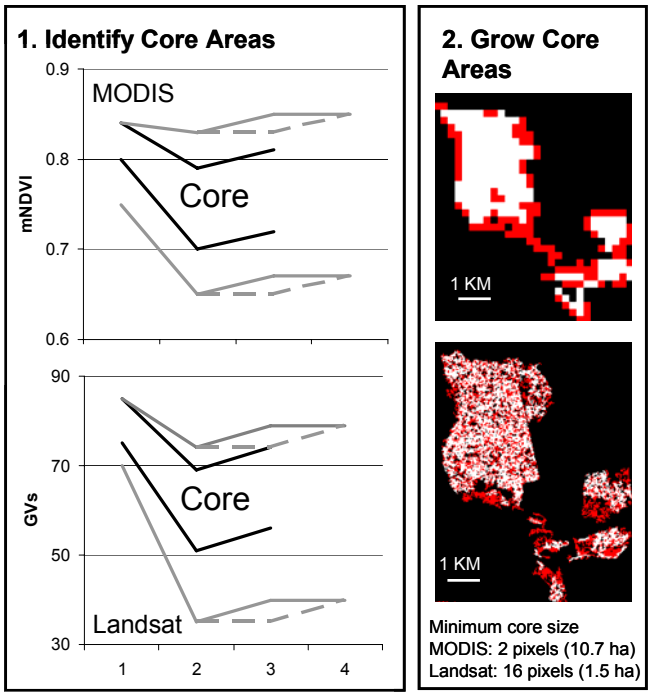

3. Calculate Spatial and Spectral Metrics to Classify Burn Scar Confidence

	Landsat		MODIS	
Metric	**Remove**	**HC***	**Remove**	**HC***
Size	-	>1.5 ha	<15 ha	>50 ha
Perimeter:Area	>0.05	<0.04	>0.012	-
Mean Greenness	-	<62	>0.81	>0.71 and <0.8
Interior Fraction	-	-	<0.5	>0.6

*** High confidence (HC) subset of forest burn scars**

BDR Trajectory Parameters

	1. Pre-Burn	2. Burn		3. Recovery	4. 2 yr Recovery
MODIS	Minimum	Drop	Range	Minimum	Minimum
Core	0.8	-0.05	0.70-0.80	+ 0.02	
Growth	0.75	-0.01	0.65-0.83	+0.01	+ 0.01
Landsat					
Core	75	-11	50-70	+ 6	
Growth	70	-6	35-75	+ 5	+ 1

Figure 3-3: The BDR algorithm has three main processing steps: 1) MODIS (top) and Landsat (bottom) time series trajectories are used to identify candidate core areas of canopy damage from fire (black) and growth regions (gray). Dashed lines show the range of values for 2-year recovery in growth regions. See table (bottom) for pre-burn, drop, burn, and recovery parameter ranges for each BDR trajectory. 2) Large core areas (white) are joined to adjacent growth areas (red) to generate forest burn scars. 3) Individual burn scars are classified as low and high confidence based on spatial and spectral metrics. Small or linear burn scars are removed from consideration; high-confidence burn detections are large and non-linear, with burn values intermediate between damages from deforestation and logging.

is the percentage of an individual burn scar that is not edge, calculated based on the reduction in burn scar size after applying a majority filter to the initial results using a 3 x 3 pixel window. These spatial and spectral statistics form the basis of a burn scar confidence classification in which large burn scars with low perimeter-area ratio, high interior fraction, and low average greenness are considered most confident. Characteristics of low and high-confidence burn scars were derived from calibration data. Low confidence burn scars at Landsat resolution have high perimeter-area ratio typical of the dendritic pattern of selective logging operations; MODIS low-confidence detections are small or linear edge effects common along class boundaries at moderate resolution (Figure 3-4). The final outputs of the automated BDR approach are annual maps of canopy damage from fire in which each burn scar is classified as high or low confidence according to spatial and spectral metrics.

In summary, the BDR algorithm applied to time series of Landsat GVs data searches for core areas of contiguous canopy damage from fire that are at least three times larger than previously documented for selective logging, uses recovery in years 1-2 after damage to differentiate forest burning from deforestation, and corrects the final burn scars to eliminate potential logging artifacts based on the shape (perimeter-area ratio) and degree of canopy damage within each burn scar (mean GVs). The minimum burn scar size in Landsat-based results is 1.5 ha, equivalent to the smallest core area considered by the algorithm.

The BDR algorithm applied to time series of MODIS mNDVI also begins with large core areas to search for canopy damage from fire (≥10.7 ha), and initial results are corrected to eliminate potential edge effects with cleared areas or small

burn scars that cannot be well-characterized by moderate resolution data (<3 250 m pixels, (Morton *et al.*, 2005). MODIS results are then classified according to confidence levels by size, shape, and mean mNDVI in the year of burn detection. High confidence burn scars are large (>50 ha), non-linear (interior fraction >0.6), with intermediate mNDVI values between potential logged areas (>0.8) and deforested regions (<0.71).

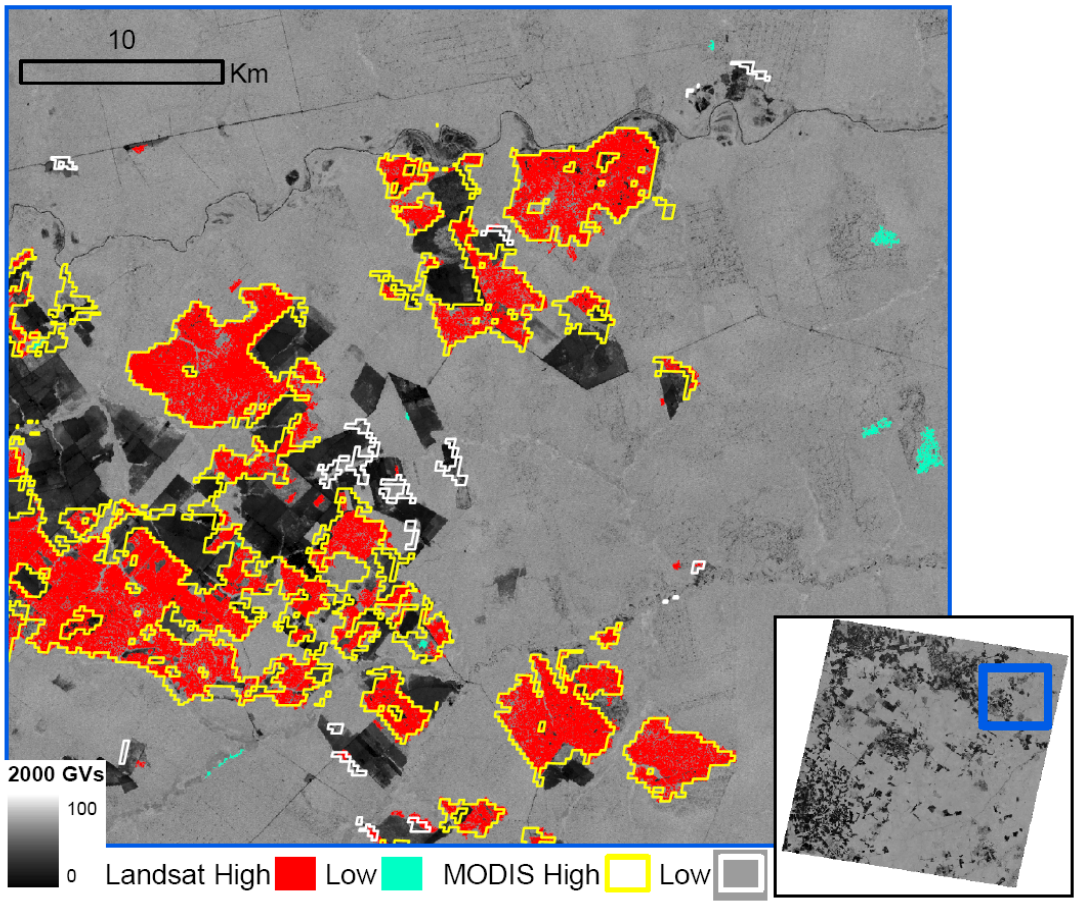

Figure 3-4: Landsat and MODIS 1999 forest burn scar results classified according to high and low confidence based on spatial and spectral metrics for a subset of the study area (inset). The background image shows the shade-normalized green vegetation fraction (GVs) for 2000.

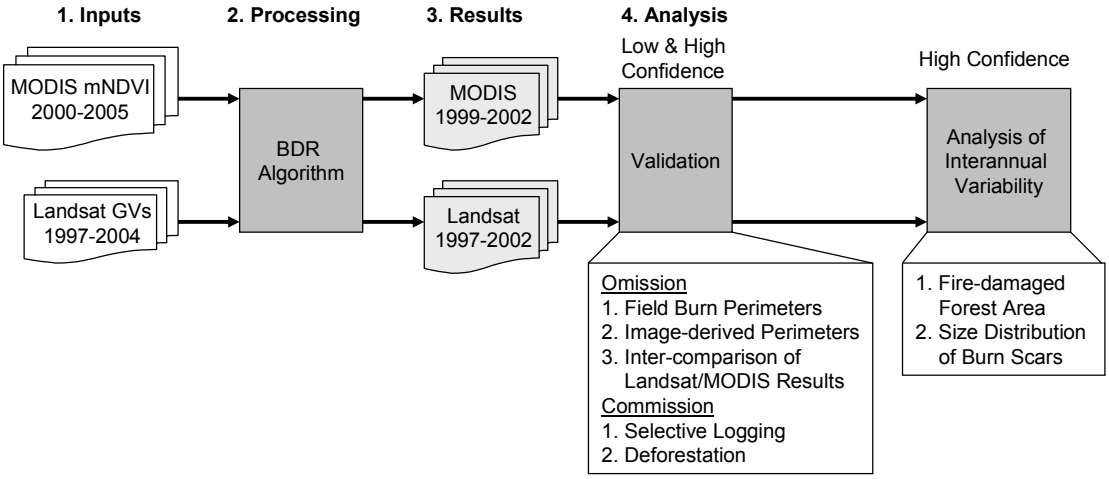

Figure 3-5: Flow diagram of data processing and analysis for annual maps of fire-damaged forest area from the BDR algorithm applied to time series of MODIS and Landsat data. We compared low and high-confidence burn scars to validation data on burned forest, selective logging, and deforestation, but only high-confidence burn scars were used to examine interannual variability in burn scar size and total fire-damaged forest area.

3.3.5 Validation

The accuracies of burn scars from the BDR algorithm were evaluated using four independent validation datasets and an inter-comparison of high-confidence Landsat and MODIS results (Table 3-1). Figure 3-5 summarizes the overall approach for validation and analysis of results from the BDR algorithm. Omission and commission were calculated on a per-pixel and per-polygon basis. Per-pixel comparisons quantified the total overlap between validation data and fire-damaged forest. Per-polygon analyses quantified the overlap between BDR results and validation data for individual validation polygons (perimeters) of different sizes. By stratifying omission and commission errors by polygon size, this study quantified the advantages and disadvantages of the BDR algorithm applied to high and moderate resolution time series. The accuracies of both low and high-confidence detections

were evaluated in order to 1) test whether spatial and spectral metrics derived from calibration data reduced the overlap with independent estimates of logging and deforestation, and 2) evaluate the potential for MODIS to identify small burn scars, since low-confidence results from MODIS include all burn scars <50 ha. Each validation dataset is briefly described below.

Field observations of fire-damaged forest were collected during June-September of 2001 and 2003. In each year, field transects along existing roads targeted fire scars visible in coincident high-resolution imagery. The location and perimeter of each forest burn scar was recorded using a hand-held Global Positioning System (GPS) unit. The date and ignition source for each fire was determined using a combination of satellite data and information from landowners. Immediately following field campaigns, field-mapped burn perimeters were identified in coincident high-resolution data (ASTER or Landsat TM/ETM+) to complete portions of the burn perimeter that were not accessible during fieldwork. The total fire-damaged forest area mapped during fieldwork was 145 km^2 in 18 forest burn scars that ranged in size from 27-5,086 ha (Table 3-2).

An additional validation dataset of burned forest perimeters from 1999 was generated through visual inspection of Landsat imagery from 1999-2001. Spatial and spectral characteristics of field-mapped forest burn scars were used to identify similar features within the study area. A total of 145 forest burn scars from 1999 (1767.9 km^2), ranging in size from 13-14,462 ha, were digitized within the study area to test omission of canopy damage from fire in the BDR results (Figure 3-6). For per-polygon analyses, this study used linear regression to determine whether the area of

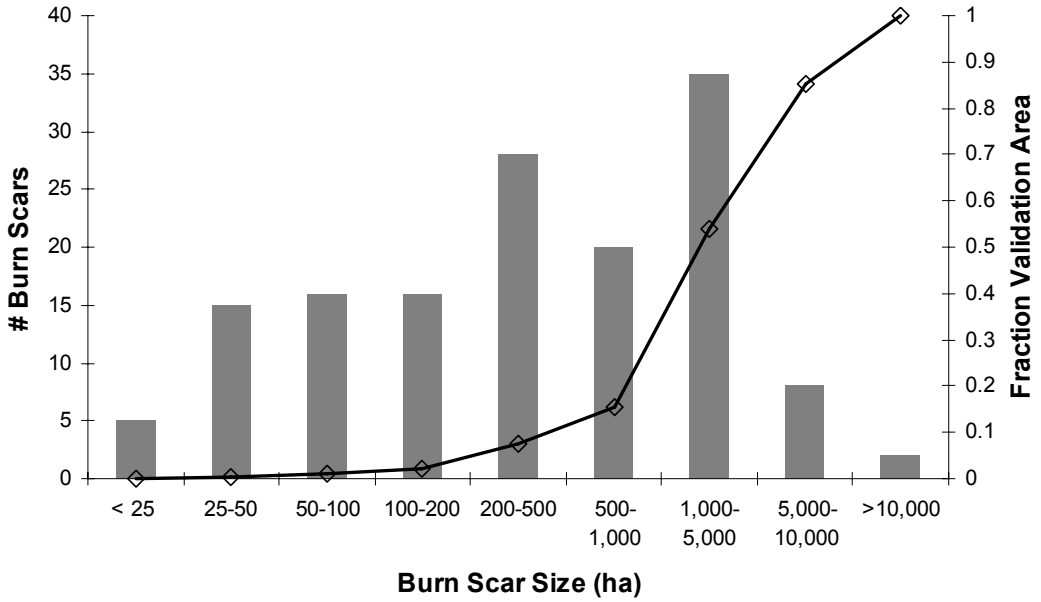

Figure 3-6: Number of burn scars (bars) and cumulative contribution to total validation fire-damaged forest area (◊) by size class for 145 validation burn scars from 1999 identified in Landsat imagery.

fire-damaged forest identified in Landsat and MODIS results within individual validation burn scars was similar for burn scars of different sizes. We ran separate regression analyses for large (>500 ha) and small (<500 ha) burn scars.

Agreement between fire-damaged forest results from Landsat and MODIS time series was used as an additional validation test since canopy damages are captured differently in high and moderate resolution data. Subtle damages from selective logging are less likely to be detected with moderate resolution data than with data from Landsat-like sensors (Asner *et al.*, 2004), while mixed pixel effects at class boundaries typical at MODIS resolution are less likely to occur with higher resolution data (Morton *et al.*, 2005). Therefore, detection by both MODIS and

Landsat BDR results increases the confidence of an individual burn scar. To compare the burn scar results from moderate and high resolution data, linear regression was used to determine whether the area identified in Landsat results (y) was similar to the area identified in MODIS results (x). Separate regression analyses were run for large (>500 ha) and small (<500 ha) burn scars. The fraction of the total fire-damaged forest in high-confidence burn scars that was detected at both Landsat and MODIS resolutions was also calculated.

Independent datasets on selective logging (Asner *et al.*, 2005) and deforestation (INPE, 2007) were used to characterize potential commission errors in the Landsat and MODIS results of fire-damaged forest. These comparisons did not provide a rigorous test of commission errors in results from the BDR algorithm because neither product was specifically designed to exclude burned forest. Instead, evaluation of overlap between canopy damage from fire, selective logging, and deforestation was useful to characterize the nature and extent of classification confusion among disturbance types in southern Amazonia. As shown in Table 3-1, overlap between deforestation events >25 ha and fire-damaged forests was further defined according to post-clearing land use based on results from Morton *et al.* (2006). Finally, accounting methods differ between the BDR algorithm and datasets of selective logging and deforestation. For fire-damaged forest, early dry-season images capture evidence of forest burning during the previous dry season. Selective logging and deforestation damages are assigned to the year in which they were mapped, representing the sum of all damages between annual images. For validation, this study compared fire-damaged forests, selective logging, and deforestation

identified in the same year (e.g., burn damages from 1999 were compared with selective logging from 2000, and burn damages from 2002 were compared with 2003 deforestation). For consistency, this study described validation comparisons using the year of burn damages.

3.4 Results

3.4.1 Validation: Omission

Field and image-derived forest burn scars were used to quantify omission in results from the automated BDR algorithm applied to Landsat and MODIS time series. Overall, the BDR algorithm accurately identified forest burn scars mapped during fieldwork (Table 3-2). Landsat results identified some canopy damage from fire in all 18 field-mapped burn scars, and MODIS results detected fire damages in all but one field-mapped burn scar in 2000 (103 ha). MODIS results captured a higher percentage of the fire-damaged forest area mapped during fieldwork than Landsat due to heterogeneity of canopy damage within the burn scar perimeters at high resolution (82% and 74%, respectively). The high-confidence subset of all burn scars reduced the area of overlap with field validation data by <1% in both Landsat and MODIS results (Table 3-2).

Fire-damaged forest results for 1999 from Landsat and MODIS also corresponded well with image-derived burn scars (Table 3-2). Landsat results detected 61% of the total fire-damaged forest area, with some canopy damage from fire detected in 143/145 burn scars. The fraction of digitized burn scars detected by Landsat was consistent for large (>500 ha, $y = 0.61x$, $R^2 = 0.96$, $n = 65$, $p<0.001$) and

Table 3-2: Detection of field and image-derived validation forest burn scars with results from the BDR algorithm applied to time series of Landsat and MODIS data.

	Validation			Landsat		MODIS	
	Obs.	Burn scars (ha)	Area (km^2)	km^2	%	km^2	%
Field							
1999	9	34, 205, 237, 496, 505, 820, 1148, 1479, 5086	96.3	78.9	82	82.8	86
2000*	2	49, 103	1.5	0.8	53	0.3	20
2001	1	979	9.7	1.1	12	2.5	25
2002	6	27, 272, 300, 632, 873, 1672	37.2	26.4	71	33.4	90
Total	18		144.7	107.2	74	119.0	82
Image							
1999**	145	(see Fig. 6)	1767.9	1071.1	61	1344.5	76

*Only year in which results were different for high-confidence burn scars than total fire-damaged forest area (Landsat: 0.6 km^2, MODIS = 0).

**Overlap of high confidence burn scars with image-derived validation data differed by <1% from total results (Landsat:1063 km^2; MODIS: 1331 km^2).

small validation burn scars (<500ha, $y = 0.68x$, $R^2 = 0.97$, $n = 81$, $p<0.001$). MODIS results detected a higher percentage of the total fire-damaged forest area (76%) but fewer individual burn scars than Landsat (136/145). Four of the 9 digitized forest burn scars without a corresponding MODIS detection were <50 ha. Automated results from MODIS underestimated the area in individual burn scars by approximately 25% for digitized burn scars of all sizes (>500 ha, $y = 0.75x$, $R^2 = 0.97$, $n = 65$, $p<0.001$; <500 ha, $y = 0.74x$, $R^2 = 0.89$, $n = 81$, $p<0.001$). The high-confidence subset of burn scars reduced the overlap with digitized fire-damaged forest area by <1% for both Landsat and MODIS results since large burn scars (>500 ha) accounted for 93% of the total digitized area (Figure 3-6).

3.4.2 Validation: Commission

3.4.2.1 Selective Logging

Maps of annual selective logging damages independently derived from Landsat data (Asner *et al.*, 2005) were used to characterize potential commission errors in results from the BDR algorithm. Overlap between selective logging and canopy damage from fire was high in 1999 but very low in 2000 and 2001 (Table 3-3). Coincident burning and logging classifications in 1999 were predominantly in high-confidence results (Table 3-3). Forest areas classified as logged and burned also overlapped with field-mapped burn scars (52%) and digitized forest burn scars (48%) in that year. In 2000 and 2001, there was little overlap between fire-damaged forest and selective logging, and most coincident detections occurred in the low-confidence burn scars. In all years, forest burning extended beyond areas of coincident logging. For example, burn scars in Landsat and MODIS results from 1999 that were also classified as logging averaged only 49% and 33% logged, respectively.

Table 3-3: Overlap between Landsat-based selective logging from Asner *et al.* (2005) and fire-damaged forest for all BDR results (Total) and high-confidence burn scars (HC) from Landsat and MODIS time series. Total high confidence fire-damaged forest area (HC Area) and the percentage of HC Area that overlapped with selective logging are also shown.

	Logged	Landsat	Landsat Overlap			MODIS	MODIS Overlap		
	Area	HC Area	Total	HC		HC Area	Total	HC	
Year*	(km^2)	(km^2)	(km^2)	(km^2)	%	(km^2)	(km^2)	(km^2)	%
1999	2587.6	1508.1	653.8	633.4	42	2526.3	848.2	821.0	33
2000	1466.1	55.4	10.7	5.2	9	65.5	12.8	4.4	7
2001	1878.6	34.9	2.2	2.0	6	45.5	11.5	2.8	6

* Asner et al. (2005) assigned logging between annual Landsat images to the end image date, whereas burn damages from the BDR algorithm are attributed to previous year. As shown, year 1999 corresponds to logging in 2000, etc.

Table 3-4: Overlap between fire-damaged forest (2000-2002) and PRODES deforestation (2001-2003) (INPE, 2007) for all BDR results (Total) and high-confidence burn scars (HC). Total overlap with PRODES deforestation is further divided by size and post-clearing land use (Morton *et al*., 2006). Total high confidence fire-damaged forest area (HC Area) and the percentage of HC Area that overlapped with deforestation are also shown.

		Deforested Area (km^2)**	Landsat HC Area (km^2)	Landsat Overlap Total (km^2)	Landsat Overlap HC (km^2)		MODIS HC Area (km^2)	MODIS Overlap Total (km^2)	MODIS Overlap HC (km^2)	
Year*						**%**				**%**
2000	**Total**	**287.0**	**55.4**	**13.0**	**12.9**	**23**	**65.5**	**21.5**	**11.9**	**18**
	>25 ha									
	Cropland	78.5		0.0	0.0			0.6	0.1	
	Pasture	165.4		10.0	10.0			15.7	8.4	
	NIP	15.3		2.2	2.1			3.7	3.0	
	<25 ha	27.8		0.8	0.8			1.5	0.5	
2001	**Total**	**398.3**	**34.9**	**19.3**	**19.1**	**55**	**45.5**	**26.3**	**18.7**	**41**
	>25 ha									
	Cropland	113.5		0.0	0.0			0.9	0.0	
	Pasture	225.9		16.1	16.0			18.2	12.5	
	NIP	24.3		2.7	2.6			6.2	5.7	
	<25 ha	34.6		0.5	0.5			1.0	0.5	
2002	**Total**	**649.3**	**281.4**	**119.3**	**115.3**	**41**	**402.7**	**125.6**	**108.3**	**27**
	>25 ha									
	Cropland	235.2		13.5	13.5			4.3	1.9	
	Pasture	275.2		63.7	63.1			61.5	53.4	
	NIP	75.2		35.3	32.1			49.7	44.2	
	<25 ha	63.7		6.9	6.6			10.2	8.8	

*Burn year 2000 corresponds to 2001 deforestation due to differences in annual accounting between BDR and PRODES.

**Landsat-based annual deforestation from PRODES (INPE, 2007). Clearings >25 ha classified according to post-clearing land use (Morton et al., 2006).

3.4.2.2 Deforestation

Landsat-based maps of annual deforestation from the PRODES program (INPE, 2007) were also used to quantify potential commission errors in results from the BDR algorithm. Overlap between fire-damaged forest and PRODES deforestation occurred primarily in high-confidence burn scars (Table 3-4). The area of overlap between fire-damaged forest and deforestation was similar for Landsat and MODIS results in all years (Table 3-4).

Coincident detection of burn damages and deforestation varied according to clearing size and post-clearing land use (Table 3-4). In 2000 and 2001, confusion between deforestation and fire-damaged forest was mostly confined to large (>25 ha) forest clearings for pasture. Burn scars only overlapped with a small fraction of the individual areas cleared for pasture in those years; the average fraction of forest clearings for pasture mapped as canopy damage from fire was 28% in 2000 and 25% in 2001. In 2002, a small number of individual clearings for pasture (37/192) that were mapped as >50% fire-damaged forest accounted for 75% of the area of overlap between deforestation for pasture and fire-damaged forest in that year. Forest burn scars overlapped less frequently with deforestation classified as not in agricultural production (NIP), and did not overlap with cropland deforestation and clearings <25 ha except in 2002 (Table 3-4).

Table 3-5: Fire-damaged forest area detected by the BDR algorithm using Landsat and MODIS time series for all forest burn scars (Total) and high-confidence burn scars (HC). Coincident detections at both high and moderate resolution (overlap) were derived from high-confidence burn scars.

Year	Total Fire-damaged Forest Area (km^2)	HC Fire-damaged Forest Area (km^2)	Overlap (km^2)*
Landsat			
1997	150.3	123.6	
1998	41.6	38.6	
1999	1549.9	1508.1	1435.8
2000	67.5	55.4	28.1
2001	35.9	34.9	17.4
2002	290.5	281.4	185.6
MODIS			
1999	2788.7	2526.3	2317.3
2000	143.4	65.5	52.4
2001	88.9	45.5	40.4
2002	507.8	402.7	359.5

* Forest burn scars with high-confidence detections in Landsat and MODIS results during 1999-2002.

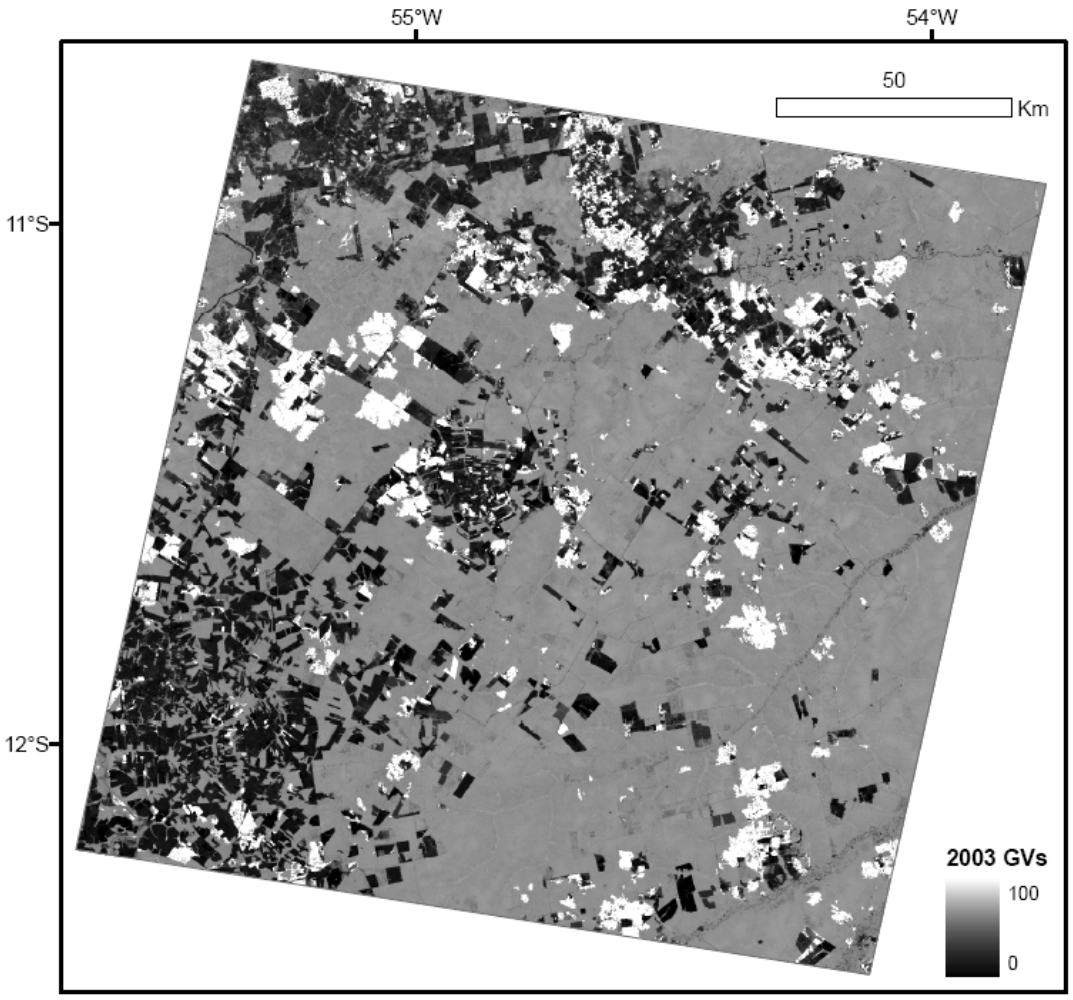

Figure 3-7: Total Landsat high confidence fire-damaged forest area during 1997-2002 (white) impacted 10% of the forested area in 1997. Forested regions appear gray and deforested areas appear black in the background image of the study area (2003 shade-normalized green vegetation fraction, GVs).

3.4.3 Interannual Variation in Fire-Damaged Forest, 1997-2002

The majority of fire-damaged forest mapped with Landsat and MODIS time series was not associated with the 1997-1998 ENSO. Fire-damaged forest area from Landsat in 1999 was 10 and 15 times greater than the amount of canopy damage from fire during 1997 and 1998, respectively (Table 3-5). Similarly, <1% of MODIS fire-

damaged forest area in 1999 was identified as burned forest in 1998 in Landsat results (12 km^2).

Interannual variation in fire-damaged forest area was similar between results from the BDR algorithm applied to Landsat and MODIS time series (Table 3-5). The location of individual burn scars during 1999-2002 was also similar between moderate and high resolution results. MODIS burn scars with corresponding Landsat detections accounted for over 91% of all MODIS high confidence fire-damaged forest area (Table 3-5).

In the southern Amazon study area, the total Landsat high confidence fire-damaged forest area during 1997-2002 was 2136 km^2 (Table 3-5), equivalent to 10% of all forest in the study area in 1997 (Figure 3-7). The total area in high confidence burn scars during 1999-2002 at MODIS resolution was 2832 km^2 (13% of 1997 forested area).

3.4.4 Burn Scar Sizes

The contribution of large and small burn scars to total fire-damaged forest area varied interanually (Figure 3-8). Very large burn scars (>500 ha) were only mapped in years with highest fire damages (1999, 2002). However, these largest burn scars contributed the majority of canopy damage from fire during 1997-2002. Burn scars >500 ha accounted for 56% of the Landsat fire-damaged forest area during 1997-2002 and 78% of the MODIS fire-damaged forest area during 1999-2002.

Small burn scars (<50 ha) in Landsat results were common in all years but contributed only 12% of the total fire-damaged forest area over the study period.

Small burn scars contributed 46% of total fire-damaged forest area in years with lowest canopy damage from fire (1998, 2001).

The estimated size of individual burn scars was larger from MODIS than from Landsat, but the exact relationship between MODIS and Landsat-based area was strongly dependent on burn scar size. For very large burn scars (>500 ha), MODIS-based burn scar size was consistently twice that derived from higher resolution data: 1999 ($y = 0.52x$, $R^2 = 0.92$, $n = 79$, $p<0.001$) and 2002 ($y = 0.49x$, $R^2 = 0.94$, $n = 19$, $p<0.001$). The correlation between MODIS and Landsat-based burn scar size was lower for smaller burn scars (<500 ha), and the slope of the linear fit was more variable (1999: $y = 0.23x$, $R^2 = 0.47$, $n = 200$, $p<0.001$; 2000: $y = 0.40x$, $R^2 = 0.82$, $n = 38$, $p<0.001$; 2001: $y = 0.23x$, $R^2 = 0.56$, $n = 30$, $p<0.001$; and 2002: $y = 0.37x$, $R^2 = 0.68$, $n = 105$, $p<0.001$).

3.5 Discussion

The BDR algorithm is a fully-automated approach to estimate the annual extent of canopy damage from understory fires in Amazon forests. The use of a time series approach enabled accurate identification of fire-damaged forest areas and improved separability of burning from logging and deforestation for cropland and pasture compared to single-date methods. Results from the BDR algorithm applied to time series of Landsat and MODIS data demonstrate the high degree of interannual variability in the extent of fire-damaged forest. Surprisingly, fire-damaged forest in 1999 was an order of magnitude higher than during the 1997-1998 El Niño. Large burn scars (>500 ha) were also detected in 2002, highlighting potential

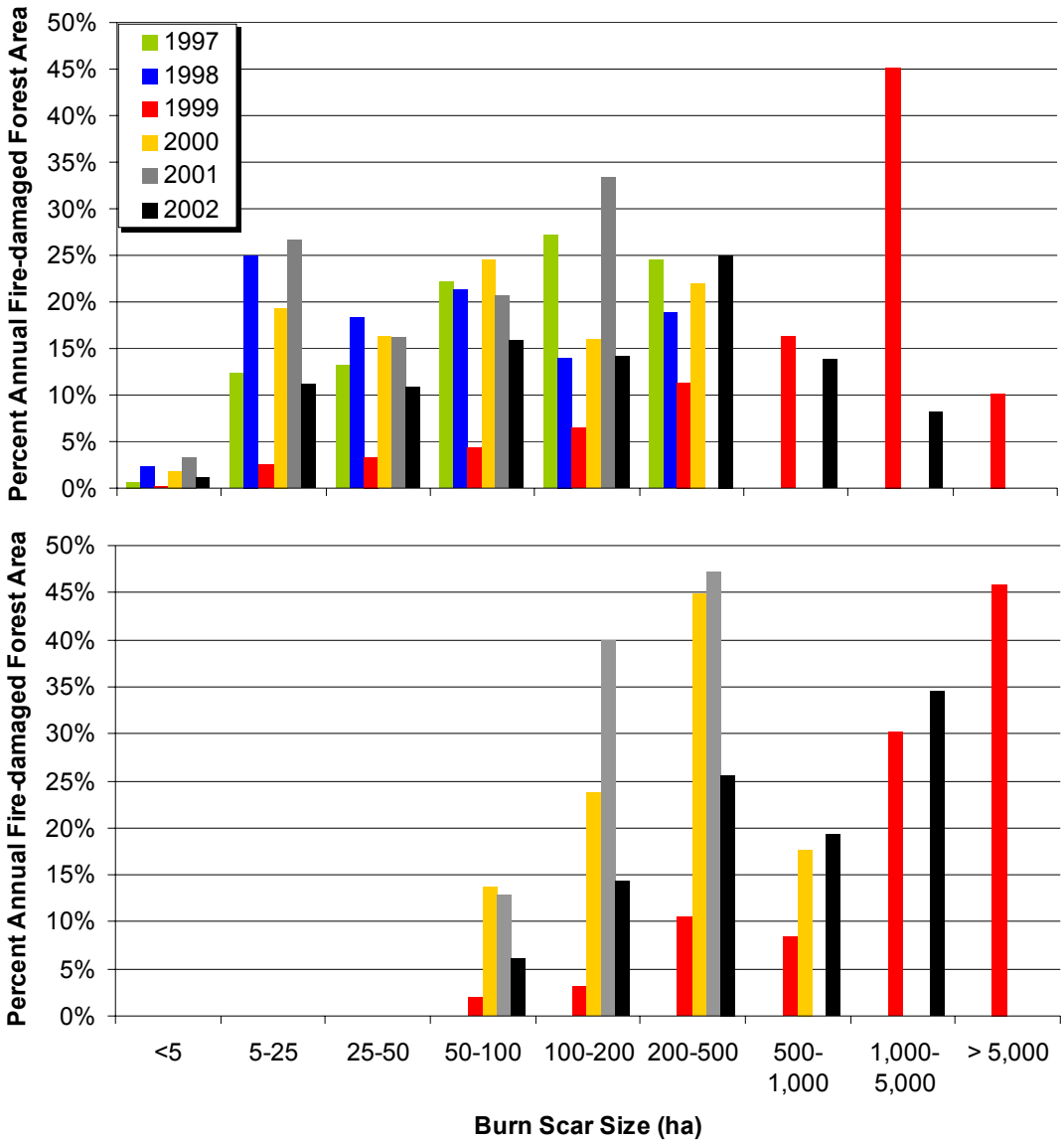

Figure 3-8: Percent contribution from burn scars of different sizes to annual high-confidence fire-damaged forest area for the BDR algorithm applied to time series of Landsat (top) and MODIS (bottom).

differences in the relationship between climate and fire in this study area compared to other Amazon regions (e.g., Barbosa & Fearnside, 1999; Nepstad *et al.*, 2004; Alencar *et al.*, 2006). Our results illustrate the potential to address critical questions

concerning climate and fire risk in Amazon forests when the BDR algorithm is applied over larger areas.

Both Landsat and MODIS time series were suitable for mapping canopy damage from fire using the BDR algorithm. MODIS results captured a higher fraction of the area in field validation burn scars and had very similar commission of selective logging and deforestation compared with Landsat results. Landsat resolution was essential for high-confidence detection of small burn scars (<50 ha), but results from this study demonstrate that moderate resolution data are suitable for identifying burn scars >50 ha which contributed the majority of fire-damaged forest area in every year. Thus, moderate resolution satellite data may be suitable to provide estimates of fire-damaged Amazon forest at a regional scale.

MODIS and Landsat data have complementary characteristics for mapping canopy damage from fire in tropical forests using time series of satellite data. Lower data volumes and a more homogenous disturbance signature in 250 m MODIS data facilitated automated BDR processing; some canopy damage was not detected at Landsat resolution because damaged pixels were not contiguous, interrupting the search portion of the BDR algorithm. Improvements to the BDR algorithm, such as improved characterization of burn scar fragments, or data filtering techniques (e.g., Souza *et al*., 2005a) could improve automated burn scar detection in Landsat or other higher-resolution satellite time series. As shown in Figure 3-2, values of Landsat GVs were less stable over time than mNDVI derived from MODIS for intact forest areas, likely due to interannual variability in the timing of image acquisition and atmospheric conditions. Cloud cover may also limit the degree to which time-series

processing of high resolution data can be conducted in less seasonal tropical forest regions (Asner, 2001). Accurate geolocation (Salomonson & Wolfe, 2004), atmospheric correction (Vermote *et al.*, 2002), and bi-weekly data mosaics may therefore facilitate the use of MODIS data for regional scale studies of fire-damaged tropical forests. Nevertheless, high-resolution satellite data may still be required for studies in regions with only small burn scars and to characterize canopy damage within the burn perimeters identified using the BDR algorithm with moderate resolution data. As demonstrated here, Landsat data are also an essential link between field and satellite-based observations.

The BDR approach successfully isolated fire-damaged forest from areas of selective logging in years with low fire activity (2000-2001, when <0.4% of logging was classified as burning and <9% of burning was also classified as logging). Given previous reports of low sensitivity to fine-scale canopy damages from selective logging in moderate resolution data (e.g., Asner *et al.*, 2004), the high degree of confusion between MODIS-based burn scars and logging in 1999 was unexpected (821 km^2 represented 31% of logging and 33% of canopy damage from fire). Overlap between validation burn scars and selective logging suggests that logging and burning may have occurred in the same year (1999) or that burning re-exposed evidence of selective logging prior to 1999. Clarifying the role of logging for generating both fuels and ignition sources for forest fires in Amazonia during years with extensive forest fire damages is an important subject for future study.

Overlap between deforestation and fire-damaged forest in both Landsat and MODIS results suggests that PRODES may have overestimated the amount of

deforestation in the study area. Because the BDR algorithm identifies areas of fire-damaged forest based on forest recovery over time, it is likely that the areas of overlap between burn scars and deforestation were never fully cleared for agricultural use. Our results further suggest that cropland expansion may be a more important driver of recent deforestation than previously reported because most overlap between burning and PRODES deforestation was associated with clearing for pasture (Morton *et al.*, 2006). Lower overlap between mechanized forest clearing for cropland and fire-damaged forest may be a result of seasonal differences in the timing of fires for deforestation; fires for cropland deforestation occur earlier in the dry season than fires for pasture deforestation when surrounding forests may be less flammable (Morton *et al.*, 2008). However, confusion between forest fires and deforestation cannot be completely resolved by combining independent data products derived from different methods.

Development of an integrated time-series approach to separately account for the contributions from understory fires, selective logging, and deforestation to annual forest damage would satisfy information needs for both policy and science applications. All three types of forest disturbance could be identified in time series of data from Landsat-like sensors by combining methods demonstrated in this study to follow fire damages and deforestation over time with techniques to detect spatial attributes of forestry infrastructure (Asner *et al.*, 2005; Matricardi *et al.*, 2005; Souza Jr. *et al.*, 2005a). Time series of MODIS data could be used to estimate fire-damaged forest and deforestation in an internally-consistent manner, given that MODIS-based results in this study were largely insensitive to subtle canopy damages from selective

logging. Any integrated approach that requires several years of satellite imagery will not replace the need for operational deforestation monitoring (INPE, 2006) or global burn scar mapping (e.g., Roy *et al.*, 2008; Giglio *et al.*, submitted). As presented here, the BDR algorithm can only map canopy damages from fire with high confidence on a two-year delay. However, longer time horizons under discussion for policy and market mechanisms to reduce carbon emissions from deforestation and degradation (REDD) may permit this type of retrospective approach (Gullison *et al.*, 2007), given the substantial differences in carbon losses from understory fires (e.g., Barlow *et al.*, 2003; Alencar *et al.*, 2006; Balch *et al.*, 2008), selective logging (e.g., Asner *et al.*, 2005), and deforestation (Houghton *et al.*, 2000; van der Werf *et al.*, in press-b).

Interannual variation in fire-damaged forest area was high within the study area in southern Amazonia. Fires damaged 10% of all forest in the study area during 1997-2002, and three quarters of all canopy damage from fire occurred during 1999. In contrast to findings in this study, Alencar *et al.* (2006) reported extensive fire damages in 1998 for a neighboring study area in northern Mato Grosso state, Brazil. Localized differences in site conditions, land use, forest structure, disturbance history, or climate that generate spatial heterogeneity in understory forest fire damages merit further study. Once burned, Amazon forests may be more susceptible to future fires based on the influence of canopy damage on forest microclimate and fuels (Cochrane *et al.*, 1999). Using a longer time series, the BDR approach could also be used to characterize the frequency of fires in previously-burned forest to evaluate long-term

changes in the structure of tropical forest ecosystems from frequent fire exposure (Cochrane & Schulze, 1999; Barlow & Peres, 2008).

Very large burn scars were only mapped during years with extensive forest burning, consistent with previous findings of greater penetration of understory fires in periodic high-fire years (Cochrane & Laurence, 2002; Alencar *et al.*, 2004; Alencar *et al.*, 2006). Based on published understory fire spread rates of 0.1 – 0.5 m/min (Cochrane *et al.*, 1999; Balch *et al.*, 2008), the largest fires in 1999 may have burned continuously for approximately two weeks. Whether high fire damages in these years were linked with climate (e.g., Ray *et al.*, 2005) or an increase in fuel availability (Alvarado *et al.*, 2004; Balch *et al.*, 2008), prolonged rainless periods once understory fires begin appear necessary for individual fires to damage large areas.

3.6 Uncertainties

Several limitations of the BDR algorithm should be taken into account. Omission of fire-damaged forest was tested using field and image-derived validation burn scars, and commission errors were evaluated using independent data on selective logging and deforestation in the region. However, several additional sources of uncertainty may lead to an underestimate of fire-damaged forest in this study. Understory fires that do not generate any canopy damage will not be detected by the BDR algorithm. Similarly, fires that generate very low or very high canopy damage will be considered low confidence detections to minimize potential classification errors with selective logging and deforestation, respectively. During sequential forest disturbance events, such as fire following selective logging (Souza Jr. *et al.*, 2005a),

fire damages that follow the network of skid roads and log decks installed during forestry operations may not be considered high confidence burn scars in the BDR approach. Finally, immediate abandonment of partially-cleared areas or installation of plantation forests could generate a recovery trajectory similar to burned forest, leading to commission errors with the BDR approach. Data on land abandonment and plantation forests were not available, but based on field knowledge of the study region, these practices are rare relative to widespread damages from understory fires, selective logging, and deforestation for agricultural use.

3.7 Conclusions

The BDR algorithm is a novel method to identify temporal and spatial characteristics of burned forest in time series of satellite data. Time series information from a minimum of three consecutive years permits detection of two changes—a reduction in green vegetation following fire and immediate recovery of canopy material in subsequent years. The results from this study demonstrate that both Landsat and MODIS time series are suitable for isolating understory forest fire damages from selective logging and deforestation in Amazonia using the BDR algorithm.

Mapping the annual extent of canopy damage from understory fires in Amazonia is critical to improve estimates of carbon emissions from forest degradation to meet both scientific and policy objectives (Gullison *et al.*, 2007). This study confirms that periodic high fire years contribute substantially to forest degradation in southern Amazonia, but extensive burning in the study area did not

coincide with the 1997-1998 ENSO as reported in previous studies. Applying the BDR algorithm to longer time series over larger study areas will improve understanding of relationships among climate, land use, and forest fire activity in Amazonia.

Chapter 4: A Positive Fire Feedback in Southern Amazon Forests

4.1 Summary

Initial anthropogenic understory fires may increase Amazon forest flammability. This positive fire feedback is one potential mechanism for savannization of tropical forests under current climate conditions. Testing the savannization hypothesis over large areas requires annual satellite data to determine the frequency of understory fire damages and characterize vegetation recovery following repeated burning. This chapter describes the combination of field observations and a moderate resolution satellite time series to create annual maps of burned Amazon forest (1999-2005) and deforestation (2000-2006) for the upper Xingu River watershed in the Brazilian state of Mato Grosso. This study tests the hypotheses that fire-damaged forest area is highest during dry years and that repeated fire exposure reduces satellite-measured vegetation greenness compared to initial burn damages as herbaceous vegetation replaces closed-canopy forest. The results from this study suggest that burned forests are an extensive and long-term component of frontier landscapes in southern Amazonia. The area of fire-damaged forest during the MODIS era was equivalent to the area deforested for cropland and pasture, and combined damages from fire and deforestation totaled 30% of the initial forested area outside of the Xingu Indigenous Park. Contrary to the first study hypothesis, annual fire-damaged forest did not show a consistent trend with precipitation anomalies derived from the Tropical Rainfall Measuring Mission (TRMM) satellite during

1998-2005. Highest fire damages in 1999 (8,815 km^2) did coincide with low accumulated (6/98-5/99) and dry season (6/99-8/99) rainfall, but precipitation was average and anomalously wet preceding elevated forest fire damages in 2002 and 2004, respectively. Approximately 20% of all forests damaged by fire burned two or three times during 1999-2005 with an average fire return interval of 3.2 years. Comparable recovery of dry-season greenness two years after first, second, and third burns implied a continued dominance of deep-rooted, woody vegetation in fire-damaged forest areas. While three fires in 5-7 years did not lead to evidence of savannization in satellite-based measures of vegetation greenness, higher frequency of fire damages in previously-burned than unburned forests supports the hypothesis of a positive fire feedback in southern Amazon forests.

4.2 Introduction

Widespread fires in tropical forests more than doubled estimates of atmospheric carbon emissions from annual deforestation during the 1997-1998 El Niño event (Nepstad *et al.*, 1999b; van der Werf *et al.*, 2004; van der Werf *et al.*, in press-a) and demonstrated the sensitivity of humid forest types to severe degradation from fire during drought conditions (Barbosa & Fearnside, 1999; Cochrane *et al.*, 1999; Page *et al.*, 2002). Fires in tropical forests may initiate a positive feedback in which canopy gaps from fire-killed trees alter the forest microclimate, drying leaf litter and accumulated woody fuels, thereby making future fires more likely (Cochrane & Schulze, 1999). Repeated exposure to fire may eventually convert tropical forest into fire-adapted grasslands or woodlands, a process described as

savannization, with dramatic consequences for carbon storage, regional climate, and biodiversity (Cochrane *et al.*, 1999; Cochrane & Schulze, 1999; Malhi *et al.*, 2008). In Amazonia, the extent of fire-damaged forests has been estimated for ENSO years (Barbosa & Fearnside, 1999; Elvidge *et al.*, 2001; Cochrane & Laurence, 2002; Phulpin *et al.*, 2002; Alencar *et al.*, 2006) and other drought conditions (e.g., Brown *et al.*, 2006), but the frequency of fire damages have never been determined from annual satellite data over large regions. Estimating the frequency of fire damages under current climate is critical to understand how anthropogenic fire use may accelerate Amazon forest dieback from climate change (e.g., Cox *et al.*, 2000; Cox *et al.*, 2004; Malhi *et al.*, 2008).

Fire risk in Amazon forests is a function of climate, fuels, and ignition sources (Nepstad *et al.*, 1999b; Alencar *et al.*, 2004; Nepstad *et al.*, 2004; Ray *et al.*, 2005; Balch *et al.*, 2008). Previous studies have identified important linkages between annual or dry-season precipitation and fire risk for regions of eastern and central Amazonia (Holdsworth & Uhl, 1997; Cochrane & Schulze, 1999; Nepstad *et al.*, 2004; Ray *et al.*, 2005; Aragão *et al.*, 2007; Zeng *et al.*, 2008). The increase in fuels from selective logging has also been cited as a critical precursor to forest fires (e.g., Uhl & Buschbacher, 1985; Holdsworth & Uhl, 1997; Nepstad *et al.*, 1999b), and recent work in southern Amazonia suggests that fuel availability may be more important than rainfall for fire risk in more seasonal forest types (Balch *et al.*, 2008). Ignitions are most concentrated along the arc of deforestation, where rapid conversion of forest for cropland and pasture is the primary source of satellite fire detections (Morton *et al.*, 2008). The Brazilian state of Mato Grosso is a focal point for studies

on forest fires because of seasonal climate (see methods) and the highest rates of logging (Asner *et al.*, 2005), deforestation (INPE, 2007), and satellite-based fire detections (Morton *et al.*, 2008) of any Amazon region during this decade. In addition, previous studies have presented conflicting results for the importance of climate and fuels as the source of interannual variability of fire damages in Mato Grosso (Chapter 3; Alencar *et al.*, 2006; Balch *et al.*, 2008).

Understory fires in Amazon forests can result in severe and long-term changes in forest structure. Field measurements of canopy mortality from initial fire exposure range from 6-44% (e.g., Holdsworth & Uhl, 1997; Barbosa & Fearnside, 1999; Cochrane & Schulze, 1999; Pinard *et al.*, 1999; Barlow *et al.*, 2003; Haugaasen *et al.*, 2003; Ivanauskas *et al.*, 2003; Balch *et al.*, 2008). Recurrent fires in previously-burned forests further reduce live canopy (Cochrane *et al.*, 1999; Cochrane & Schulze, 1999; Gerwing, 2002; Barlow & Peres, 2008), although fire severity in later fires may depend on the frequency of fire damages (Balch *et al.*, 2008). Satellite-based studies of Amazon forests have quantified percent tree cover (e.g., DeFries *et al.*, 2002; Hansen *et al.*, 2002) and reductions in live canopy associated with selective logging (Asner *et al.*, 2004) and forest fires (Cochrane & Souza, 1998; Souza Jr. *et al.*, 2005a). However, evidence for the reduction in live canopy from repeated burning observed in field studies has not been confirmed using systematic satellite measurements.

This chapter describes how field observations and a moderate resolution satellite data time series were combined to create annual maps of burned forest and deforestation for the upper Xingu River watershed in the Brazilian state of Mato

Grosso. The goals of this study were to assess the interannual variability in fire-damaged forest area, frequency of recurrent fire damages, and relationship between burned forest and deforestation in the region. Maps of fire-damaged forest were used to conduct the first large-scale test of two prevailing hypotheses regarding fire risk and damages from repeated burning in Amazon forests. Specifically, this study tested the hypothesizes that: 1) forest fire damages would be more extensive in years with low rainfall, and 2) recurrent fires in would reduce satellite-based measurements of vegetation greenness in years following second and third fires, consistent with the replacement of closed-canopy tropical forests by herbaceous vegetation.

4.3 Methods

4.3.1 Study Area

This study evaluated the spatial extent and frequency of forest disturbance from fire in the headwaters of the Xingu River, a main tributary of the Amazon River with its origin in the Brazilian state of Mato Grosso (Figure 4-1). The study area incorporates the southern extent of closed-canopy Amazon forests. Analysis was restricted to fire-damaged forests in this study, excluding fire-adapted Cerrado savanna-woodland physiognomies common below 14° S latitude in the watershed. Prior to analysis, geographic information system (GIS) data layers for non-forest (INPE, 2007) and river corridors (SEPLAN-MT, 2004) were used to mask Cerrado vegetation types and seasonally-inundated vegetation, respectively. Approximately 87% of the 112,800 km^2 study area was forested in 2000 (97,690 km^2). The Xingu

Indigenous Park covers the central portion of the study region and contained 23% of all forest in 2000 (22,129 km^2).

Forests in the Xingu River watershed range in height from 20 – 30 m (Vourlitis *et al.*, 2001; Lefsky *et al.*, 2005; Balch *et al.*, 2008), with total above-

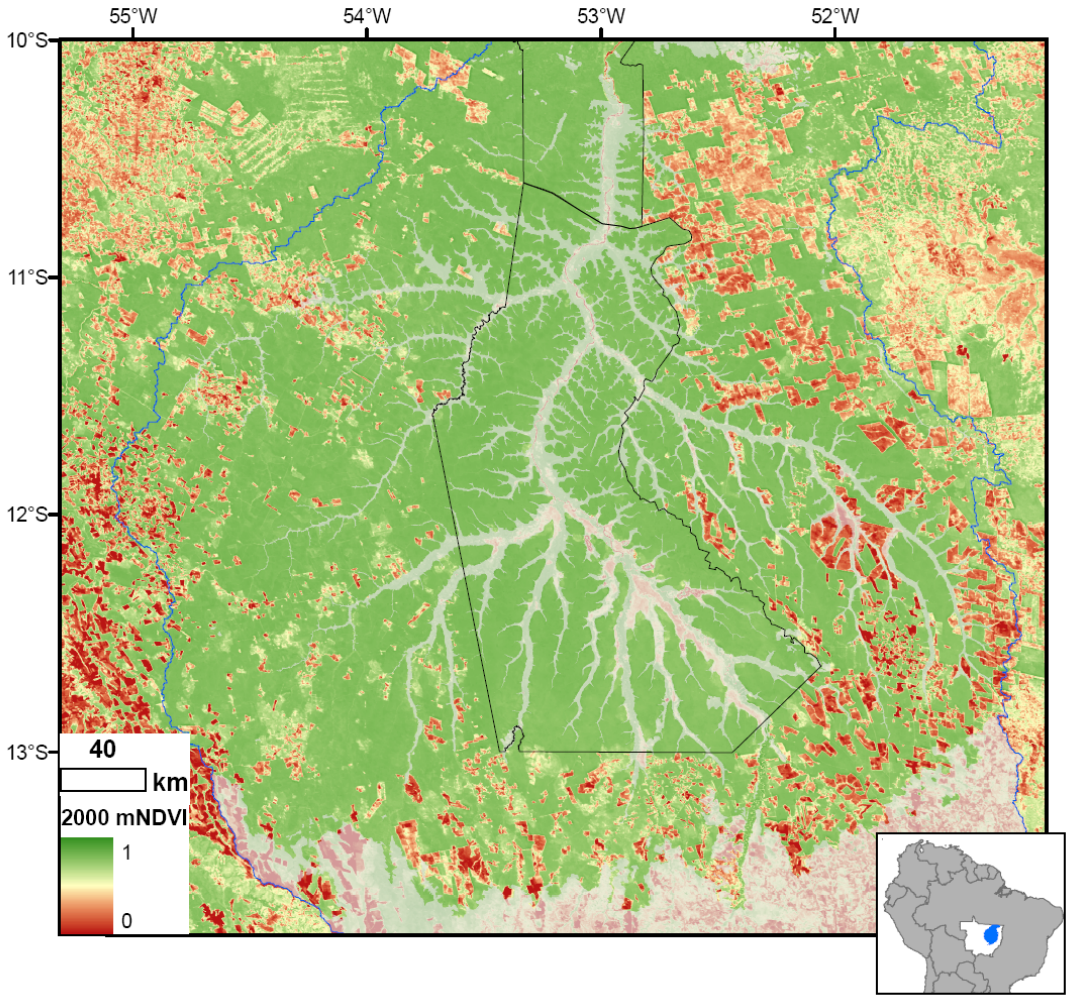

Figure 4-1: MODIS mean dry-season NDVI (mNDVI) in 2000 for the upper Xingu River watershed (blue) in the Brazilian state of Mato Grosso (inset, white). The Xingu Indigenous Park (black outline) occupies the center of the study area. Forested areas are shown in green, grasslands and Cerrado in shades of yellow, and bare soils typical of cropland in dry-season months appear red. Within the Xingu River watershed, Cerrado and inundated vegetation along river courses that were excluded from the analysis are masked in light-gray tones.

ground live biomass exceeding 300 Mg/ha in some areas (Monteiro *et al.*, 2004; Souza Jr. *et al.*, 2005b). Soils are primarily well-drained and nutrient-poor ultisols (Vourlitis *et al.*, 2001). Precipitation averaged 1886 ± 99 mm/yr during 1998-2006 (see description of precipitation data below). Forest fire risk in the study region is exacerbated by frequent fire use for deforestation during May-September when the area receives little or no precipitation (Morton *et al.*, 2008).

4.3.2 Precipitation Data

Precipitation data derived from the Tropical Rainfall Measuring Mission (TRMM) sensor were used to estimate annual and seasonal rainfall anomalies for the study region. The TRMM 3B43 V6 product provides a monthly estimate of precipitation rates at 0.25-degree spatial resolution based on a combination of satellite and rain gauge data (Huffman *et al.*, 2007). Precipitation in the upper Xingu River basin is highly seasonal; average annual rainfall ranged from 1700-2000 mm yr^{-1} during 1998-2006 with little or no precipitation during June-August and <100 mm per month in May and September. Within the study area, average rainfall during this period increased along a south-north gradient by ~100 mm per degree latitude (R^2=0.79, $p<0.001$).

Previous studies have suggested two mechanisms by which precipitation anomalies may increase forest flammability. Lower precipitation during severe drought conditions may lead to a deficit in soil water during the subsequent year (e.g., Nepstad *et al.*, 1999a; Nepstad *et al.*, 2004; Aragão *et al.*, 2007). Similarly, flammability and fire spread rates in intact tropical forests increase during extended rainless periods as declining relative humidity dries leaf litter and other fine fuels on

the forest floor (e.g., Cochrane & Schulze, 1999; Ray *et al.*, 2005; Brown *et al.*, 2006). Long periods without rain may also be necessary to burn large areas, since fire spread rates in Amazon forests are typically <0.5 m/min (Chapter 3; Cochrane & Schulze, 1999; Balch *et al.*, 2008). Two rainfall anomaly measurements were calculated using TRMM data for the study area to test these hypotheses. The annual anomaly in accumulated precipitation during 1998-2005 was calculated from total rainfall in the year prior to burning (e.g., June 2000 – May 2001 for fires in 2001). Dry season rainfall anomalies were calculated for June-August precipitation in the year of forest burning (1999-2005).

4.3.3 MODIS Time Series 2000-2007

Data from the Moderate Resolution Imaging Spectroradiometer (MODIS) sensor onboard the Terra satellite were used to develop a time series of annual mean dry season normalized difference vegetation index (mNDVI) at 250 m spatial resolution following methods described in Chapter 3. Briefly, cloud-free observations of NDVI (MOD13 Q1 V4 product (Huete *et al.*, 2002)) from seven 16-day composite images during May-August (day of year 129-225) were used to derive annual mNDVI data layers for 2000-2006. Data for 2007 were generated using Collection 5 MODIS algorithms since processing for MODIS products switched from Collection 4 to Collection 5 in January 2007. Intact forest areas in the study region showed small differences (<0.5%) in mNDVI values derived for 2001 and 2002 from Collection 4 and Collection 5 data products. However, more substantial differences between collections occurred over Cerrado vegetation and near water bodies from changes to the internal water mask. Therefore, Collection 5 data from 2007 were

only used to confirm forest regrowth in previously-burned areas (2004, 2005) and deforestation for forest areas cleared in 2006.

4.3.4 Mapping Canopy Damage from Fire with the Burn Damage and Recovery Algorithm

The Burn Damage and Recovery (BDR) algorithm is a time-series approach to distinguish fire-related canopy damages from other types of forest degradation (Chapter 3). The BDR algorithm utilizes up to four years of mNDVI data to identify the trajectory of damage and recovery of burned forest over time (see Figure 3-2). Although canopy damages from multiple types of forest disturbance may appear similar in a given year, the BDR trajectory over multiple years for canopy damage from fire is unique. Previous application of the BDR algorithm to time series of Landsat and MODIS data demonstrated the ability to isolate burned forest from logging and deforestation for a subset of the current study area (Chapter 3).

This study applied the BDR algorithm to a time series of MODIS mNDVI data to map fire-damaged forest area during 1999-2005. Forest that burned in 1999 was first mapped using MODIS data from 2000-2002, and forest that burned in 2005 was detected in 2006 and confirmed based on mNDVI recovery in 2007. Since the BDR algorithm uses satellite data from the early dry season period to identify evidence of canopy damage from fires in the previous year, the algorithm does not technically map burned area (Lentile *et al.*, 2006). Instead, this study characterized fire effects on canopy trees in the MODIS-based maps of fire-damaged forest area from the BDR algorithm. Only high-confidence burn scars >50 ha were used to analyze interannual variability in the extent and frequency of forest burning in the

study region during this period. Additional details regarding the BDR algorithm development can be found in Chapter 3.

4.3.5 Deforestation

The MODIS mNDVI time series was also used to identify deforestation in the study region during 2001-2006. Forest areas converted for cropland or pasture have distinct non-forest phenology in years following clearing (Morton *et al.*, 2006), and mNDVI values for pasture and cropland deforestation consistently remain below 0.65 (e.g., Figure 3-2). To confirm forest conversion and subsequent non-forest land use, only forested regions with MODIS mNDVI <0.65 in two consecutive years during 2000-2007 were mapped as deforestation. This approach to identify deforestation is internally consistent with maps of burned forest. All deforestation data derived from the MODIS time series approach were used to assess total deforestation and deforestation of previously-burned forests, but only individual deforestation events >20 ha (>3 MODIS 250 m pixels) were used to identify burned forest that was adjacent to new deforestation based on established limitations on the size of individual clearings that can be reliably identified using moderate-resolution satellite data (Morton *et al.*, 2005; INPE, 2006).

4.3.6 Validation Data

Field observations of fire-damaged forest were collected during June-September of 2001 and 2003-2006. In each year, field transects targeted historic fire scars visible in coincident high-resolution imagery and accessible via existing roads. The location and perimeter of each forest burn scar was recorded using a hand-held

Global Positioning System (GPS) unit, and the date and ignition source for each fire was determined using a combination of satellite data and information from landowners. Immediately following field campaigns, observations and mapped burn perimeters were identified in coincident high-resolution data (e.g., Advanced Spaceborne Thermal Emission and Reflection Radiometer (ASTER), 15 m spatial resolution) to complete portions of the burn perimeter that were not accessible during fieldwork. In total, 117 field observations of burned forest (925 km^2) were used to validate satellite-based estimates of canopy damage from understory fires (Table 4-1). A subset of field-mapped burn scars (368.4 km^2) burned more than once. For field observations of repeated understory fires, the detection performance of the BDR algorithm was calculated separately for canopy damages from first, second, and third fires.

Field observations of deforestation from 2004 and 2005 were collected in a similar manner. A total of 205.1 km^2 of new deforestation for pasture and cropland was observed during field campaigns in 2004-2006 (Table 4-1). Field observations of

Table 4-1: Field observations of forest that burned during 1999-2005 in the upper Xingu River study area.

Year	Observations	Fire-damaged forest area (km^2)
1999	16	277.3
2000	1	0.5
2001	5	53.4
2002	34	305.0
2003	12	120.9
2004	31	118.5
2005	18	49.5
Total	117	925.0

2004 deforestation were used previously to validate Landsat and MODIS-based deforestation detections (Morton *et al.*, 2005). Validation comparisons considered the percent of field-mapped deforestation events of different sizes that was correctly identified using the MODIS time series approach.

4.3.7 Statistical Analyses

Two approaches were used to test the hypothesis that repeated exposure to fire reduces satellite-based estimates of vegetation greenness. First, the effect of multiple fires in the same location was evaluated. Analyses were conducted separately for areas that burned two times (burn 1 versus burn 2) and three times (burn 2 versus burn 3) during the study period using paired t-tests (SAS System v9.1, The SAS Institute, Cary, NC). Analyses were also conducted separately for both "burn" and "recovery" mNDVI values, because it is ecologically plausible that the effects of multiple fires may appear as greater canopy damage immediately following fire (e.g., Cochrane *et al.*, 1999) or a reduction in the rate of forest recovery during subsequent years (e.g., Zarin *et al.*, 2005; Malak & Pausas, 2006). Burn values were defined as the mNDVI for the year in which each fire was mapped (~7-9 months post-burn), and recovery values were defined as the mNDVI for the year after fire damages were mapped (see Figure 3.2). However, in this short time series, burn number was highly correlated with calendar year for areas burned three times (burn 1: 1999-2001, burn 2: 2001-2005, burn 3: 2003-2005), thus making it difficult to isolate the effect of multiple burns from other conditions that vary interanually.

The second approach explicitly accounted for potential interannual differences in burn and recovery mNDVI values. These analyses included all areas that burned in a given year, grouped by burn number, to evaluate whether fire damages in the same year were similar regardless of previous disturbance history. The mean burn and recovery mNDVI values for first, second, and third fires were plotted for each year, and the pairwise comparisons from first to second and second to third fires were calculated using unpaired t-tests (SAS System v9.1, The SAS Institute, Cary, NC). Although this analysis loses the spatial consistency of the repeated measures t-test in the first approach, it minimizes potential interannual differences in mNDVI resulting from variability in climate and atmospheric conditions.

Due to large sample sizes typical of remote sensing analyses, a meaningful effect size was defined for differences in mNDVI values in addition to testing for statistically significant differences in group means. Based on parameters in the BDR algorithm used to map burned forest areas (Chapter 3), only mean mNDVI differences >0.01 were considered to be meaningful in this study. This effect size also exceeds the interannual variation in mean mNDVI for intact forest during 2001-2005 shown in Figure 3.2 (range = 0.873 – 0.88).

4.4 Results

4.4.1 Validation

Field observations of burned forest were used to assess the detection performance of the BDR algorithm for individual burn scars of different sizes and recent fire history. The automated BDR algorithm successfully detected 81.7% of the

fire-damaged forest area mapped during fieldwork, and the percentage of individual burn scars in which MODIS detected canopy damage from fire increased with burn scar size (Table 4-2). Very large burn scars (>500 ha) accounted for 91% of all field validation area, and MODIS results captured 83% of the area in these largest burn scars.

Automated detection of multiple burning events in the same location improved as the number of years between fires increased (Table 4-3). The BDR

Table 4-2: Detection of field validation burned forest perimeters as a function of burn scar size using the BDR algorithm applied to the time series of MODIS data.

	Field Validation		MODIS	
Size (ha)	Obs.	Area (km^2)	Area (km^2)	% Detection
<25	16	2.15	0.38	17.50%
25-50	8	2.84	0.43	15.09%
50-100	17	11.32	5.42	47.87%
100-500	29	67.56	47.44	70.21%
500-1000	18	135.93	103.30	76.00%
1000-5000	26	518.53	434.61	83.81%
>5000	3	186.90	164.26	87.88%
Total	117	925.24	755.83	81.69%

Table 4-3: Percentage of field validation data detected by the BDR algorithm for areas burned multiple times.

Multi-year burns	Field (km^2)	1st Burn	2nd Burn	3rd Burn
1999,2002	70.24	94.42%	87.09%	
1999,2003	40.78	91.18%	84.47%	
1999,2004	49.58	83.55%	90.80%	
2001,2004	5.04	63.83%	80.85%	
2003,2005	9.39	87.43%	37.14%	
1999,2001,2004	6.12	80.70%	20.18%	70.18%

algorithm applied to time series of MODIS data detected only 29% of fire-damaged forest that burned again after two years, but detection performance increased to 79% for field validation burn scars with 3 years between fires. Validation data with 4 years (84%) or 5 years (91%) between fires had the highest detection rates for repeated burning with the automated BDR algorithm.

Field observations of deforestation for cropland and pasture in 2004 and 2005 were used to quantify omission errors from the time series approach to detect deforestation. Only two small validation areas in 2005 had no corresponding detections in MODIS results (2 and 21 ha). Overall, MODIS detected 83% of the validation deforested area (Table 4-4).

4.4.2 Interannual Variation in Burned Forest

Interannual variation in fire-damaged forest area within the study region was high. More than half of all forest fire damages occurred in 1999, while fire-damaged

Table 4-4: Detection of field-observed deforestation according to clearing size in 2004 and 2005 using the MODIS time-series approach.

	2004 Validation		MODIS '04	2005 Validation		MODIS '05
Size	#	ha	ha (%)	#	ha	ha (%)
<25 ha	19	161	149 (93)	6	90	43 (48)
25-50	9	365	349 (96)	2	65	38 (58)
50-100	8	687	612 (89)	12	919	505 (55)
100-200	8	1074	854 (80)	10	1514	1079 (71)
200-500	11	2686	2263 (84)	11	3416	2803 (82)
>500	6	6657	6169 (93)	4	2875	2186 (76)
Total*	61	11630	10396 (89)	45	8879	6653 (75)

*Including all MODIS deforestation detections during 2003-2006 increased the percentage of validation area detected in 2004 (94%, 10,967 ha) and 2005 (81%, 7,210 ha).

Table 4-5: Fire-damaged forest area (FDFA) during 1999-2005 and the contribution from first, second, and third fires to FDFA in each year. Interactions between burned forest and deforestation (Defor.) are shown separately for fire-damaged forest that was subsequently deforested, FDFA adjacent to new deforestation (2002-2006), and total deforestation identified in the MODIS time series during 2001-2006. All areas are shown in km^2.

Year	FDFA*	1st**	2nd	3rd	Burned, Defor.	Mean Annual Defor. Rate***	Adjacent to Defor.****	MODIS Defor.
1999	8814.6	8814.6			1550.3	3.52%		
2000	488.6	488.6			154.2	7.89%		
2001	362.3	256.8	105.5		58.3	5.36%	41.2	822.8
2002	2553.8	1263.5	1290.2		124.3	2.43%	380.5	866.2
2003	1196.7	825.5	360.4	10.8	30.3	2.53%	592.1	4413.4
2004	2008.5	1019.3	660.7	328.4			1053.6	3260.0
2005	904.7	497.6	284.1	123.0			428	1900.5
2006								1123.0
Total	16329.2	13165.9			1917.5		2495.4	12386.0

* Total fire-damaged forest area (FDFA), including repeated fires in previously-burned areas.

** Net FDFA during the study period.

*** Mean annual percent deforestation during 2002-2006 of fire-damaged forest.

**** Burned forest area adjacent to MODIS deforestation events >20 ha.

forest mapped in 2001 was <5% of the burned forest area in 1999 (Table 4-5). Forest fires were concentrated in the southwestern portion of the study area in years with low burned forest area (2000, 2001, and 2005), whereas burned forest was common across the entire study area in years with highest burning (1999, 2002-2004). Less than 3% of total forest burning during 1999-2005 occurred within the Xingu Indigenous Park (476.7 km^2).

There was no consistent relationship between burned forest area and annual or dry-season precipitation anomalies (Figure 4-2). The three years with highest burning (1999, 2002, and 2004) had different precipitation patterns. Highest burned forest area during 1999 coincided with anomalously low accumulated rainfall in the year

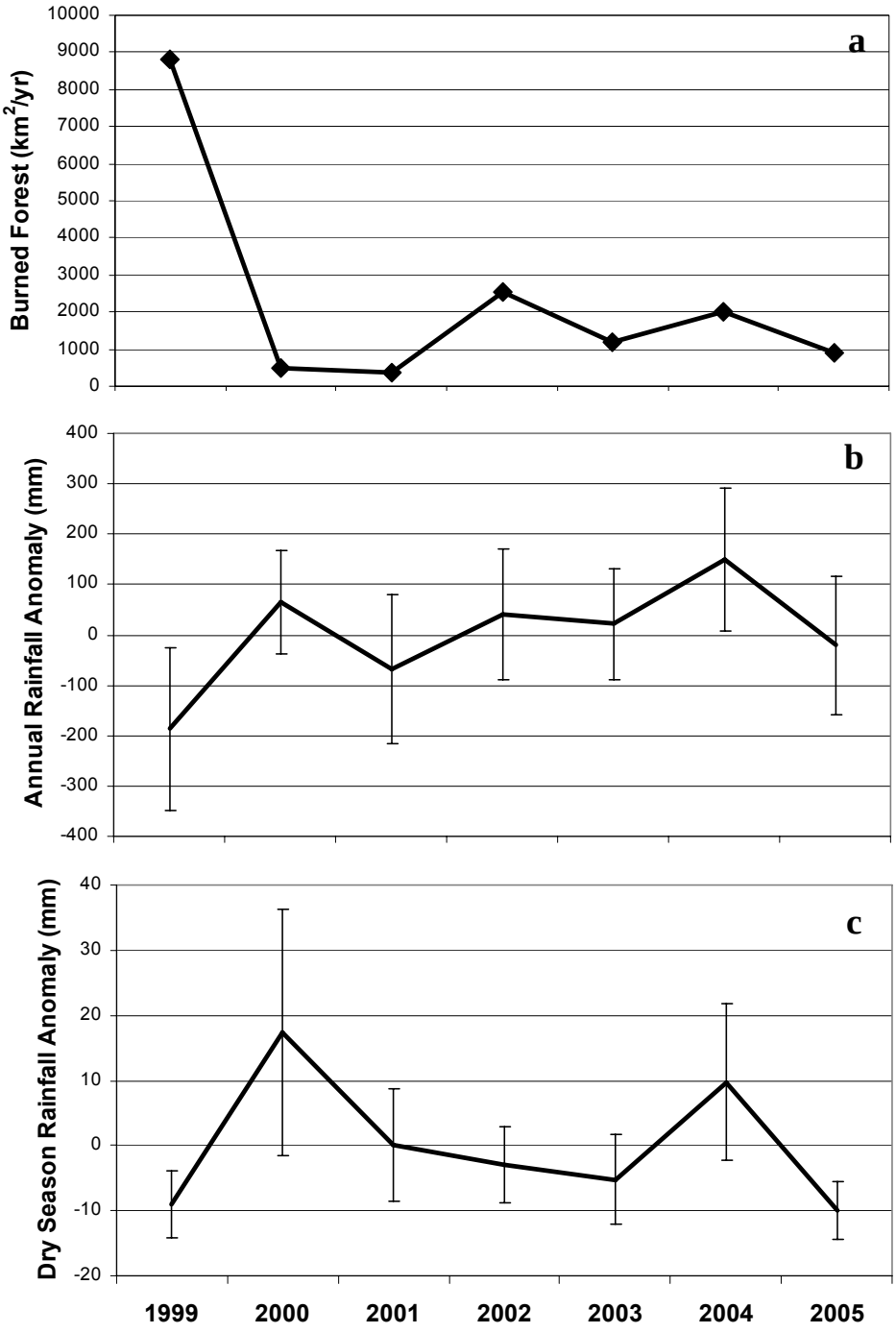

Figure 4-2: Relationship between the annual extent of burned forest (a) and mean annual precipitation anomalies ± 1 S.D. during 1998-2005 of accumulated rainfall in the year (June-May) before burning (b) and dry season rainfall (June-August) in the year of forest fire damages (c).

prior to burning (6/98 – 5/99) and dry season precipitation (6/99 – 8/99). However, accumulated and dry-season precipitation were average in 2002, and in 2004, both rainfall measures were anomalously high. Dry-season precipitation was lowest in 2005, but fire-damaged forest was not elevated in this year. Lowest forest fire damages in 2001 coincided with average accumulated and dry-season rainfall.

Although average rainfall during the study period was higher in the northern portion of the study region, only three rainfall anomalies showed consistent north-south trends across the study area. Accumulated precipitation in 2005 (6/04 – 6/05) was lower in the southern portion of the study area by ~100 mm per degree latitude ($R^2 = 0.46$, $p<0.0001$). Dry-season precipitation in 1999 was lower in the northern portion of the study area by 4 mm per degree latitude ($R^2 = 0.53$, $p<0.0001$). Finally, wetter than normal conditions during dry-season months in 2000 was driven by higher rainfall in the northern portion of the study area (14 mm per degree latitude, $R^2 = 0.47$, $p<0.0001$).

4.4.3 Recurrent Forest Fires

More than 20% of all forest damaged by fire burned more than once during 1999-2005 (Figure 4-3). Half of the forest that burned during 2002 and 2004 had burned previously (Table 4-5), with some areas burning every two years. The average fire return interval for areas burned multiple times during the study period was 3.2 years. Fires were five times more common in previously-burned than unburned forests; during 2001-2005, 24% of forests burned in 1999-2003 burned for a second time, while only 4.4% of unburned forests (3,862.7 km^2 of a possible 88,386.8 km^2) were damaged by fire during this period (Table 4-5). After accounting

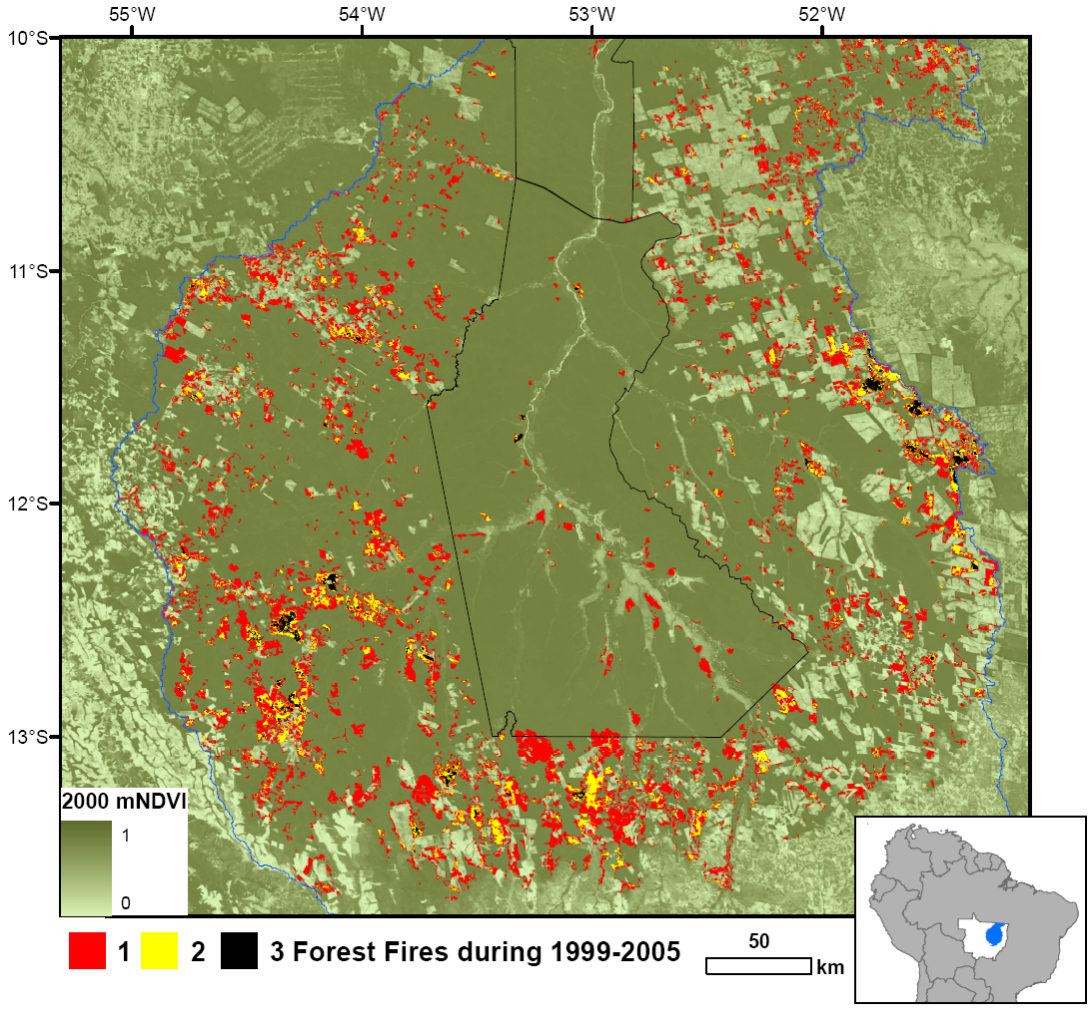

Figure 4-3: Forests burned one, two, or three times during 1999-2005 within the upper Xingu River watershed (blue) in eastern Mato Grosso State (inset, white). The Xingu Indigenous Park (black outline) occupies the center of the study area.

for repeated burning, the total fire-impacted forest area in this study was 13,165.9 km^2, two-thirds of which burned for the first time in 1999 (Table 4-5).

The effect of recurrent fires on satellite-based measures of vegetation greenness was also evaluated (Figure 4-4). In each year except 2005, mean burn mNDVI values were significantly lower for areas burning for the second time compared with areas burning for the first time. Unexpectedly, mean burn mNDVI

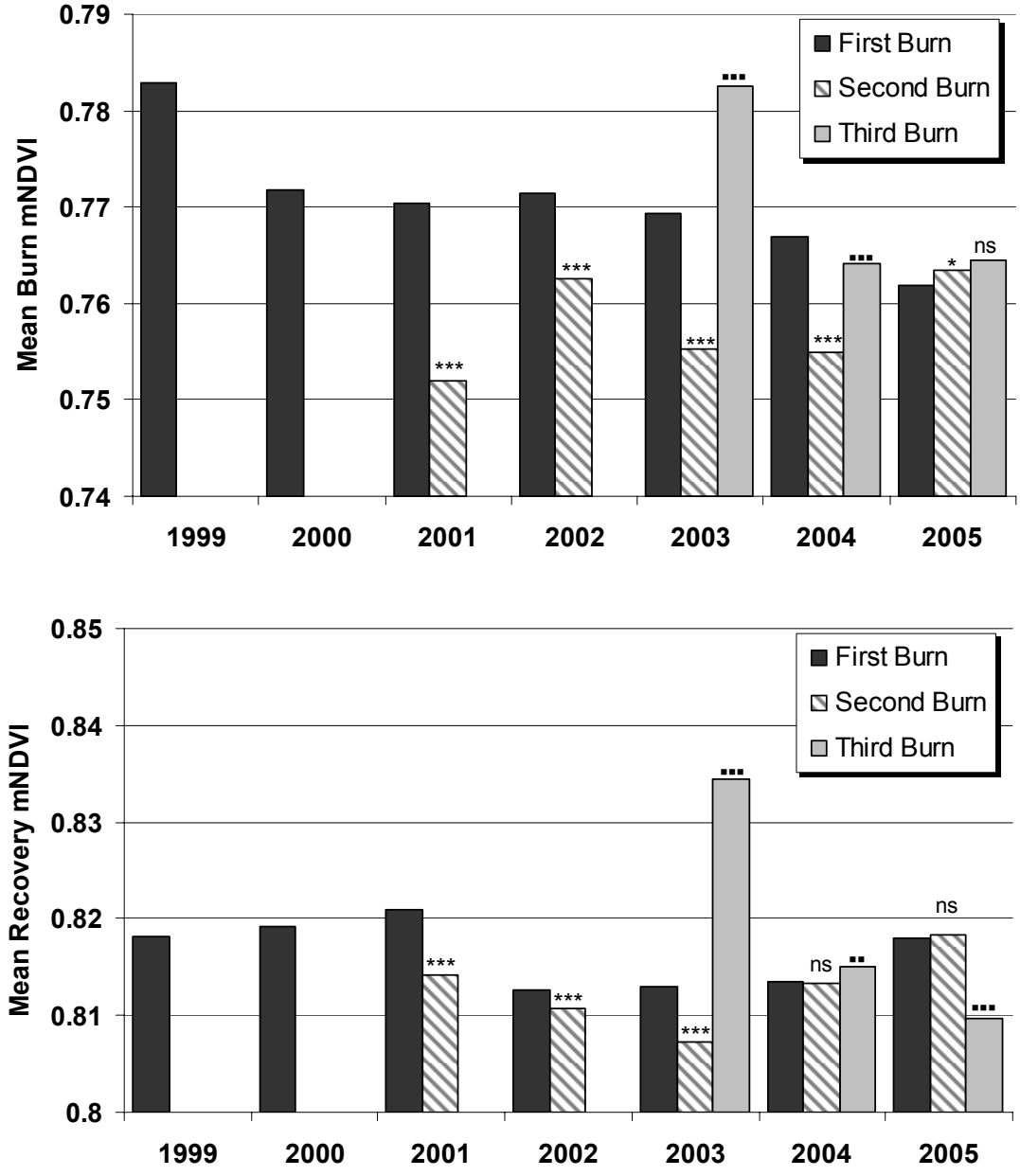

Figure 4-4: Effect of multiple burns on burn (upper) and recovery mNDVI values (lower). Symbols signify the level of statistical significance between mean mNDVI values in each year for first and second burns (stars) and second and third burns (squares) using t-tests: *** $p<0.0001$, ** $p<0.001$, * $p<0.01$, ns = not significant. Sample sizes for burned forest area in each year as a function of burn number can be found in Table 4-4. Note that results for the third burn in 2003 are based on substantially smaller burned forest area (10.8 km^2) than any other estimate.

values were higher for areas burning for the third time compared with areas burning for the second time. Statistically significant differences between first and second fires were consistent between per-year (t-tests, Figure 4-4) and per-pixel statistical tests (paired t-test, mean = 0.782 and 0.759, respectively, $p<0.0001$). Mean burn mNDVI values were more similar for second and third fires in the per-pixel analysis (paired t-test, 0.766 and 0.765, respectively, $p = 0.012$).

The impact of recurrent fires on recovery mNDVI values was similar to results for burn mNDVI, although the patterns were less consistent between statistical approaches. After controlling for burn year, mean recovery mNDVI values between areas burning for the second time compared with areas burning for the first time were not meaningfully different (>0.01) during any year (Figure 4-4). Damages from a third fire in 2003-2005 had mixed effects on recovery mNDVI (Figure 4-4). In the per-pixel analysis, recovery mNDVI declined significantly with each subsequent fire ($p<0.0001$), although mean recovery mNDVI values for the second and third fires were not meaningfully different (0.819 and 0.814, respectively). Between first and second fires, mean recovery mNDVI declined from 0.827 to 0.812 in the per-pixel analysis.

4.4.4 Deforestation of Burned Forests

Only a small fraction of burned forest identified in this study was deforested for cropland or pasture by 2006. Deforestation of previously-burned forest averaged 3.6% per year (Table 4-4). Outside of the Xingu Indigenous Park, deforestation rates during 2002-2006 were slightly higher for unburned forests (18.5% of 62,395 km^2) than for forest that burned in 1999-2003 (17.1% of 11,241

km^2). Only two areas of new deforestation >20 ha were mapped within the Xingu Indigenous Park during the study period totaling 0.5 km^2.

Fire-damaged forest during 1999-2005 that was not subsequently deforested (11,247.8 km^2) was nearly as extensive as MODIS-based deforestation during 2001-2006 (12,386 km^2). Combined, forest fires and deforestation altered 30.7% of the forested area in 2000 outside of the indigenous reserve (Figure 4-5).

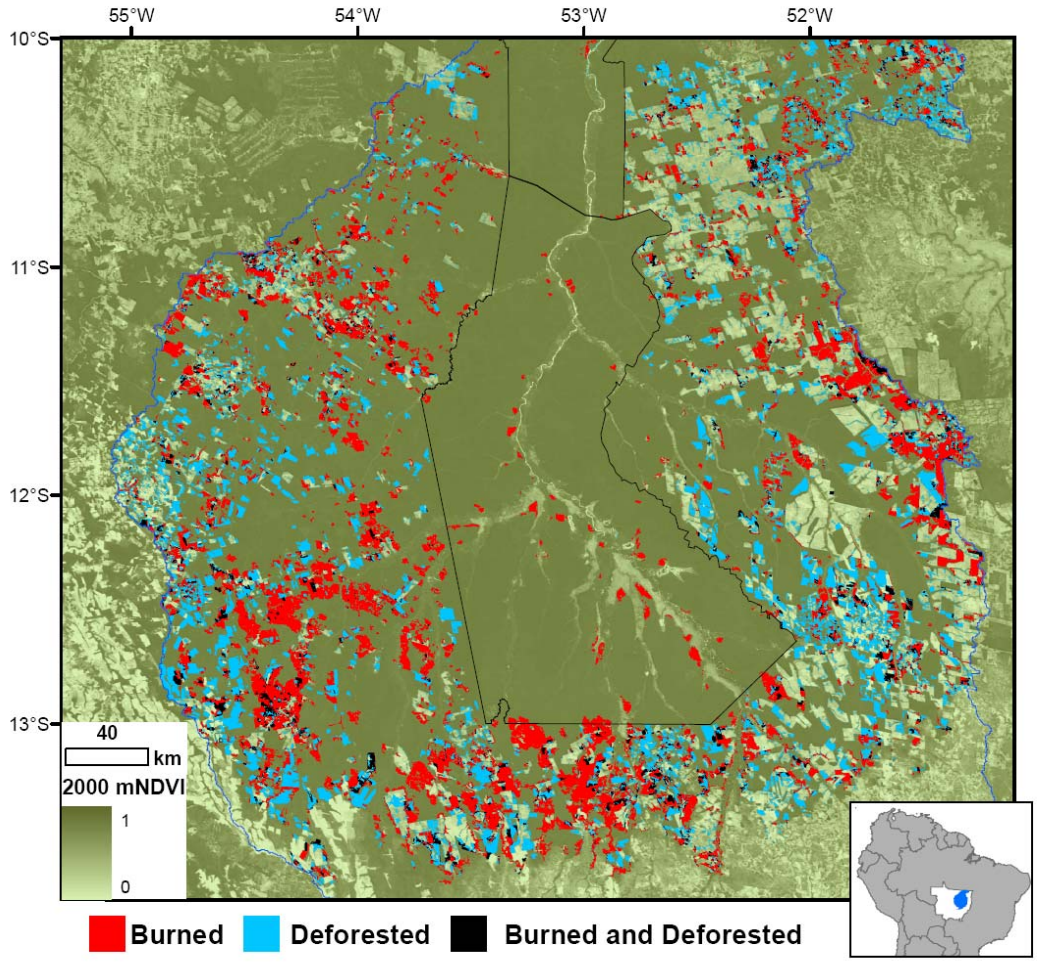

Figure 4-5: Understory forest fires in 1999-2005 (red) and deforestation during 2001-2006 (blue) damaged 30.7% of the forested area in 2000 outside of the Xingu Indigenous Park (black outline) in the upper Xingu River basin (blue outline). Burned forests that were later deforested are shown in black.

Burned forest was often adjacent to areas of new deforestation, and half of the annual burned forest in 2003-2005 adjoined deforestation events >20 ha (Table 4-5). However, there was no consistent trend for all years in the relationship between deforestation and burning. Highest deforestation rates in 2003 were not coupled with an increase in fire-damaged forest area, and lower deforestation in 2005 did not reduce the fraction of forest burning adjacent to new clearing relative to other years. During 2001-2005, fire-damaged forest adjacent to new clearing was evenly divided between first (52.6%) and repeated fires (second: 36.8%, third: 10.6%).

4.5 Discussion

Burned forests are an extensive and long-term component of the frontier landscape in southern Amazonia. Periodic high-fire years and low deforestation rates of burned forest led to 11,250 km^2 in cumulative forest fire damages during 1999-2005, doubling the amount of forest damaged by deforestation alone in this study. Deforestation rates for burned forest were lower than for unburned forest in this study and half the rate previously reported for logged forests in Mato Grosso (Asner *et al.*, 2006), suggesting that canopy damages from understory forest fires identified by the BDR approach were not an immediate precursor to conversion for cropland or pasture in this region. Combined damages from fire and deforestation impacted more than 30% of forests outside the Xingu Indigenous Park in less than a decade. The following sections consider the results from this study in the context of the study hypotheses regarding the role of precipitation in determining the interannual

variability in burned forest area and satellite-based evidence of damages from recurrent forest fires.

4.5.1 Interannual Variation in Burned Forest

4.5.1.1 Rainfall

Interannual variability of burned forest area in this study did not clearly support previous findings about the role of rainfall in forest fire risk determined for other Amazon regions. Extensive canopy damage from fire in 1999, when two-thirds of all forests damaged by fire in the study were burned, did occur following anomalously low precipitation. However, more than 2,000 km^2 of forest burned in 2002 and 2004 when rainfall was average and anomalously wet, respectively. Dry conditions similar to 1999 did not recur during the study period to confirm the combined influence of accumulated and dry-season precipitation anomalies for fire exposure in southern Amazonia. Previous reports of extensive forest fires associated with drought during El Niño Southern Oscillation (ENSO) phenomena (e.g., Barbosa & Fearnside, 1999; Cochrane & Laurence, 2002; Alencar *et al.*, 2006) could not be tested with the MODIS time series, but results in Chapter 3 demonstrate that annual fire damages for a subset of the Xingu River basin in Mato Grosso were 10 times higher in 1999 than during the 1997-1998 ENSO. Drought conditions in western Amazonia during 2005 also led to forest burning and an overall increase in satellite-based fire detections (Brown *et al.*, 2006; Aragão *et al.*, 2007; Morton *et al.*, 2008; Zeng *et al.*, 2008). Dry-season precipitation was anomalously low during 2005 in the study region, but forest fire activity was not markedly higher in that year. Finally, Nepstad *et al.* (2004) estimated extreme forest fire risk in southern Amazonia during

2001 based on modeled soil water deficits; however, 2001 had the lowest fire-damaged forest of any year in this study.

The contribution from repeated burning to annual forest fire damages may partially account for the variable relationship between forest fires and precipitation in years with high fire activity in this study (1999, 2002, and 2004). In 2002 and 2004, 50% of the total burned area occurred in forests with at least one prior fire. In previously-burned forests, either wet or dry conditions may lead to higher fuels for additional fires; wet years may promote understory fuel buildup (grasses, woody shrubs, and trees) typical of fire risk in savanna ecosystems (e.g., Govender *et al.*, 2006), whereas drought conditions may stress or kill large or fire-damaged canopy trees (e.g., Nepstad *et al.*, 2007). The length of the satellite time series limits further insight into the role of precipitation in fire risk for burned and unburned forests because fire histories for forests burned in 1999 cannot be established using MODIS data.

4.5.1.2 Ignitions

Deforestation for cropland and pasture may be an important source of forest fire ignitions in southern Amazonia. By the end of the study period, half of all burned forest areas were adjacent to large deforestation events. Deforestation fires are hotter and burn longer than other fire types in Amazonia (Schroeder *et al.*, 2008b), yet higher deforestation rates in 2003 and 2004 did not increase total burned area or the fraction of forest fires adjacent to new clearings. Direct conversion of forest to cropland in Mato Grosso was also highest in these years, while the area converted to pasture did not change in 2003-2004 relative to other years during 2000-2005 (Morton *et al.*, 2006; Morton *et al.*, 2007b). Fires for pasture deforestation typically

occur later in the dry season than fires for cropland expansion when forests may be most flammable after 3-5 months with little rainfall (Morton *et al.*, 2008). Thus, more deforestation, and more frequent fire usage during the conversion process, may not lead to an increase in forest fire damages if areas are cleared and burned when the risk of forest fires is low.

Other ignition sources were also responsible for forest fire damages in this study. Fire damages in the Xingu Indigenous Park occurred despite little measurable deforestation. Inside the indigenous area, fires are frequently set in the grassland regions that border the Xingu River and its tributaries for hunting purposes (Nepstad *et al.*, 2006a); M. Shimabukuro, personal communication). Fire is used for a variety of management purposes outside of reserve, and previous studies have linked forest fire activity in Amazonia with charcoal production (Alencar *et al.*, 2004) and burning in cattle pastures (Uhl & Buschbacher, 1985; Cochrane *et al.*, 1999; Alencar *et al.*, 2004). Given the ubiquity of ignition sources in frontier landscapes and seasonal climate in southern Amazonia, fuels may more be more important than climate or specific land uses in determining fire risk in seasonal Amazon forests (Alvarado *et al.*, 2004; Balch *et al.*, 2008).

4.5.2 Impact of Recurrent Fires on Amazon Forests

Recurrent fire damages did not lead to evidence of savannization in satellite-based measures of vegetation greenness. Burn mNDVI values were consistently lower between first and second fires, similar to reports from field studies of higher canopy-tree mortality from repeated fires in Amazon forests (e.g., Cochrane *et al.*, 1999; Cochrane & Schulze, 1999; Gerwing, 2002; Barlow & Peres, 2008). However,

the increase in burn mNDVI between second and third fires and comparable recovery mNDVI values following first, second, and third fires were inconsistent with the study hypothesis that mNDVI would decrease as function of burn number (Cochrane & Schulze, 1999).

Despite burning three times in 5-7 years, dry-season vegetation greenness was higher in the years following fire than would be expected for grass-dominated cover types. During June-August, a dense canopy of deep-rooted vegetation is necessary to maintain a high level of satellite-based greenness because of very low rainfall (average <5 mm/month) in the study region (Holdsworth & Uhl, 1997; Ichii *et al.*, 2007). Rapid recovery of mNDVI following fire is consistent with field observations that pioneer trees, tree sprouts, lianas, and other woody vegetation quickly regain dominance following initial and repeated burns (Kauffman, 1991; Cochrane & Schulze, 1999; Gerwing, 2002; Barlow & Peres, 2008) and previous satellite-based studies showing high fractional tree cover in previously-burned forests (Souza Jr. & Roberts, 2005; Souza Jr. *et al.*, 2005b). While recurrent fire damages did not lead to evidence of savannization in satellite-based measures of vegetation greenness in this study, more frequent fires in previously-burned than unburned forests provides the first satellite-based evidence for a positive fire feedback in Amazon forests (Cochrane & Schulze, 1999).

Changes in forest structure and species composition from repeated fires may also render burned forests more susceptible to future fires despite continued dominance of woody vegetation (Barlow & Peres, 2008). Barlow & Peres (2008) described the impact of recurrent fires in Amazonia as “secondarization” since forest

composition following fires shifts to favor pioneer species. Long-term changes in the amount of carbon stored in above-ground biomass could be large if repeated fires trap forests in early succession. By combining remote sensing results from this study with an ecosystem model, it may be possible to quantify carbon losses from changes in forest structure following repeated burning in southern Amazonia.

Whether forests in southern Amazonia may eventually be converted to open-canopy or grass-dominated vegetation types through repeated fires may ultimately depend on the relationships among the frequency of additional fire damages, ability of forest trees to resprout following fire, and influence of climate change on temperature and precipitation patterns. The overall frequency of fires mapped in this study and higher detection rates for field-mapped burns at 3+ year frequencies are consistent with findings that fuels may limit annual or biannual fire activity in seasonal Amazon forests (Balch *et al.*, 2008). Whether fires can eventually become too frequent to allow trees to recover carbon stores that enable resprouting is an important question for future research (Kauffman, 1991; Bond & Midgley, 2001). Previous studies of the impact of fire on forest recovery have documented reduced secondary forest growth rates in slash-and-burn agricultural systems in Amazonia after 5 or more fires (Zarin *et al.*, 2005) and long-term loss of resilience in Mediterranean ecosystems following recurrent burning (Malak & Pausas 2006, Wittenberg *et al.*, 2007). Using a longer time series, it may be possible to examine recovery from additional fires (4+) in Amazon forests and monitor recovery over multiple years following fire to compare recurrent fire damages in southern Amazonia with findings in these previous studies. Finally, long-term changes in

climate may also exacerbate impacts from repeated burning in tropical forests (Malhi *et al.*, 2008).

4.5.3 Study Limitations and Uncertainties

Fine-scale spatial and temporal heterogeneity in precipitation may be important for fire risk in southern Amazonia, but these questions could not be directly addressed using monthly TRMM precipitation data at 0.25 degree resolution. For example, the number of consecutive days without rain is important for fuel moisture in less seasonal regions of Amazonia (Holdsworth & Uhl, 1997; Cochrane & Schulze, 1999; Ray *et al.*, 2005). Future work to establish the precise timing and duration of forest fires identified in this study would help clarify whether accumulated or dry-season precipitation is more important for initial fire damages and repeated burning of previously-burned forests in southern Amazonia. The coarse resolution of the TRMM data may also mask spatial variability in precipitation within the Xingu River basin. Interestingly, fire damages were spatially concentrated in average and wet years with little forest burning, but burned forests were widely distributed across the study area in high-fire years. Regional-scale climate mechanisms that lead to fuel buildup, such as extreme temperatures or wind events, could also explain widespread fire activity in years with highest burned forest area (e.g., Carvalho *et al.* 2004).

Several aspects of the BDR algorithm could contribute to the patterns in satellite-based vegetation greenness observed following repeated burning in this study. First, burned forest with mNDVI <0.65 would be excluded by the BDR algorithm to avoid confusion with deforestation in the classification approach, potentially leading to an underestimate of the extent of burned forest and an

overestimate of mean canopy greenness following fire. Second, burned forests that do not recover following fire are also not included in results from the BDR algorithm. However, burned forests with low mNDVI or that did not recover following fires were not a large fraction of the field-observed fire damages, given the high detection rates of field validation data with the BDR algorithm. Third, forests that burn on annual basis will not be detected by the BDR algorithm, and biannual burning may be underestimated with this approach based on comparisons with field validation burn scars. Results in this study are consistent with reduced fire risk observed by Balch *et al.* (2008) in forests with frequent burning due to decreased fuels immediately following fire. Nevertheless, the frequency and extent of burning that generates patterns other than the BDR trajectory merit further study. Finally, studies of fire effects in Amazon forests with high-resolution satellite data have documented fine-scale spatial heterogeneity in canopy damages (Chapter 3; Cochrane & Souza, 1998; Cochrane *et al.*, 1999; Souza Jr. *et al.*, 2005a). Rapid regrowth of woody vegetation may overtop small patches of herbaceous vegetation that established following fire, preventing their detection using moderate resolution optical satellite data. Although individual patches of herbaceous vegetation were not large enough to alter the aggregate surface reflectance from burned forest regions, changes in understory species composition may increase the risk of larger grass-dominated patches following future fires.

Our time-series approach to map deforestation has several advantages over methods that classify forest loss using a single observation, but moderate resolution data may underestimate the area of individual clearings. Omission of field validation

areas with the time-series approach was lower than previously reported for single-date methods with MODIS data (Morton *et al.*, 2005; Ferreira *et al.*, 2007). By using the same mNDVI time series with mutually exclusive criteria, deforestation maps are internally consistent with maps of burned forests. However, it is possible that burned forest with very high canopy damage or forests burned every year could be classified as deforestation using this method. Our approach only estimates the total forest area converted to non-forest land uses for at least two years. As a result, the time-series method may underestimate the area of forest that was completely cleared but immediately abandoned or converted to a forest plantation. Limitations of all MODIS-based deforestation detection methods include less reliable estimates of deforested area without calibration of results using high-resolution data (Morton *et al.*, 2005; Hansen *et al.*, in press). Finally, due to differences in methodology, deforestation results from this study cannot be directly compared to results from other methods that identify deforestation based on imagery from a single year (e.g., INPE, 2007; Hansen *et al.*, 2008).

4.6 Conclusions

This study examined the interannual variability in understory fire damages and deforestation for a study region in southern Amazonia using a time series of satellite data. In total, understory forest fire damages during 1999-2005 were as extensive as deforestation during 2001-2006. Forest burning identified by the BDR algorithm was not the initial phase of forest conversion, as deforestation rates for unburned forest were actually higher than rates estimated for previously-burned forest

areas. Interannual variability in the extent of burned forest was large, and widespread fire damages were mapped in both dry and wet years. Therefore, results from this study suggest that drought conditions may not be necessary for extensive forest fire damages in southern Amazonia.

Repeated fire activity in previously-burned forests was common, and over 20% of all fire-damaged forest in the study burned more than once during 1999-2005. Satellite-based estimates of vegetation greenness decreased between first and second fires, but recovery of mNDVI in the year after fire damages was comparable among areas burning for the first, second, and third times. While recurrent fire damages did not lead to evidence of savannization in satellite-based measures of vegetation greenness, frequent understory fires in previously-burned forests provides satellite-based evidence of a positive fire feedback in southern Amazon forests. Forest succession following fire damages may therefore promote a positive fire feedback in burned forests through changes in forest structure and composition.

Chapter 5: Modeling Long-Term Changes in Amazon forest Structure from Repeated Exposure to Land-Use Fires

5.1 Summary

Anthropogenic understory fires lead to a short-term increase in Amazon forest flammability. Whether previously-burned forests become trapped in an early-successional state, similar to secondary forests, depends on the rates of recurrent fire exposure and forest recovery. This chapter describes the development of a new height-structured fire sub-model for the Ecosystem Demography (ED) model to evaluate long-term changes in forest structure and composition from a positive fire feedback in southern Amazon forests under a range of land-use scenarios. ED models vegetation height and the fraction of the landscape in short vegetation, and these attributes were used to develop estimates of fire risk and fire spread, respectively, in the new fire sub-model. Satellite-based estimates of canopy damage from understory fires (Chapter 4) and selective logging were used to calibrate model scenarios of continued land use in the Xingu basin study area over decadal and century timescales. To quantify the specific impacts from fire, model scenarios with combined disturbances from selective logging and understory fires were compared to a scenario with only selective logging. In this study, all scenarios were run under constant current climate to focus on the impact of recurrent fire damages on forest structure rather than feedbacks from climate variability on fire risk. Combined impacts from a century of selective logging and fire spread decreased total forest biomass in the upper Xingu basin by 46% (0.4 Pg C) and doubled the fraction of biomass in early-

successional trees compared to the forest control scenario. Change in forest biomass from the Logging scenario was intermediate between Century scenarios with and without fire spread, emphasizing the importance of fire spread for maintaining a positive fire feedback under current rates of fire ignitions. Scenarios in this study are likely to be conservative since they do not include additional forest losses from deforestation or potential increases in forest flammability from changes in climate. Future work is needed to incorporate climate-related feedbacks on forest flammability in order to assess the relative contributions from a positive fire feedback and climate change to potential Amazon forest dieback.

5.2 Introduction

Several models have suggested that large-scale dieback of Amazon forests may occur during this century due to positive feedbacks with global and regional climate (Werth & Avissar, 2002; Cox *et al.*, 2004; Malhi *et al.*, 2008). A positive feedback between warming climate from increasing greenhouse gas concentrations and terrestrial carbon losses from respiration accelerates the loss of tropical forest from the Amazon region in some general circulation models (GCMs) (Cox *et al.*, 2000; Cox *et al.*, 2004) but not others (e.g., Zeng *et al.*, 2004; Friedlingstein *et al.*, 2006). Additional deforestation for agriculture may also destabilize the strong coupling between vegetation and local rainfall, leading to forest dieback if the spatial pattern or total quantity of deforestation interrupts regional precipitation patterns (Zeng *et al.*, 1996; Werth & Avissar, 2002; Oyama & Nobre, 2003; Soares-Filho *et al.*, 2006). However, neither the carbon-cycle nor land-use feedback with climate

consider direct impacts from land use on forest cover such as fragmentation, selective logging, or fire that may enhance Amazon dieback.

A third positive feedback mechanism that may accelerate forest loss in Amazonia is the increased fire risk from changes in forest microclimate and fuels following initial understory fire exposure (Cochrane & Schulze, 1999). Canopy damage from fire increases the amount of light reaching the forest floor, drying leaf litter and other fuels that promote fire spread (Holdsworth & Uhl, 1997; Cochrane & Schulze, 1999). Woody debris from fire-killed trees and rapid regrowth of herbaceous vegetation, lianas, seedlings, and tree sprouts in canopy gaps following fire also increases the amount of available fuels for future fires (Uhl & Buschbacher, 1985; Kauffman, 1991; Cochrane & Schulze, 1999; Gerwing, 2002; Monteiro *et al.*, 2004; Balch *et al.*, 2008; Barlow & Peres, 2008). Recurrent exposure to land-use fires in previously-burned forests leads to additional loss of canopy and understory trees, especially newly-established pioneer tree species with low fire tolerance (Ivanauskas *et al.*, 2003; Barlow & Peres, 2008), perpetuating fire risk by reinitiating forest succession. The positive feedback ends when regrowth and infilling from adjacent trees closes canopy gaps from previous fires and reestablishes a moist forest microclimate resistant to fire spread (Holdsworth & Uhl, 1997; Cochrane, 2003). Thus, the competing mechanisms in this feedback are the frequency of understory forest fires and rate of gap closure in fire-damaged forests. Initially referred to as "savannization" (Cochrane *et al.*, 1999), this feedback has recently been characterized as "secondarization" since recovery of woody vegetation (dominated by pioneer tree species) in burned forests is more similar to secondary forest than savanna (Chapter

4; Barlow & Peres, 2008). The potential for widespread conversion of tall, closed-canopy forest into short stands dominated by early-successional tree species could reduce biodiversity associated with mature forests (Barlow & Peres, 2006; Peres *et al.*, 2006) and net carbon storage in Amazon forests, enhancing carbon-cycle feedbacks with climate (e.g., Friedlingstein *et al.*, 2006).

Understanding the impacts from recurrent land-use fires on Amazon forest structure, species composition, and carbon storage necessitates the use of an ecosystem model, yet no existing model has addressed these questions. Fire is a critical determinant of vegetation distribution worldwide (Bond *et al.*, 2005), but many ecosystem models do not include disturbance from fire, including the TRIFFID model used in the Hadley Centre GCM (Cox, 2001). Other ecosystem models link forest fire damage to soil or fuel moisture (e.g., Sheffield Dynamic Global Vegetation Model (DGVM), Bond *et al.*, 2005), total above-ground biomass (TAGB), or both (e.g., Ecosystem Demography (ED), Moorcroft *et al.*, 2001). However, in humid forest types, fuel moisture limits fire risk despite large stocks of TAGB (Saatchi *et al.*, 2007).

Recently, the influence of land use on forest fire risk has been incorporated into process-based ecosystem models. Several models now include anthropogenic fire ignitions, based on proxy variables such as population density, and variable fire spread with changing climate following approaches developed by Rothermel (1972) (e.g., (Lund-Potsdam-Jena (LPJ-DGVM), Thonicke *et al.*, 2001; Venevsky *et al.*, 2002, C. Prentice, personal communication), (Canadian Terrestrial Ecosystem Model (CTEM), Arora & Boer, 2005), and (ED3, G. Hurtt, personal communication)). The

ED model has also been modified to include fire suppression (Girod *et al.*, 2007). Of this new class of ecosystem models that have been used to study anthropogenic fires, only the ED model includes height-structured vegetation. Therefore, the ED model was chosen to explore the increased fire risk in previously-burned Amazon forests as a function of vegetation height, forest structure, and anthropogenic ignitions.

This chapter presents the initial steps towards mechanistic representation of the positive fire feedback in Amazon forests using the ED model. A new height-structured fire sub-model was developed in this study that explicitly accounts for anthropogenic ignitions and increases in fire risk from changes in forest structure following selective logging and understory fires. Key aspects of the fire feedback mechanism, such as partial canopy mortality from fire and the duration of increased fire risk following previous burning, can be modeled directly using ED because the model tracks the fate of individual forest gaps. ED also estimates the fraction of the landscape in each size class and age since last disturbance, and this information was used to determine the amount of fire spread between forest patches. The new fire model was implemented in the original version of ED that was specifically parameterized for the Amazon region (Moorcroft *et al.*, 2001). In this study, ED was run with the height-structured fire sub-model under scenarios of constant current climate in order to focus on the impact of recurrent fire damages on forest structure rather than feedbacks from climate variability on fire risk.

The goal of this work was to estimate the change in carbon storage and forest composition from selective logging and recurrent fire exposure over decadal and century time scales for a study area in southern Amazonia. Satellite-based estimates

of selective logging (Asner *et al.*, 2005) and the average annual extent of canopy damage from fire in Chapter 4 were used to parameterize current rates of land use in ED. Results from land-use scenarios were compared to a forest control scenario without land use to assess the short (10-year) and long-term (100-year) impacts from selective logging and recurrent fire exposure on forest structure, composition, and total biomass. To quantify the specific impacts from fire in southern Amazon forests, model scenarios with combined disturbances from selective logging and understory fires were compared to a scenario with only selective logging. Finally, model scenarios at both time scales were used to assess the potential for a positive fire feedback based on the fraction of the landscape in a fire-prone forest structure.

5.3 Methods

5.3.1 Ecosystem Demography (ED)

ED is an individual-based terrestrial ecosystem model, formulated as a plant simulator coupled to established sub-models of below-ground hydrology and decomposition (Hurtt *et al.*, 1998; Moorcroft *et al.*, 2001). Individuals of different plant functional types (PFTs) compete in ED for local light, water, and nutrients. ED differs from most other large-scale terrestrial models by formally scaling up physiological processes through vegetation dynamics to ecosystem scales, while simultaneously modeling natural disturbances, land use, and the dynamics of recovering lands (Moorcroft *et al.*, 2001; Hurtt *et al.*, 2002; Hurtt *et al.*, 2004). The mathematical scaling approach in the ED model approximates the proportion of the landscape in each size class, PFT, and time since last disturbance using two partial

differential equations (Hurtt *et al.*, 1998; Moorcroft *et al.*, 2001). Therefore, the model can be conceptualized as running at two different scales—one at the scale of an individual canopy tree or canopy-tree gap (e.g., 15m x 15m) and a larger scale at which all gaps have the same prescribed climate and soils (e.g., 1° x 1°) and exogenous disturbances such as fire control influence sub-grid scale heterogeneity in the size and age of individual gaps.

Two key attributes of the ED model for the study of a positive fire feedback in Amazon forests are height-structured vegetation within each forest gap and the ability to track recovery from disturbance at the landscape scale. These two components of the fire feedback mechanism, the influence of forest structure on fire risk and the competing rates of disturbance frequency and vegetation recovery that maintain fire risk, have not previously been assessed using an ecosystem model.

This study uses the initial version of the ED model developed for the Amazon region (Moorcroft *et al.*, 2001). The model includes four PFTs: grass and early (ES), mid (MS), and late-successional trees (LS). All ED model runs were conducted with climate and soils data at 1° x 1° resolution from the International Satellite Land Surface Climatology Project (ISLSCP) Initiative I (Meeson *et al.*, 1995). Similar to Moorcroft *et al.* (2001), average climate from 1987-1988 was used for all model years.

5.3.2 Fuels

In the original ED fire sub-model, fire risk increased linearly with TAGB (Moorcroft *et al.*, 2001). Field studies in savanna and tropical forest environments support the importance of fuel buildup for fire risk (Govender *et al.*, 2006; Balch *et*

al., 2008), but fuel moisture, which may limit fire spread in tropical forests (Ray *et al.*, 2005), has a non-linear relationship with forest height and TAGB (Uhl & Buschbacher, 1985; Holdsworth & Uhl, 1997; Cochrane & Schulze, 1999; Ray *et al.*, 2005). Further, because understory fires in Amazon forests only consume a portion of available leaf litter, coarse woody debris, and short understory vegetation (Cochrane *et al.*, 1999; Balch *et al.*, 2008), fuel availability is also height dependent. Therefore, this study builds a new fuel-fire sub-model to address the non-linear aspects of fire risk with forest structure in the ED model.

5.3.3 Height-Structured Fire Sub-Model

This section describes the development of a new fire sub-model for ED that specifically accounts for variations in fire risk according to fuel height, canopy structure, and human land use ignitions. The new height-structured fire sub-model has three components: fuel amount (F_a), fuel quality (F_q), and fire ignitions (F_i):

$$\lambda_F(y,t) = \sum_{y=1}^{Q} 1 - e^{-FaFqFi} \qquad (5\text{-}1)$$

In this formulation, the fire disturbance rate (λ_F) in patch y at time t is summed over all gaps (Q) within the patch. As in the original fire model, annual fire disturbance for each grid cell is calculated as the area-weighted average of λ_F in each patch during the year.

The components of the fire model are defined as follows:

$$F_a(y,t) = C_1 + \sum_{i=1}^{R_y} B_a * \left(\frac{1}{h^2}\right) \qquad (5\text{-}2)$$

F_a combines all biomass in the fast soil carbon pool (C_1), comprised primarily of leaf litter, with a fraction of the biomass in short plants based on tree height (h). Individual plants (R) ≤5 m contribute a fraction of their above-ground biomass (B_a) to F_a. Fuel development is non-linear over time. In the oldest patch, F_a peaks 10-15 years following model initiation (Figure 5-1). Survivorship from understory fires also depends on height. Mortality of individual plants <5 m is 100%, consistent with reports from field studies of highest mortality in small diameter classes (e.g., Haugaasen *et al.*, 2003). Trees >5 m in height have a 50% mortality rate from fire, similar to the high end of the published range for initial fires, but lower than mortality

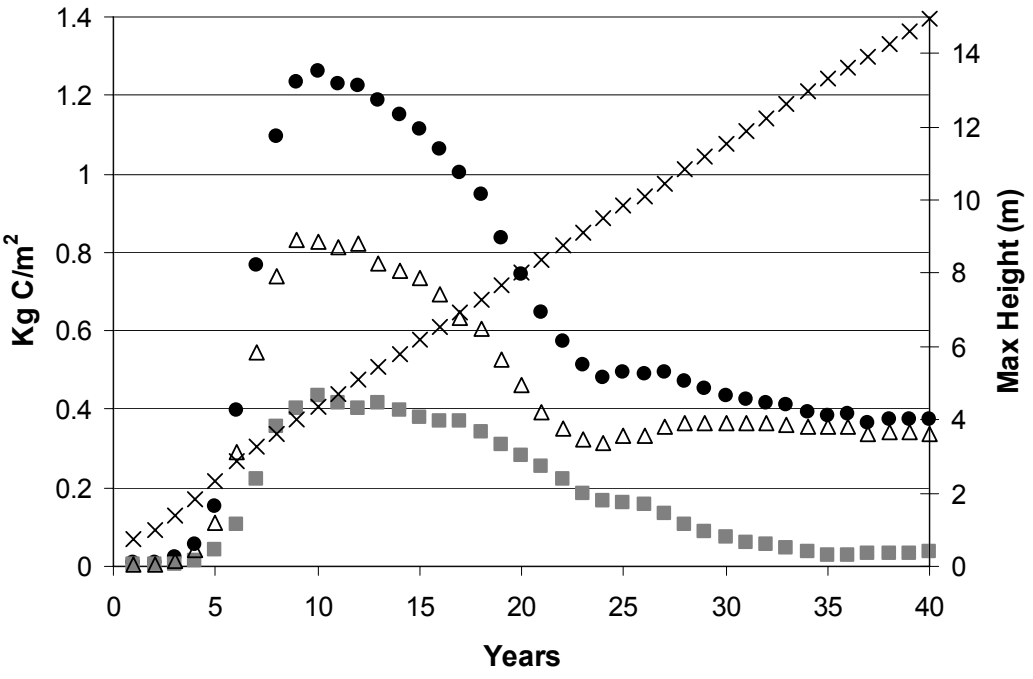

Figure 5-1: Fuel amount (●, kg C/m^2) in the oldest forest patch from model initiation to 40 years. Fuel amount is calculated as the sum of fast soil carbon (Δ) and a fraction of the biomass in short vegetation (■). Maximum height (X) in the patch is shown on the secondary y-axis.

rates of repeated burning of fire-damaged forests (Holdsworth & Uhl, 1997; Cochrane & Schulze, 1999; Gerwing, 2002; Barlow & Peres, 2008). Fire-killed canopy trees are added to soil carbon pools.

F_q is defined as a function of average canopy height per patch ($\bar{h}$), calculated as the mean height of all cohorts:

$$F_q(y,t) = 10 * e^{-0.23\bar{h}} \quad (5\text{-}3)$$

Previous versions of the ED model have also included a link to seasonal water stress as an indicator of fuel quality and fire risk (Moorcroft *et al.*, 2001; Hurtt *et al.*, 2002). Water stress was excluded from this version of the height-structured fire sub-model because 1) this study considered the risk and impact of fire under constant climate conditions, 2) climate at 1° x 1° resolution was relatively homogenous across the study site, and 3) the importance of drought or other climate factors for understory fire risk in southern Amazonia remains uncertain (Chapter 4). The exponential function was implemented to scale $F_q = 1$ when $\bar{h} = 10$ m based on previous findings about the influence of canopy height on forest microclimate and fire spread in eastern Amazonia (Uhl & Buschbacher, 1985; Uhl & Kauffman, 1990; Ray *et al.*, 2005). In addition to canopy height and precipitation, Ray *et al.* (2005) also linked fire spread rate to leaf area index (LAI). Like many ecosystem models, ED does not generate a realistic representation of seasonal changes in LAI over Amazon forests (Saleska *et al.*, 2003; Huete *et al.*, 2006; Ichii *et al.*, 2007). Therefore, this version of the fire model uses canopy height as a proxy variable for insolation rather than directly calculating seasonal light levels based on LAI.

F_i is a measure of fire ignitions from land use. In this study, F_i is implemented as a step function linked to land-use activity:

$F_i = 0.03$ if land use is present, otherwise (5-4)

$F_i = 0$

F_i was set to reproduce current rates of understory fire in Chapter 4 (as described in section 5.3.6). F_i could also be parameterized directly from satellite-based fire detections (e.g., Chapter 2) or linked to scenarios of deforestation and land management (Soares-Filho *et al.*, 2006). This initial parameterization for F_i results in peak fire risk 5-10 years following canopy disturbance, and the fire disturbance rate in logged patches remains elevated for several decades compared to intact forest areas (Figure 5-2).

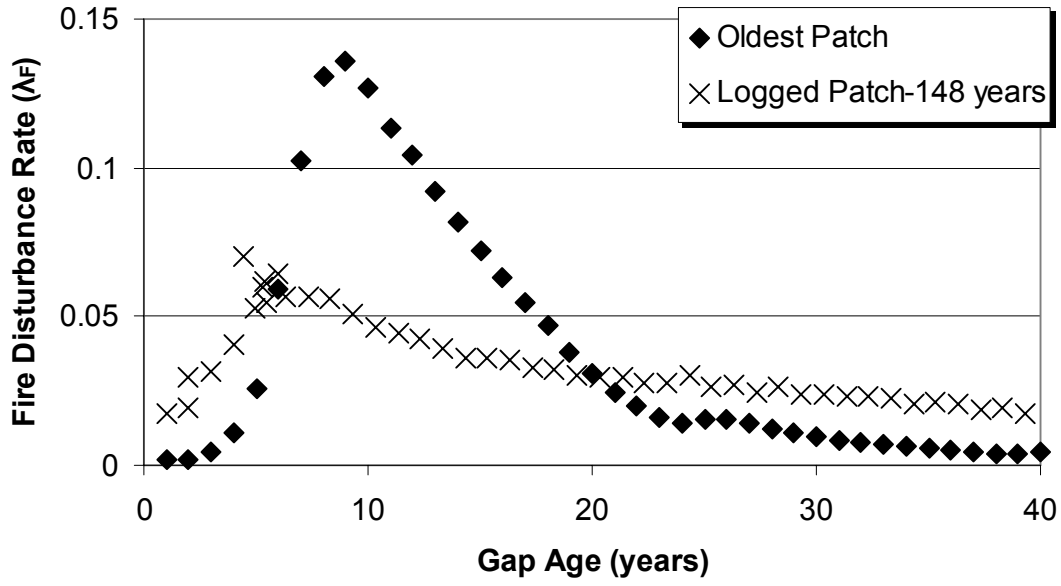

Figure 5-2: Fire disturbance rate (λ_F) from the new height-structured fire sub-model for two patches, the oldest patch (created at time = 0) and a patch resulting from selective logging at time = 148 years.

5.3.4 Fire Spread

ED is a pseudo-spatial, individual-based ecosystem model; the composition and height structure of vegetation within each gap are known, but the x and y locations of each tree and gap within a forest patch are not known (Moorcroft *et al.*, 2001). The pseudo-spatial nature of ED therefore influences the representation of inherently spatial processes such as fire spread. In this study, two model formulations were used to bracket the potential range of fire spread between forest patches. The first formulation is similar to the original fire model described by Moorcroft *et al.* (2001); a fire that begins in any patch spreads equally to all patches. Throughout the study, this model formulation is simply described as "spread." The second formulation considers the opposite case, "no spread," in that a fire may only burn a fraction of the patch in which it begins. The "no spread" model formulation therefore emphasizes the importance of a positive fire feedback because only patches that become flammable due to selective logging or previous understory fires are burned at each time step. The following section describes the calculation of fire damages in spread and no-spread scenarios in more detail.

The new height-structured fire sub-model was implemented with and without fire spread. For ED model runs with fire spread, all patches contribute to the calculation of the fire disturbance rate (λ_F) for the grid cell according to their canopy height (Fq) and fuel amount (Fa) when ignitions are present (Fi). If land-use fires occur in the grid cell, all patches are equally affected because all patches are equally interconnected (Moorcroft *et al.*, 2001). For ED model runs without fire spread, λ_F was calculated and applied locally to each patch. In reality, fire damages in Amazon

forests exhibit both tendencies. Satellite-based results in Chapter 4 suggest that half of the area of fire-damaged forest in recent years was a result of fire spread into unburned forests. However, evidence for higher fire risk in previously-burned forests from satellite-based studies (Chapter 4) and field surveys (e.g., Alencar *et al.*, 2004) is consistent with the implementation of the fire model in ED without fire spread.

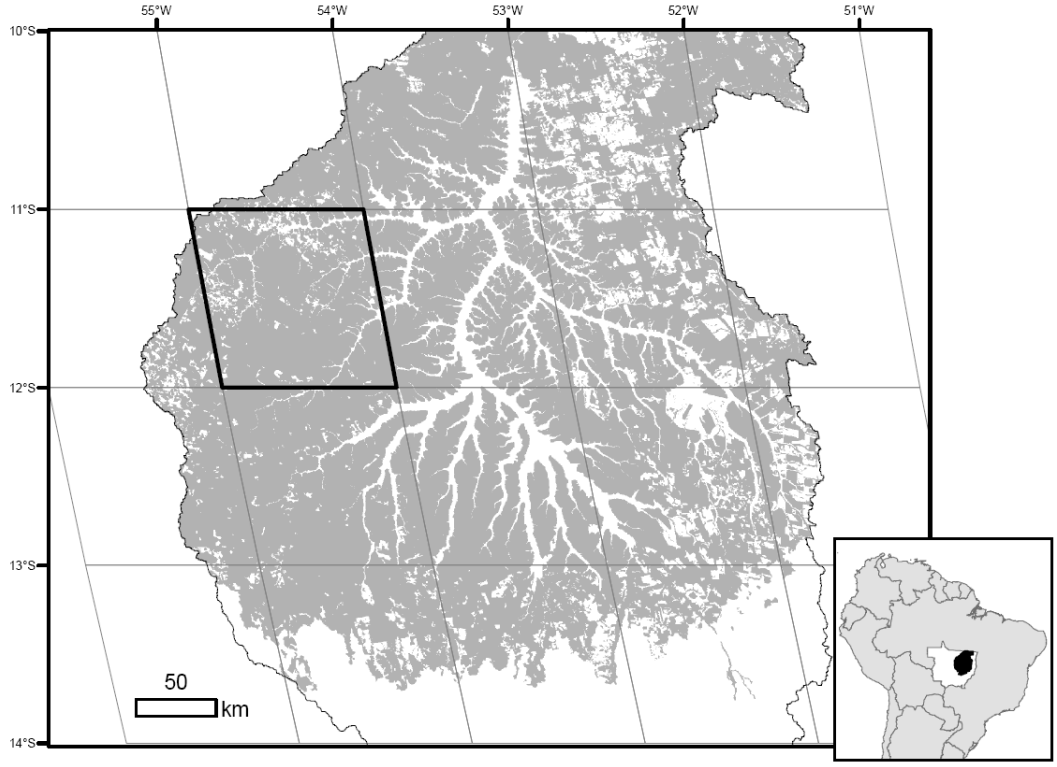

Figure 5-3: Forested areas in 2000 (gray) and 1° x 1° ED model grid cells within the Xingu River basin (black) in the Brazilian state of Mato Grosso (inset, white). Detailed modeling runs were conducted for a single model cell near Sinop, Mato Grosso (11.5° S, 54.5° W, dark black outline).

5.3.5 Study Area

This study evaluated the changes in forest structure and composition from scenarios of land use for a study area in the Brazilian State of Mato Grosso (Figure 5-3). The upper Xingu River basin study area included 97,690 km^2 of forest in 2000 (Chapter 4). ED model results for each 1° x 1° grid cell (e.g., basal area) were multiplied by the forested area in each grid cell in 2000 to generate forest area-weighted average values for the entire Xingu study region. Three model variables were calculated at this scale: total biomass, fraction of biomass in ES trees, and basal area.

One model cell near the city of Sinop was also chosen for detailed model runs of monthly vegetation dynamics that could not be easily assessed at the larger scale (Figure 5-3). Results for the Sinop study site illustrate the evolution of changes in forest structure and composition in each scenario. The detailed model results were also used to evaluate short-term changes in biomass, net ecosystem productivity (NEP), and forest composition. Finally, model output for the Sinop site was used to characterize relative changes in canopy height and patch ages among scenarios because these variables are not included in the regional output. Sinop model runs were only used for relative comparisons and were not scaled to represent a specific forest area.

5.3.6 Calibration: Current Rates of Logging and Understory Fires

A combination of satellite and field-based studies were used to parameterize the rates of selective logging and understory fire damages for scenarios of land use. The average rate of selective logging in the Xingu study area during 2000-2002 was

3.1% yr^{-1} (Asner *et al.*, 2005). Data for selective logging during 1999-2000 were excluded from the calculation of current logging rates based on substantial overlap between logging and burning in that year (Chapter 3). The relationship between satellite-based estimates of logged area and field measurements of canopy gap fraction were used to translate logging rates into canopy gaps as represented in the ED model (Asner *et al.*, 2002; Asner *et al.*, 2004). Selective logging includes canopy damage from harvesting individual trees (mean = 3-7 trees ha^{-1}, Asner *et al.*, 2005) and ground damages from skid trails, roads, and log decks (patios). The range of total area-integrated gap fraction from conventional and reduced-impact logging was 5-22% (Asner *et al.* 2002), and the high end of this range was used to estimate the increase in canopy damage from current rates of selective logging (3.1% logged x 22% gaps within the logged area = 0.07%). Therefore, 2.1% of the study area experienced treefall gaps during each year in scenarios with selective logging (1.4% background mortality + 0.07% canopy mortality from logging). Average rates of canopy damage from understory fires were derived from MODIS-based results of the total fire-damaged forest during 1999-2005 in Chapter 4 (2.4% yr^{-1}). In model tests for the Sinop site, a fire ignition rate (*Fi*) of 0.03 led to a fire disturbance rate of approximately 2.4% per year when combined with selective logging at 2.1% per year. In all scenarios with fire, the annual rate of fire ignitions was held constant. However, rates of fire disturbance varied over time depending on the amount of fire-prone forest in each scenario.

5.3.7 Land-Use Scenarios

Four land-use scenarios were developed to evaluate the impact of selective logging and understory fire damages at current rates over decadal and century time scales:

- **1. Forest Control**: No land use, canopy-tree gaps from natural disturbances occur at a rate of 1.4% yr^{-1} (Moorcroft *et al.*, 2001).
- **Business as usual (BAU)**: Forest disturbances from selective logging (**2. Logging**) or combined damages from selective logging and understory fires (with fire spread (**3. Fire Spread**) and without fire spread (**4. Fire no-spread**), as described in Section 5.3.4) occur at current rates over two time scales:
    a. **Century**: Canopy damage from selective logging and understory fires begins in model year 100 and continues until the end of the model period (year 200).
    b. **Decade**: Canopy damage from selective logging and understory fires begins in model year 100 and continues for 10 years at present rates (model years 100-110). In model years 111-200, no land use occurs and canopy-tree gaps only occur from natural disturbances (1.4% yr^{-1}).

BAU scenarios of Logging, Fire Spread, and Fire no-spread were run for decadal and century timescales for a total of seven model runs (six land-use scenarios and the Forest Control). At the end of each model scenario (e.g., time = 200 years), the relative changes between the Forest Control and land-use scenarios were assessed

regarding total forest biomass, the fraction of the total biomass in ES trees, and attributes of forest structure such as mean canopy height and age since last disturbance. For the decade scenarios, the Sinop study site was used to consider the change in biomass between control and land-use scenarios at year 110, the duration of biomass recovery after land use ended, and the short-term impacts from disturbance on NEP.

ED was used to derive the initial distribution of forest heights and ages for each land use scenario in the Sinop and Xingu study areas based on potential vegetation at year 100. For comparison, one scenario (Century Spread) was run with land use beginning in year 1, 25, 50, 100, and 200 to test the sensitivity of model results to initial forest conditions.

5.3.8 Biomass Validation

Modeled above-ground live biomass (AGLB) from ED for the Xingu study region was compared to a recent satellite-based estimate of AGLB for the Amazon region (Saatchi *et al.*, 2007). Total above-ground biomass in ED was converted from kg C/m^2 to AGLB assuming forest biomass is 50% C by weight. Since Saatchi *et al.* (2007) included data from the MODIS sensors through 2004 in their calculation of forest biomass, MODIS-based deforestation estimates from Chapter 4 were used to exclude areas that were deforested during 2000-2004 before calculating average forest biomass in each 1° x 1° grid cell. Saatchi *et al.* (2007) classified AGLB into 11 categories; the high end of the AGLB range for each class was chosen to estimate average biomass of forested areas in 2004.

5.4 Results

5.4.1 Xingu Biomass

Estimated AGLB in ED was very similar to satellite-based estimates for the Xingu study area (Figure 5-4). The range of biomass values for all 1° x 1° grid cells was consistent between approaches (ED: 103-170 Mg/ha, Saatchi *et al.*: 83-180 Mg/ha). Overall, the forest area-weighted average AGLB in the Xingu study area from ED (135.4 Mg/ha) was 9% lower than the satellite-based approach (149.2 Mg/ha).

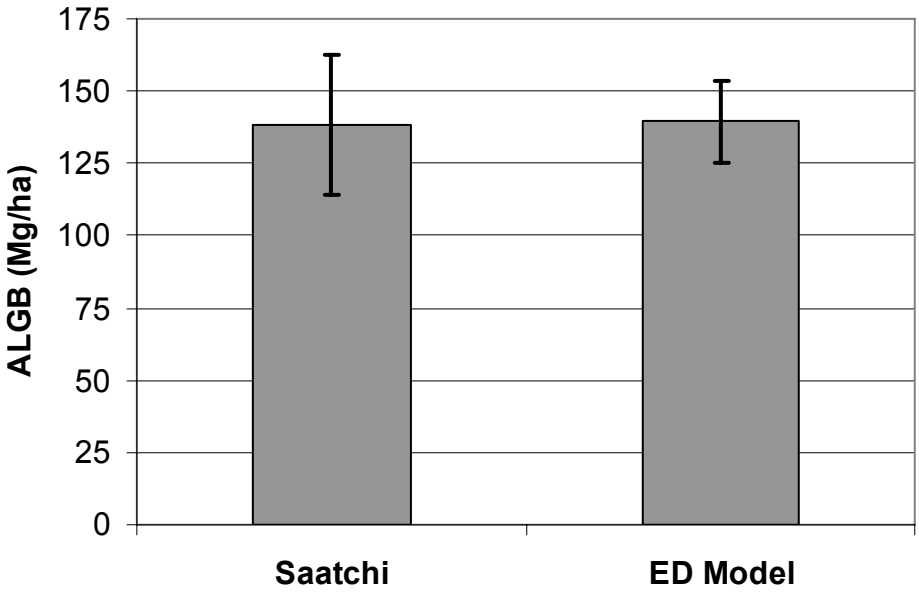

Figure 5-4: Comparison of mean (± 1 S.D.) above-ground live biomass (AGLB) from ED to satellite-based estimates of AGLB from Saatchi *et al.* (2007) for all 1° x 1° grid cells in the Xingu study region.

5.4.2 Century Scenarios

Century land-use scenarios of selective logging and understory fire reduced total biomass in the study area by 0.19-0.4 Pg C (22-46%) compared to the Forest Control scenario (Table 5-1). The greatest reduction in total biomass occurred for the Century Spread scenario, which was 46% lower than the Forest Control scenario, and approximately 30% lower than either the Logging scenario or the Century scenario without fire spread (Table 5-1). Figure 5-5 shows the evolution of changes in above-ground biomass for each model scenario at the Sinop site to a similar end point as in Table 5-1.

Table 5-1: ED model results in year 200 for the Xingu study area from Forest Control and land-use scenarios. Values for total biomass, fraction of biomass in early-successional (ES) trees, and basal area in year 200 were calculated as forest area-weighted means from all 1° x 1° grid cells in the Xingu study area. Values for mean canopy height and age since last disturbance were only calculated at the Sinop site for each scenario.

Model Scenarios	Total Biomass (Pg C)	ΔBiomass (% of Control)	% Biomass in ES Trees	Basal Area (m^2/ha)	Mean Canopy Height (m)*	Mean Age Since Last Disturbance (years)*
Control	0.871	X	31.1	25.1	10.2	66.6
Decade Spread	0.859	-1.4%	33.1	25.0	9.5	62.9
Decade (no spread)	0.854	-2.0%	32.6	24.9	9.9	65.5
Logging	0.64	-26.6%	45.6	21.0	8.5	47.9
Century Spread	0.468	-46.3%	58.4	16.9	8.4	22.6
Century (no spread)	0.68	-22.0%	41.0	21.5	9.0	46.4

* Mean canopy height and age singe last disturbance were calculated at the Sinop study site.

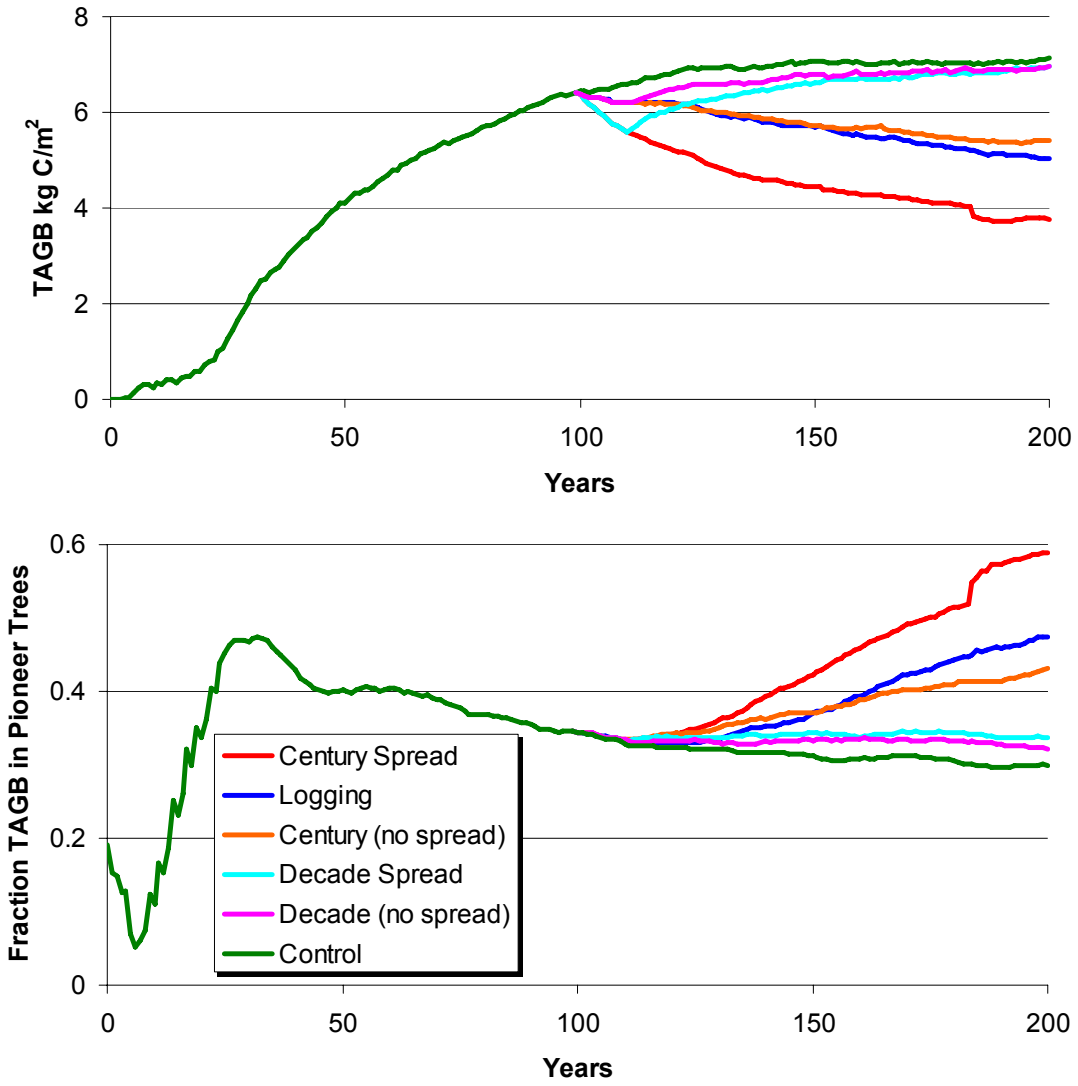

Figure 5-5: Annual total above-ground biomass (TAGB, top) and the fraction of TAGB in pioneer (early-successional trees) (bottom) for the Sinop site from the forest Control scenario and five 'Business as Usual' land use scenarios calibrated based on current rates of logging and understory fire damage.

A century of land use at current rates also led to large changes in forest composition, measured as the fraction of all forest biomass in ES (pioneer) trees (Table 5-1). For the Century Spread scenario, the fraction of biomass in pioneer trees

was nearly double that of the Forest Control in year 200 (Table 5-1). The Century no-spread scenario increased the fraction of biomass in ES trees during the first 50 years of land use compared to the Logging scenario (Figure 5-5), but Logging ultimately led to a higher fraction (45.6%) of forest biomass in ES trees (Table 5-1).

Changes in forest structure from land use were also most pronounced in the Century Spread scenario, with a 33% decline in average basal area and 19% reduction in mean canopy height relative to the Forest Control (Table 5-1). However, high canopy mortality during logging disturbances (100% for trees >10 m) led to a similar decrease in mean canopy height (8.5 m). Mean basal area was similar between Logging and Century no-spread scenarios.

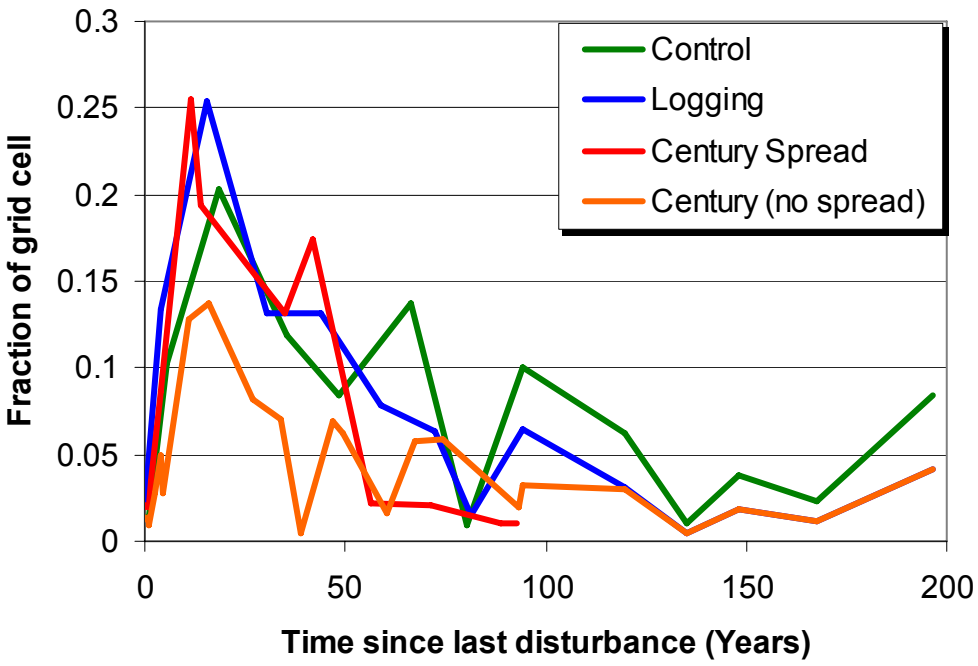

Figure 5-6: Distribution of patch age since last disturbance in year 200 for Century scenarios at the Sinop study site.

The mean age since last disturbance was similar between the Logging and Century no-spread scenarios (Table 5-1), but the fraction of the landscape in patches <30 years since last disturbance differed between scenarios. The Century no-spread scenario led to three types of forest patches at the Sinop site in year 200 (Figure 5-6). Half of the study site was in patches <30 years since last disturbance, 40% were age 30-100, and approximately 10% of the landscape was in patches that were not disturbed by land use (>100 years since last disturbance). In contrast, in the Logging scenario only 41% of the site was in patches <30 years since last disturbance and 11% were older than 100 years. Fire spread had the largest impact on mean age since last disturbance (Table 5-1); 63% of the study site was in patches <30 years since last disturbance and no patches were older than 100 years.

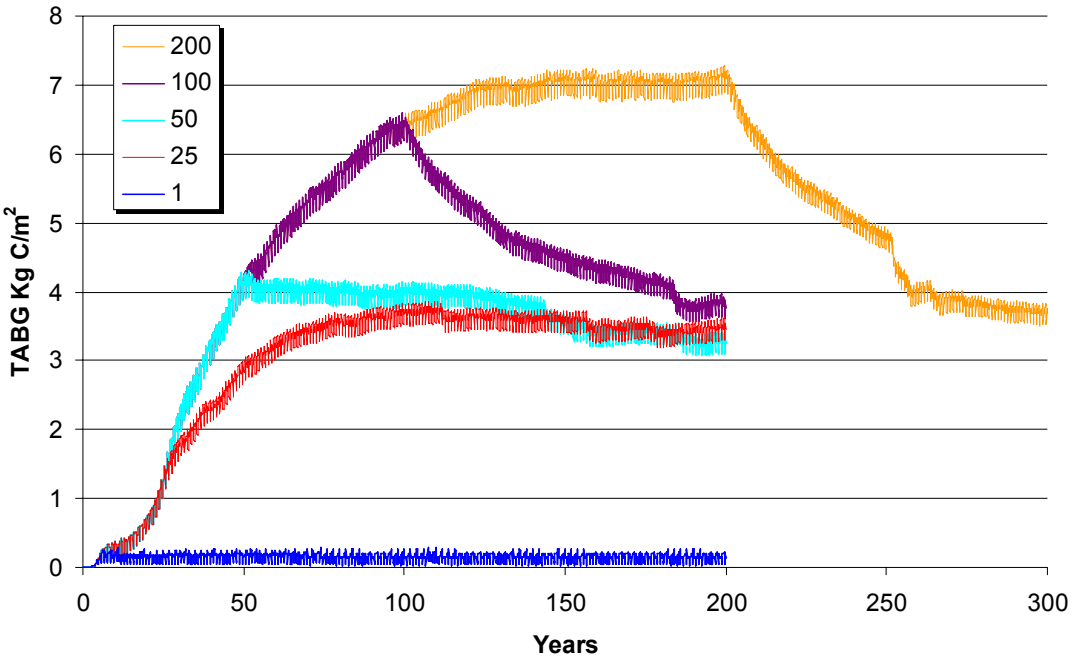

Figure 5-7: Total above-ground biomass (TAGB) at the Sinop study site under the Century Spread scenario with land use beginning in year 1, 25, 50, 100, and 200.

In order to test the sensitivity of model results to initial forest conditions, the Century Spread scenario was run with land use beginning in different years (Figure 5-7). Initiating land use during the first model year prevented trees from becoming established at the Sinop site (Figure 5-7). Trapping the entire study site in low vegetation was not possible once trees became established. Instead, initiating land use in year 25-200 led to a new equilibrium state of ~3.5 kg C/m^2 in all Century Spread scenarios based on the current rate of fire ignitions, F_i. The number of years of land use required to reach this new equilibrium did vary from approximately 60 years when land use was initiated in young forests (≤50 years) or old forests (200 years) to 85 years when land use was initiated in year 100.

5.4.3 Decade Scenarios

Land use in the Decade scenarios at the Sinop site led to short-term reductions in above-ground biomass and NEP (Figure 5-8). Biomass returned to pre-land use levels after logging and fire ceased, but the duration of biomass recovery differed between Decade scenarios with fire spread (25 years) and without fire spread (7 years). By year 200, the difference in total biomass between the Decade scenarios and the Forest Control was ≤2% (Table 5-1). NEP decreased to near 0 by the end of the land-use decade in the scenario with fire spread. Compared to the forest control, average annual NEP for the decade was 48% and 31% lower for scenarios with and without fire spread, respectively (Figure 5-8).

The major impact from a decade of land use was the increase in the fraction of the landscape in recently-disturbed patches (Table 5-2). In the Decade Spread scenario, nearly 60% of the Sinop site was in patches <30 years old in year 110, and

43.9% of the site was in patches disturbed by land use (<10 years old, Table 5-2). Changes in forest structure and landscape composition were similar for Decade no-spread and Logging scenarios in year 110. Mortality of large trees from land-use

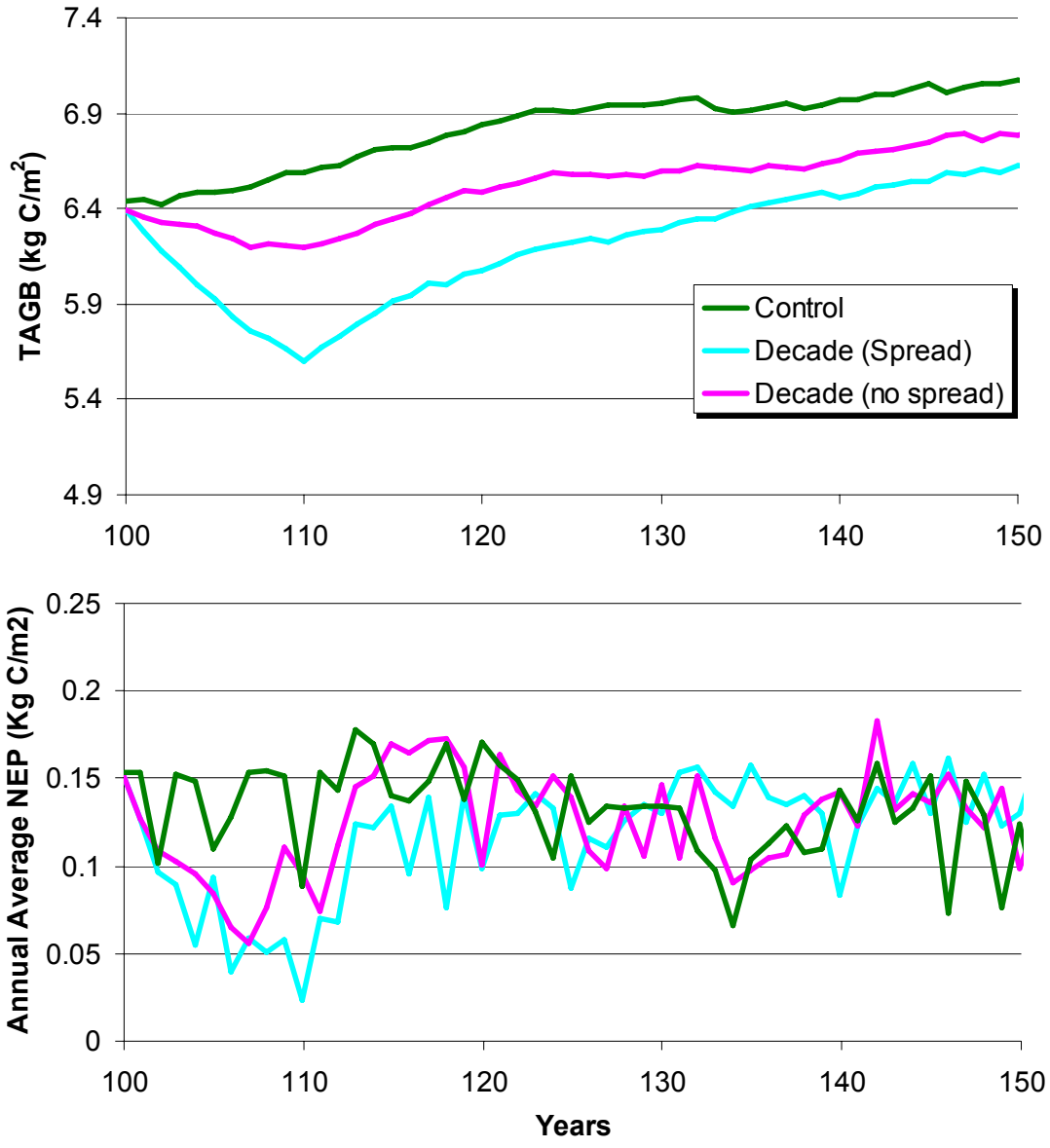

Figure 5-8: Total above-ground biomass (TAGB, top) and net ecosystem production (NEP, bottom) for Control and Decade scenarios of land use with and without fire spread at the Sinop study site.

Table 5-2: ED model results for the Sinop study site from Forest Control, Logging, and Decade land-use scenarios in year 110.

Model Scenarios	Basal Area (m^2/ha)	Mean Canopy Height (m)	Mean Age Since Last Disturbance (years)	<30 Years Since Last Disturbance	<10 Years Since Last Disturbance
Control	25.0	8.0	55.7	45.2%	23.4%
Logging	23.8	7.7	51.9	49.3%	29.0%
Decade Spread	21.5	7.7	42.6	59.2%	43.9%
Decade (no spread)	23.5	7.7	51.6	49.3%	20.9%

decreased the mean basal area in all land-use scenarios relative to the Forest Control in year 110 with the greatest decrease for the Decade Spread scenario.

Changes in forest structure and composition from land use in the Decade scenarios at the Sinop site were still evident at the end of the model period (Table 5-1, Figure 5-5). Compared to the forest control scenario, the Decade Spread scenario at the Sinop site had lower mean canopy height (-6.9%) and a higher fraction of biomass in ES trees (3.7%, Figure 5-5). The Decade scenario without fire spread had 3% lower mean canopy height and 3.2% higher fraction of biomass in ES trees than the control (Table 5-1, Figure 5-5). Across the entire Xingu study area, differences in the fraction of biomass in ES trees for Decade Spread and no-spread scenarios were slightly lower than at the Sinop site (2% and 1.5%, respectively, Table 5-1).

5.5 Discussion

This chapter describes a new height-structured fire sub-model for the ED model that mechanistically reproduces a positive feedback from selective logging and land-use fires in Amazon forests. Results from model scenarios with current rates of selective logging and understory fires demonstrate that impacts from continued land use on forest structure, composition, and carbon storage may be large. Combined impacts from a century of selective logging and fire spread decreased total forest biomass in the upper Xingu basin by 46% (0.4 Pg C) and doubled the fraction of biomass in ES trees compared to the Forest Control scenario. Change in forest biomass from the Logging scenario was intermediate between Century scenarios with and without fire spread, emphasizing the importance of fire spread for maintaining a positive fire feedback under current rates of selective logging and fire ignitions. The results from this study suggest that widespread secondarization of Amazon forests is possible through a positive fire feedback in logged and burned forests following a century of land use at current rates. Reductions in net carbon storage from frequent fire damages could therefore enhance carbon-cycle climate feedbacks (Friedlingstein *et al.*, 2006). Finally, model scenarios in this study are conservative because they do not include additional forest losses from deforestation (Soares-Filho *et al.*, 2006) or increased forest fire risk from climate changes (Malhi *et al.*, 2008).

Short-term changes in vegetation dynamics from a decade of logging and fire spread substantially decreased carbon uptake at the Sinop site relative to the Forest Control scenario. The change in NEP reported for the Decade scenarios is conservative, however, because fire emissions were not included in the estimate of

net productivity. These results suggest that current rates of forest disturbance, even in the absence of additional deforestation, may reduce or eliminate net carbon uptake by intact forests in southern Amazonia. Recent estimates of carbon uptake by tropical forests (e.g. (Baker *et al.*, 2004) that do not include the influence of forest disturbances from land use may therefore overestimate the potential carbon sink in tropical forests.

Short-term land use in the Decade scenarios also resulted in long-term changes in forest structure from the legacy of selective logging and forest burning on species composition. Biomass losses from a decade of combined damages from selective logging and understory fires were recovered in 7-25 years after land-use ended, but changes in mean canopy height were still evident at the end of the modeling period 90 years later. The combined disturbances from logging and fire spread damaged 44% of the landscape in only 10 years; the establishment of ES trees following these disturbances also led to changes in forest composition that persisted to the end of the modeling period.

Model outcomes depended on the implementation of fire spread in the ED model. Fire damages in both Century scenarios with fire trapped more than half of the Sinop study site in forest patches <30 years since last disturbance, but the Century Spread scenario ultimately damaged every forest patch, leading to a pronounced "pioneer effect." The Logging scenario also promoted the growth of pioneer species, but the pioneer effect was magnified in scenarios with fire spread. The pioneer effect in the Century scenario without fire spread was similar to the Logging scenario despite higher rates of forest disturbance during the initial 50 years of land use.

Reduced rates of fire disturbance in later years in the Century no-spread scenario resulted from a model artifact in which survivors from burned and logged patches were combined at each time step. Ultimately, this process reduced fire risk in the new patch because taller cohorts from logged areas increased mean canopy height. Results from the Century no-spread scenario should therefore be interpreted with caution. Ultimately, fire spread scenarios led to greater changes in forest structure and composition relative to the Logging scenario despite initial expectations that no-spread scenarios would emphasize the positive fire feedback.

This study identified several priority areas for future improvements in modeling the positive fire feedback in Amazon forests that could be implemented using a version of the ED model with sub-grid cell land use (e.g., Hurtt *et al.*, 2002). First, knowledge of the sub-grid cell fraction of cropland, pasture, logged, and burned forests would allow fire spread to occur differently in logged or burned forest types (secondary forests) than in primary forest. Independent calculation and application of fire damages to secondary and primary forests would create intermediate cases of fire spread between the bracketing examples presented in this study. Second, only one disturbance type was applied to each patch in a given year. Future development of a fire model that permits logging and burning in the same year, as documented in Chapter 3, could be used to assess the specific role of logging for fire spread. Finally, model scenarios of land use in this study begin from conditions of potential vegetation to assess relative changes between land use and control scenarios. ED can also be initialized using an estimate of vegetation conditions from field or lidar data (e.g., Hurtt *et al.*, 2004) or patterns of historic land use (e.g., Hurtt *et al.*, 2002).

Improving the depiction of initial forest conditions is a priority for future work, especially to improve estimates of short-term (1-10 year) carbon fluxes from repeated burning in Amazonia, since the fire feedback mechanism is sensitive to initial forest conditions.

The height-structured fire sub-model developed in this study focused on the non-linear relationship between fire risk and canopy height that governs the positive feedback from land-use fires in Amazon forests. This attribute of the feedback mechanism has not previously been incorporated into an ecosystem model. However, the fire feedback mechanism is complex, and variations in land use (Uhl & Buschbacher, 1985; Holdsworth & Uhl, 1997; Alencar *et al.*, 2004) and climate (Cochrane & Laurence, 2002; Alvarado *et al.*, 2004) may also contribute to spatial and temporal variability in the strength of the positive feedback from land-use fires in Amazonia. Several options for future research to address key attributes of climate and land use in the fire feedback mechanism are briefly considered below.

The simple approach to model anthropogenic fire ignitions in this study links fire activity with human presence for selective logging, but future modeling studies could also consider additional complexities in the fire feedback mechanism in Amazon forests from the timing, type, and location of anthropogenic fire ignitions (Chapter 2; Chapter 4; Alencar *et al.*, 2004). The highest density of fire ignitions in Amazonia occurs in areas of active deforestation (Chapter 2), and the timing and location of land-use fires derived from satellite observations differs from previous modeling approaches tied to the seasonality of lightning strikes (Arora & Boer, 2005) or population density (Venevsky *et al.*, 2002), respectively. Locally-varying ignition

rates could be derived directly from satellite-based active fire detections (Chapter 2), burned area (Roy *et al.*, 2008; Giglio *et al.*, submitted), or other fire models (e.g., Cardoso *et al.*, 2003; Arima *et al.*, 2007) to investigate the relative importance of fire ignitions, fuels, or forest structure for understory fires in different Amazon regions.

Climate variability has a complex relationship with fire risk in Amazon forests. Seasonal changes in precipitation, temperature, relative humidity, and wind may influence three components of fire in Amazon forests: fuel amount, fuel quality, and fire size or duration of burning (Chapter 3; Chapter 4; Alvarado *et al.*, 2004; Nepstad *et al.*, 2004; Ray *et al.*, 2005; Alencar *et al.*, 2006; Brando *et al.*, 2007; Balch *et al.*, 2008; Zeng *et al.*, 2008). Satellite-based studies of the extent and frequency of forest fire damages suggest that key factors for fire risk in Amazon forests may differ between humid forest types in central and western Amazonia and seasonal forest types common along the existing arc of deforestation in eastern and southern Amazonia (Chapter 4; Cochrane & Laurence, 2002; Alencar *et al.*, 2006). In central and western Amazonia, moist conditions in the forest understory generally limit forest fire activity to drought years (Barbosa & Fearnside, 1999; Ray *et al.*, 2005; Alencar *et al.*, 2006; Aragão *et al.*, 2007; Zeng *et al.*, 2008) despite accumulation of leaf litter on the forest floor during dry-season months (Goulden *et al.*, 2004). In contrast, forests in southeastern Amazonia have a drier microclimate throughout a 3-5 month dry season, but fires in standing forest appear limited by insufficient leaf litter and other fine fuels (Balch *et al.*, 2008). The increase in fuels from leaf shedding following dry-season cold fronts (Alvarado *et al.*, 2004) may partially explain years with extreme burning in southern Amazonia such as 1999 (Chapter 3, Chapter 4). Amazon

forest phenology may also contribute to regional variability in dry-season fuel availability (Huete *et al.*, 2006). Therefore, modeling the link between climate and fire risk in Amazon forests may require accurate representation of litter moisture in humid forest types and litter production in seasonal forest types with changing climate. By incorporating aspects of climate sensitivity into a height-structured model of the positive fire feedback in Amazon forests, future modeling studies could improve projections of potential synergies between climate change and land-use fires in Amazonia for potential dieback of tropical forest in the region.

In summary, the new height-structured fire sub-model developed in this study demonstrates the potential impacts from a positive fire feedback in logged and burned forests under current rates of land use and constant climate. Short-term reductions in biomass and NEP in the Decade scenarios indicate that current rates of land use may further enhance atmospheric carbon emissions from deforestation in southern Amazonia (Chapter 2). Following a century of land use, the combination of selective logging and fire spread led to secondarization of forests in southern Amazonia. Recurrent fire damages maintained changes in forest structure and composition, leading to large losses in net carbon storage relative to the Forest Control and Logging scenarios. This study also outlines areas for future research to improve the depiction of fire spread, land-use fires, and climate-related aspects of the positive fire feedback in an improved version of the in the height-structured fire sub-model.

5.6 Conclusions

This chapter describes the development of a new height-structured fire sub-model in ED to evaluate the long-term changes in Amazon forest structure from repeated exposure to land-use fires. The new fire model uses characteristics of vegetation height and the fraction of the landscape in a fire-prone forest structure as modeled in ED to develop estimates of fire risk and fire spread, respectively. The height-structured fire sub-model was calibrated using satellite-based estimates of recent selective logging and understory fires in the Xingu basin study area, and model scenarios of continued land use at current rates over decadal and century time scales under constant current climate were used to assess the long-term impacts consequences of logging and fire on forest structure, composition, and total biomass.

Results from this study suggest that combined forest damages from logging and understory fires could reduce net carbon storage in the upper Xingu basin by 22-46% within 100 years without enhanced fire risk from climate change or additional deforestation. The Century Spread scenario resulted in the greatest changes in forest structure and composition relative to the Forest Control and Logging scenarios. Thus, fire spread was essential to maintain changes in forest structure and composition from a positive fire feedback under current rates of fire ignition and selective logging. Reductions in carbon storage from a positive fire feedback in Amazon forests could accelerate the large-scale dieback of Amazon forests projected due to carbon-cycle feedbacks with climate change (Cox *et al.*, 2004). Because climate changes could also increase forest flammability, future work is needed to incorporate climate-related aspects of the positive fire feedback into the height-structured fire sub-model in this

study in order to assess the relative contributions from land use and climate change to potential Amazon forest dieback.

Chapter 6: Conclusions and Policy Implications from the Dissertation and Directions for Future Research

6.1 Summary

The four individual studies in this dissertation develop and integrate satellite remote sensing and ecosystem modeling approaches to address three priority research questions regarding understory fires in Amazon forests, as outlined in Section 1.5. This final chapter summarizes the key findings from the dissertation related to these initial questions (Section 6.1). Section 6.2 presents an additional set of synthetic conclusions based on multiple lines of evidence from data in Chapters 2-5 concerning the impacts of land-use fires on Amazon forest structure. Section 6.3 considers the implications of these conclusions for improving management of land-use fires in Amazonia and satellite-based monitoring of deforestation and degradation in the region. Finally, Section 6.4 suggests avenues for future research based evidence for interannual and regional variation in the role of climate for understory forest fires in Amazonia.

6.2 Dissertation Summary and Conclusions Related to Priority Research Areas

The individual studies in this dissertation examine the impacts of anthropogenic fires on forests in southern Amazonia using satellite remote sensing and ecosystem modeling approaches. Chapter 2 describes the spatial and temporal patterns of fire use for deforestation and agricultural maintenance based on the local

frequency of fire detections from the MODIS sensors. Land-use fires for deforestation and agricultural maintenance frequently escape their intended boundaries and burn into adjacent Amazon forests (Figure 1-2). Chapter 3 develops an automated approach to identify canopy damage from these understory forest fires in time series of annual satellite data and tests the method in a region with concentrated land-use fire activity in the Brazilian State of Mato Grosso (Figure 2-1). The time-series approach was applied to a larger study area in Chapter 4 to quantify the extent and frequency of understory fires in southern Amazon forests. Results from Chapter 4 showing recurrent fire damages in previously-burned forest support the hypothesis of a positive fire feedback in Amazon forests from land-use fires (Figure 1-3). Finally, Chapter 5 builds a new height-structured model of fire risk in Ecosystem Demography (ED), an advanced ecosystem model, to assess the short and long-term carbon consequences of a positive fire feedback in Amazon forests. Model scenarios, calibrated using estimates of fire-damaged forest from Chapter 4, test the influence of continued fire use under current climate conditions for Amazon forest structure and composition.

The main conclusions from the dissertation regarding the priority research areas outlined in Section 1-5 are summarized below:

1. How has the trend towards intensification of agricultural production in southern Amazonia altered the use of fire for deforestation?

Changes in the frequency and duration of fire use for the expansion of mechanized cropland into Amazon forest areas have increased the combustion

completeness of the deforestation process compared to less intensive methods of forest clearing. Data in Chapter 2 demonstrate that patterns of repeated fire detections in the same ground location are largely confined to areas of active deforestation in Amazonia (Table 2-1, Figure 2-1), where trunks, stumps, and woody roots can be piled and burned many times in the same dry season in preparation for agriculture. Post-clearing land use, rather than clearing size, largely determines the intensity and duration of fire use during the deforestation process; deforestation for cropland doubled the average frequency and duration of satellite-based fire detections compared with deforestation for pasture (Figure 2-2, Figure 2-4, Figure 2-5). Frequent fire use for cropland expansion may increase the combustion completeness of the deforestation process to near 100% (Figure 2-6), generating fire emissions 2-4 times higher than estimated for previous decades (e.g., Houghton *et al.*, 2000). Finally, because cropland deforestation from multiple years may contribute to fire activity in any given year (Figure 2-5), a decrease in deforestation may not reduce fire activity in that year (Table 2-2). This 'carryover' of ignitions also extends the period over which fires for deforestation may lead to understory fires in adjacent forests.

2. What is the extent and frequency of forest damages from understory fires in southern Amazonia?

Canopy damage from understory fires was widespread in southern Amazonia and frequent fire damages in previously-burned forests were common. Understory fires occurred in all years during 1997-2005 in the southern Amazon study areas (Table 3-5, Table 4-5). The average annual extent of fire-damaged forests and

deforestation were similar (Figure 4-5), but interannual variability in forest damage from understory fires was high (Table 3-4, Table 4-5). Unexpectedly, fire-damaged forest was not highest during ENSO years (1997-1998, Table 3-5) as reported previously for study areas in southern and eastern Amazonia (e.g., Alencar *et al.*, 2006). Canopy damage from fire was most extensive in 1999, the driest year during the study period (Figure 4-2), but widespread burning also occurred during 2002 and 2004 (Table 3-5, Table 4-5). Very large burn scars (>500 ha) were only mapped during years with highest fire damages (1999, 2002), yet these largest fires contributed the majority of fire-damaged forest area (Figure 3-8). Finally, repeated burning contributed up to half of all fire-damaged forest in 2001-2005 as more than 20% of previously-burned forests burned again during this period (Table 4-5). The average fire return interval in previously-burned forests was 3.2 years, with some forests burning three times in 5-7 years (Figure 4-3, Table 4-5).

3. What are the long-term carbon consequences from changes in forest structure due to recurrent fires in Amazon forests?

Satellite and model-based evidence for "secondarization" of Amazon forests from repeated exposure to land-use fires has long-term consequences for carbon storage and forest composition. Satellite data support the hypothesis of a positive fire feedback in Amazon forests (Figure 1-3); the fraction of previously-burned forests (1999-2003) that burned a second time during 2001-2005 (23.2%) was five times higher than the fraction of initial forest damages from fire in the Xingu study area during 2001-2005 (4.4%) (Table 4-5, Section 4.4.3). However, data in Chapter 4 also

indicate a recovery of woody vegetation following multiple fires in southern Amazon forests (Figure 4-4) rather than a conversion to herbaceous cover as predicted under the "savannization" hypothesis (Cochrane & Schulze, 1999). Ecosystem modeling results in Chapter 5 suggest that the structure and composition of forests exposed to recurrent land-use fires is likely to shift from mid and late-successional trees to early-successional trees (Figure 5-5), similar to secondary forests, despite high satellite-derived canopy greenness (Figure 4-4). Scenarios with a decade of land use (selective logging and understory fire damages) at current rates led to a short-term loss in carbon storage (7-25 years, Figure 5-8) and a long-term change in forest structure, measured as the reduction in mean canopy height relative to the forest control scenario at the end of the modeling period (3-7%, Table 5-1). Scenarios of continued land use at current rates for 100 years show the potential to trap a large fraction of the landscape in a fire-prone forest structure through a positive fire feedback (Table 5-1, Figure 5-6), reducing net carbon storage by 20-46% (0.19-0.4 Pg C, Table 5-1) and nearly doubling the fraction of forest biomass in early-successional trees relative to the forest control scenario (Figure 5-5, Table 5-1).

6.3 Additional Conclusions from the Dissertation

The integration of satellite remote sensing and ecosystem modeling approaches in the dissertation improves understanding of the patterns, processes, and consequences of understory fires in southern Amazon forests. Multiple lines of evidence from data in Chapters 2-5 also give rise to three synthetic conclusions

regarding land-use fires and changes in forest structure from a positive fire feedback in southern Amazonia.

First, the expansion of mechanized cropland in southern Amazonia presents an interesting paradox in terms of land-use fires and understory fire risk. Deforestation for cropland doubles the average frequency and duration of satellite-based fire detections compared with less-intensive methods of deforestation for pasture (Figure 2-5), but multiple lines of evidence suggest that these additional ignitions do not generate a proportional increase in canopy damage from understory fires in adjacent forest areas. Deforestation for cropland in the Brazilian state of Mato Grosso peaked in 2003 (Morton *et al.*, 2006), and results in Chapter 2 indicate that Mato Grosso had the highest fraction of fires detected on 3 or more days in the same location in this year (Table 2-2). MODIS-based deforestation in the Xingu Basin study area was also highest in 2003 (Table 4-5), yet total fire-damaged forest and the fraction of fire-damaged forest adjacent to new deforestation did not increase in this year (Table 4-5). Next, in Chapter 3, cropland deforestation in 2001-2003 rarely overlapped with fire-damaged forest compared with deforestation for pasture (Table 3-4). Finally, the BDR algorithm uses data from the early dry season to identify canopy damage from fires in the previous year (Figure 3-2) because field observations and calibration data in Chapter 3 suggest that most understory fires occur at the end of the dry season. Fires for cropland deforestation are common during the early dry season (Figure 2-3), suggesting that some of the additional burning for cropland expansion may occur when forests are less flammable. Thus, more deforestation and more frequent fire usage during the conversion process in

years with peak cropland expansion into Amazon forests may not lead to an increase in understory fires if areas are cleared and burned when the risk of forest fires is low.

Second, in contrast to central and western Amazonia, drought conditions and selective logging did not appear to be necessary to burn extensive areas of forest in southern Amazonia. Widespread canopy damage from understory fires in the Xingu basin study area occurred under a range of climate conditions during 1997-2005 (Figure 4-2, Table 3-5, Table 4-5), and forest areas in the southern and eastern portions of the study area burned despite little evidence for recent logging activity in the study by Asner *et al.* (2005) (Figure 4-3). Understory fires burned forest in the Xingu Indigenous Park without evidence for selective logging or deforestation (Figure 4-5). Finally, rates of selective logging (Table 3-2) and the predicted risk of understory fires based on soil water deficits (Nepstad *et al.*, 2004) were high in 2001, but actual fire-damaged forest area was lower in 2001 than in any other year during 1997-2005 (Table 3-5, Table 4-5).

Third, burned forest is an extensive and long-term component of the frontier landscape in southern Amazonia (Table 4-5). Fire and deforestation damaged equivalent forest areas in the upper Xingu River basin (Figure 4-5). Burned forests were not rapidly converted to cropland or pasture, leaving a large stock of fire-damaged forest on the landscape (Table 4-5). A positive fire feedback in previously-burned forests enhances the changes in structure and composition from initial fire damages (Figure 5-5) and maintains the amount of burned forest on the landscape (Table 4-5, Figure 5-6). Finally, forest recovery after a decade of fire damages

rapidly offsets carbon losses from fire-killed trees (7-25 years) but the legacy of changes in forest structure and composition from fire may be long-term (>90 years).

6.4 Policy-Relevant Implications of Dissertation Conclusions

6.4.1 Lessons for Managing Land-Use Fires in Southern Amazonia

Guidelines for managing land-use fires in Amazonia were largely developed following widespread fire damages in central and eastern Amazonia during ENSO-related drought events in the 1990s (Nepstad *et al.*, 1999a). Thus, some recommendations for methods to prevent understory forest fires are most suitable for humid forest types in these regions. For example, several authors advocate the use of intact forest areas as "green fire breaks" between logged forests and pastures to prevent the escape of agricultural maintenance fires into fire-prone forests (Holdsworth & Uhl, 1997; Barlow & Peres, 2004). Findings in the dissertation that both logged and intact forests in southern Amazonia burn in all years (Table 3-3, Table 3-5, Table 4-5), not just drought years (Figure 4-2), would reduce the effectiveness of this strategy and highlight the need for regionally-specific guidelines for managing land-use fires.

Restrictions for the timing of land-use fires in Brazilian Amazonia do vary regionally based on the length of the local dry season. Current legislation limits fire use in southern Amazonia beginning in the middle of the dry season (July 15) until after rains begin (Schroeder *et al.*, in press). Findings in Chapter 2 suggest that current enforcement of this restriction is weak, given high rates of satellite-based fire detections for deforestation and maintenance fires throughout the dry season. Based

on evidence for increased fire use in the early dry season for cropland deforestation (Figure 2-3) without a corresponding increase in damages from understory fires (Table 3-5, Table 4-5), incentives to promote burning in early dry-season months may lower understory fire risk in the region.

Mechanization may further reduce the risk of fires for cropland deforestation escaping into adjacent forest areas (Table 3-4). As farmers use tractors to pile trunks, stumps, and woody roots to facilitate repeated burning (Figure 2-2) they create a fuel break along the forest edge. Fuel breaks are a fundamental component of reducing damages from understory fires in tropical forests, but tractors or other machinery needed to develop and maintain fuel breaks are typically unavailable in frontier areas (Holdsworth & Uhl, 1997; Nepstad *et al.*, 1999a; Nepstad *et al.*, 2001; Barlow & Peres, 2004). Better availability of machinery in Mato Grosso than in other Amazon regions, given rapid expansion of mechanized crop production in recent years (Morton *et al.*, 2006), offers additional policy options for creating and maintaining fuel breaks in the region. Linking fire management requirements in southern Amazonia with credit access or nascent deforestation licensing efforts, as suggested previously to encourage other agricultural "best practices" (Nepstad *et al.*, 2001; Fearnside, 2003; Nepstad *et al.*, 2006b), could facilitate the implementation of regional restrictions for fire use and fuel breaks on the landscape.

6.4.2 Satellite-Based Monitoring of Deforestation and Degradation

The dissertation presents two new methods to improve satellite-based estimates of degradation and deforestation in Amazonia that address ongoing discussions for REDD and other policy-related efforts to estimate carbon emissions

from tropical regions (e.g., Canadell *et al.*, 2007; Ramankutty *et al.*, 2007). First, the BDR algorithm provides an automated approach to estimate forest canopy damage from understory fires in tropical forests. Fire is a critical component of forest degradation (Souza Jr. & Roberts, 2005; Peres *et al.*, 2006), yet technical preparations for REDD have primarily focused on mapping deforestation and selective logging because automated approaches to map fire damages were not yet available (GOFC-GOLD, 2008). Next, the dissertation highlights the importance of a coordinated approach for mapping deforestation and degradation to avoid double-counting errors that may occur by combining individual satellite data products. Findings that selective logging and deforestation may have been overestimated in southern Amazonia have direct bearing on the calculation of baseline rates for the REDD and historic carbon fluxes from tropical deforestation (e.g., Ramankutty *et al.*, 2007). Returning to historic satellite imagery using an integrated approach such as the BDR algorithm for mapping deforestation and degradation may therefore be necessary to ensure that REDD activities produce an actual reduction in greenhouse gas emissions from land use in tropical forest regions.

The approach to identify deforestation fires in Amazonia based on the local frequency of satellite-based fire detections also has policy-relevant applications for estimating fire emissions from deforestation and mapping cropland deforestation in near-real time. Results from the dissertation indicate that the current trend towards intensification of agricultural production in southern Amazonia may result in higher fire emissions compared to previous estimates for less intensive clearing methods (e.g., Houghton *et al.*, 2000; Hirsch *et al.*, 2004). Evidence for frequent land-use fires

during the multi-year deforestation process also suggests that there is no uniform relation between fire detections and carbon losses; models that use the number of individual fire detections to estimate fire emissions could therefore benefit from the fire-frequency approach to adjust emissions from fires during the deforestation process (e.g., Freitas *et al.*, 2006; van der Werf *et al.*, 2006).

The unique pattern of high-frequency fire detections for mechanized deforestation activities may also improve the detection of cropland deforestation in near-real time. Current approaches to classify post-clearing land use rely on phenology information from the subsequent growing season (Morton *et al.*, 2006). Identifying the location of new cropland deforestation prior to the growing season based on a combination of existing deforestation monitoring approaches (e.g., INPE, 2006) and fire frequency information may therefore aid ongoing efforts to limit the purchase of soybeans and other grains from recently-deforested areas (ABIOVE, 2006).

6.5 Future Research Directions

One important goal for future research is to clarify the role of climate for understory fires in Amazon forests. Results in this dissertation suggest that canopy damage from understory fires varies interanually and regionally in Amazonia; years with highest fire damages in southern Amazonia (1999, 2002, 2004) differed from previous reports of widespread fire activity in other Amazon regions during 1997-1998 (e.g., Barbosa & Fearnside, 1999; Cochrane *et al.*, 1999; Nepstad *et al.*, 1999b; Alencar *et al.*, 2006) and 2005 (e.g., Brown *et al.*, 2006; Aragão *et al.*, 2007; Zeng *et*

al., 2008). Whether regional variation in fire-damaged forest in these years resulted from the same climate feedback for fire risk (ie, regional variation in the strength of recent climate anomalies) or different mechanisms by which forests become flammable (e.g., Alvarado *et al.*, 2004; Nepstad *et al.*, 2004; Ray *et al.*, 2005; Balch *et al.*, 2008) has important consequences for future risk of understory fires in Amazonia from climate change.

One hypothesis is that canopy phenology plays an important role in determining where fires in Amazon forests are climate or fuel-limited. The mechanism and timing of canopy leaf turnover (light—dry season, or moisture—wet season) may contribute to fire risk in standing forests by determining fuel loads when land-use fires are most common. The role of canopy phenology for fire risk has received less attention than the impact of leaf turnover on dry-season photosynthesis (Huete *et al.*, 2006), yet understanding fire-climate-phenology interactions is critical to improve the ability to forecast ecosystem responses to land use under scenarios of climate change (e.g., Malhi *et al.*, 2008).

Reductions in carbon storage from a positive fire feedback in Amazon forests (Chapter 5) could accelerate a large-scale dieback of Amazon forests projected due to carbon-cycle feedbacks with climate change (Cox *et al.*, 2004). Similarly, anticipated reductions in rainfall and increases in surface temperature from climate change (Meehl *et al.*, 2007) could enhance understory fire activity in regions with moisture-limited fire risk. By incorporating aspects of climate sensitivity into a height-structured model of the positive fire feedback in Amazon forests (Chapter 5), future modeling studies could improve projections of potential synergies between climate

change and land-use fires in Amazonia for potential dieback of tropical forest in the region. By focusing on the contribution of anthropogenic fires to changes in Amazon forest structure, the final model scenarios could generate important insight into how different land use possibilities alter the long-term response to climate change.

Appendix: List of Abbreviations

AGLB	Above-Ground Live Biomass
ASTER	Advanced Spaceborne Thermal Emission and Reflection Radiaometer
AVHRR	Advanced Very High Resolution Radiometer
BAU	Business As Usual
BDR	Burn Damage and Recovery
CBERS	Chinese-Brazilian Environmental Research Satellite
DGVM	Dynamic Global Vegetation Model
ED	Ecosystem Demography (model)
ENSO	El Niño Southern Oscillation
ES	Early-Successional trees
FDFA	Fire-Damaged forest area
GCM	General Circulation Model
GPS	Global Positioning System
GVs	Shade-normalized Green Vegetation fraction
HC	High Confidence
INPE	Instituto Nacional de Pesquisas Espaciais
ISLSCP	International Satellite Land Surface Climatology Project
LAI	Leaf Area Index
LS	Late-Successional trees
mNDVI	mean dry-season Normalized Difference Vegetation Index
MODIS	Moderate Resolution Imaging Spectroradiometer
MS	Mid-Succession trees
NDVI	Normalized Difference Vegetation Index
NEP	Net Ecosystem Productivity
NIP	Not In agricultural Production
NS	Not Signifcant
PFT	Plant Functional Type
PRODES	Monitoramento da Floresta Amazônica Brasileira por Satellite
REDD	Reducing Emissions from Deforestation and Degradation
TAGB	Total Above-Ground Biomass
TRMM	Tropical Rainfall Measuring Mission (satellite)
VCF	Vegetation Continuous Fields

Bibliography

ABIOVE. (2006). "(A Associação Brasileira das Indústrias de Óleos Vegetais-ABIOVE, e Associação Nacional dos Exportadores de Cereais-ANEC) Um programa de governança sobre soja do Bioma Amazônico." Retrieved July 2006, from http://www.abiove.com.br/informa_br.html.

Achard F, Eva HD, Stibig H-J, Mayaux P, Gallego J, Richards T, Malingreau J-P (2002). Determination of deforestation rates of the world's humid tropical forests. *Science* **297**, 999-1002.

Alencar A, Nepstad DC, Vera Diaz MdC (2006). Forest understory fire in the Brazilian Amazon in ENSO and non-ENSO years: Area burned and committed carbon emissions. *Earth Interactions* **10**, Paper 10-006.

Alencar A, Solórzano LA, Nepstad DC (2004). Modeling forest understory fires in an eastern Amazonian landscape. *Ecological Applications* **14**(4), S129-S149.

Alvarado EC, Sandberg DV, Carvalho Jr. JA, Gielow R, Santos JC (2004). Landscape fragmentation and fire vulnerability in the primary forest adjacent to recent land clearings in the Amazon arc of deforestation. *Floresta* **34**(2), 169-174.

Alves DS, Morton DC, Batistella M, Roberts DA, Souza Jr. CM (in press). The changing rates and patterns of deforestation and land use in Brazilian Amazonia. Amazonia and global change. M. Keller, J. Gash and P. Silva Dias. Stockholm, International Geosphere-Biosphere Programme (IGBP).

Aragão LEOC, Malhi Y, Roman-Cuesta RM, Saatchi SS, Anderson LO, Shimabukuro YE (2007). Spatial patterns and fire response of recent Amazonian droughts. *Geophysical Research Letters* **34**(L07701), doi:10.1029/2006GL028946.

Araujo T, Carvalho Jr. JA, Higuchi N, Brasil Jr. A, Mesquita A (1999). A tropical rainforest clearing experiment by biomass burning in the state of Pará, Brazil. *Atmospheric Environment* **33**, 1991-1998.

Arima E, Simmons CS, Walker R, Cochrane M (2007). Fire in the Brazilian Amazon: a spatially explicit model for policy impact analysis. *Journal of Regional Sciences* **47**(3), 541-567.

Arora VK, Boer GJ (2005). Fire as an interactive component of dynamic vegetation models. *Geophysical Research Letters* **110**(G02008), doi:10.1029/2005JG000042.

Asner GP (2001). Cloud cover in Landsat observations of the Brazilian Amazon. *International Journal of Remote Sensing* **22**(18), 3855-3862.

Asner GP, Broadbent EN, Oliveira PJC, Keller M, Knapp DE, Silva JN (2006). Condition and fate of logged forests in the Brazilian Amazon. *Proceedings of the National Academy of Sciences* **103**(34), 12947-12950.

Asner GP, Keller M, Pereira R, Zweede JC (2002). Remote sensing of selective logging in Amazonia: assessing limitations based on detailed field observations, Landsat ETM+, and textural analysis. *Remote Sensing of Environment* **80**, 483-486.

Asner GP, Keller M, Pereira R, Zweede JC, Silva JN (2004). Canopy damage and recovery following selective logging in an Amazon forest: Integrating field and satellite studies. *Ecological Applications* **14**(4), 280-298.

Asner GP, Knapp DE, Broadbent EN, Oliveira PJC, Keller M, Silva JN (2005). Selective logging in the Brazilian Amazon. *Science* **310**, 480-482.

Baker TR, Phillips OL, Malhi Y, Almeida S, Arroyo L, Di Fiore A, Erwin T, Higuchi N, Killeen TJ, Laurance SG, Laurance WF, Lewis SL, Monteagudo A, Neill DA, Vargas PN, Pitman NCA, Silva JNM, Martinez RV (2004). Increasing biomass in Amazon forest plots. *Philisophical Transactions of the Royal Society of London B* **359**, 353-365.

Balch JK, Nepstad DC, Brando PM, Curran LM, Portela O, de Carvalho Jr. O, Lefebvre P (2008). A negative fire feedback in a transitional forest of southeastern Amazonia. *Global Change Biology* **14**, 1-12.

Barbosa PM, Grégoire J-M, Pereira JMC (1999). An algorithm for extracting burned areas from time series of AVHRR GAC data applied at a continental scale. *Remote Sensing of Environment* **69**, 253-263.

Barbosa RI, Fearnside PM (1999). Incêndios na Amazônia Brasileira: Estimativa da emissão de gases do efeito estufa pela queima de deferentes ecossistemas de Roraima na passagem do evento "El Niño" (1997/1998). *Acta Amazonica* **29**, 513-534.

Barlow J, Peres CA (2004). Ecological responses to El Niño-induced surface fires in central Brazilian Amazonia: management implications for flammable tropical forests. *Philisophical Transactions of the Royal Society of London B* **359**, 367-380. (doi:10.1098/04-0488).

Barlow J, Peres CA (2006). Effects of single and recurrent wildfires on fruit production and large vertebrate abundance in a central Amazonian forest. *Biodiversity and Conservation* **15**(3), 985-1012.

Barlow J, Peres CA (2008). Fire-mediated dieback and compositional cascade in an Amazonian forest. *Philisophical Transactions of the Royal Society of London B* **363**, 1787-1794.

Barlow J, Peres CA, Lagan B, Haugaasen T (2003). Large tree mortality and the decline of forest biomass following Amazonian wildfires. *Ecology Letters* **6**, 6-8.

Bond WJ, Midgley JJ (2001). Ecology of sprouting in woody plants: the persistence niche. *Trends in Ecology & Evolution* **16**(1), 45-51.

Bond WJ, Woodward FI, Midgley GF (2005). The global distribution of ecosystems in a world without fire. *New Phytologist* **165**, 525-538.

Brando PM, Nepstad DC, Davidson EA, Trumbore SE, Ray D, Camargo P (2007). Drought effects on litterfall, wood productiod and belowground carbon cycling in an Amazon forest: results of a throughfall reduction experiment. *Philisophical Transactions of the Royal Society of London B*, doi:10.1098/rstb.2007.0031.

Brown IF, Schroeder W, Setzer AW, Maldonado MLR, Pantoja N, Duarte A, Marengo J (2006). Monitoring fires in southwestern Amazonia rain forests. *Eos Transactions of the American Geophysical Union* **87**(26), 253.

Canadell JG, Le Quére C, Raupach MR, Field CB, Buitenhuis ET, Ciais P, Conway TJ, Gillett NP, Houghton RA, Marland G (2007). Contributions to accelerating atmospheric CO2 growth from economic activity, carbon intensity, and efficiency of natural sinks. *Proceedings of the National Academy of Sciences*, doi10.1073/pnas.0702737104.

Cardoso MF, Hurtt GC, Moore B, Nobre CA, Bain H (2005). Field work and statistical analyses for enhanced interpretation of satellite fire data. *Remote Sensing of Environment* **96**, 212-227.

Cardoso MF, Hurtt GC, Moore B, Nobre CA, Prins E (2003). Projecting future fire activity in Amazonia. *Global Change Biology* **9**, 656-669.

Carvalho JA, Costa FS, Veras CAG, Sandberg DV, Alvarado EC, Gielow R, Serra AM, Jr., Santos JC (2001). Biomass fire consumption and carbon release rates of rainforest-clearing experiments conducted in northern Mato Grosso, Brazil. *Journal of Geophysical Research* **106**(D16), 17,877-17,887.

Carvalho JA, Higuchi N, Araújo TM, Santos JC (1998). Combustion completeness in a rainforest clearing experiment in Manaus, Brazil. *Journal of Geophysical Research* **103**(D11), 13195-13199.

Carvalho Jr. JA, Costa FS, Gurgel Veras CA, Sandberg DV, Alvarado EC, Gielow R, Serra Jr. AM, Santos JC (2001). Biomass fire consumption and carbon release

rates of rainforest-clearing experiments conducted in northern Mato Grosso, Brazil. *Journal of Geophysical Research* **106**(D16), 17877-17887.

Chomitz KM, Thomas TS (2003). Determinants of land use in Amazônia: A fine-scale spatial analysis. *American Journal of Agricultural Economics* **85**(4), 1016-1028.

Cochrane M, Alencar A, Schulze M, Souza Jr. CM, Nepstad DC, Lefebre P, Davidson EA (1999). Positive feedbacks in the fire dynamic of closed canopy tropical forests. *Science* **284**, 1832-1835.

Cochrane MA (2003). Fire science for rainforests. *Nature* **421**, 913-919.

Cochrane MA, Laurence WF (2002). Fire as a large-scale edge effect in Amazonian forests. *Journal of Tropical Ecology* **18**, 311-325.

Cochrane MA, Schulze MD (1999). Fire as a recurrent event in tropical forests of the eastern Amazon: effects on forest structure, biomass, and species composition. *Biotropica* **31**(1), 2-16.

Cochrane MA, Souza CM (1998). Linear mixture model classification of burned forests in the eastern Amazon. *International Journal of Remote Sensing* **19**(17), 3433-3440.

Cox P (2001). Description of the TRIFFID dynamic global vegetation model. Technical Note 24. Bracknell, UK, Hadley Centre**:** 16.

Cox P, Betts R, Collins M, Harris P, Huntingford C, Jones C (2004). Amazonian forest dieback under climate-carbon cycle projections for the 21st century. *Theoretical Applied Climatology* **78**, 137-156.

Cox P, Betts R, Jones C, Spall S, Totterdell I (2000). Acceleration of global warming due to carbon-cycle feedbacks in a coupled climate model. *Nature* **408**, 184-187.

DeFries RS, Achard F, Brown S, Herold M, Murdiyarso D, Schlamadinger B, Souza Jr. CM (2007). Earth observations for estimating greenhouse gas emissions from deforestation in developing countries. *Environmental Science & Policy* **10**, 385-394.

DeFries RS, Houghton RA, Hansen MC, Field CB, Skole DL, Townshend J (2002). Carbon emissions from tropical deforestation and regrowth based on satellite observations for the 1980s and 1990s. *Proceedings of the National Academy of Sciences* **99**(22), 14256-14261.

Elvidge C, Hobson V, Baugh K, Dietz J, Shimabukuro YE, Krug T, Novo E, Echavarria F (2001). DMSP-OLS estimation of tropical forest area impacted

by surface fires in Roraima, Brazil: 1995 versus 1998. *International Journal of Remote Sensing* **22**, 2661-2673.

Eva HD, Fritz S (2003). Examining the potential of using remotely sensed fire data to predict areas of rapid forest change in South America. *Applied Geography* **23**, 189-204.

Eva HD, Lambin EF (1998). Remote sensing of biomass burning in tropical regions: sampling issues and multisensor approach. *Remote Sensing of Environment* **64**, 292-315.

FAO (2006). Global forest resources assessment 2005: Progress towards sustainable forest managment. Rome, Food and Agriculture Organization of the United Nations.

Fearnside PM (2001). Soybean cultivation as a threat to the environment in Brazil. *Environmental Conservation* **28**(1), 23-38.

Fearnside PM (2003). Deforestation control in Mato Grosso: A new model for slowing the loss of Brazil's Amazon forest. *Ambio* **32**(5), 343-345.

Fearnside PM, Leal N, Jr., Fernandes FM (1993). Rainforest burning and the global carbon budget: Biomass, combustion efficiency, and charcoal formation in the Brazilian Amazon. *Journal of Geophysical Research* **98**(D9), 16733-16743.

Ferreira NC, Ferreira LG, Huete AR, Ferreira ME (2007). An operational deforestation mapping system using MODIS data and spatial context analysis. *International Journal of Remote Sensing* **28**(1), 47-62.

Foley JA, DeFries RS, Asner GP, Barford C, Bonan G, Carpenter SR, Chapin FS, Coe MT, Daily GC, Gibbs HK, Helkowski JH, Holloway T, Howard EA, Kicharik CJ, Monfreda C, Patz JA, Prentice C, Ramankutty N, Snyder PK (2005). Global consequences of land use. *Science* **309**, 570-574.

Freitas SR, Longo KM, Andreae MO (2006). Impact of including the plume rise of vegetation fires in numerical simulations of associated atmospheric pollutants. *Geophysical Research Letters* **33**(L17808), doi.10.1029/2006GL026608.

Friedlingstein P, Cox P, Betts R, Bopp L, von Bloh W, Brovkin V, Cadule P, Doney S, Eby M, Fung I, Bala G, John J, Jones C, Joos F, Kato T, Kawamiya M, Knorr W, Lindsay K, Matthews H, Raddatz T, Rayner P, Reick C, Roeckner E, Schnitzler K, Schnur R, Strassmann K, Weaver A, Yoshikawa C, Zeng N (2006). Climate-carbon cycle feedback analysis: results from the C4MIP model intercomparison. *Journal of Climate* **19**, 3337-3353.

Gerwing J (2002). Degradation of forests through logging and fire in the eastern Brazilian Amazon. *Forest Ecology and Management* **157**, 131-141.

Giglio L (2007). Characterization of the tropical diurnal fire cycle using VIRS and MODIS observations. *Remote Sensing of Environment* **108**, 407-421.

Giglio L, Csiszar I, Justice CO (2006a). Global distribution and seasonality of active fires as observed with the Terra and Aqua MODIS sensors. *Journal of Geophysical Research* **111**(G02016), doi:10.1029/2005JG000142.

Giglio L, Csiszar I, Restás Á, Morisette JT, Schroeder W, Morton DC, Justice CO (in press). Active fire detection and characterization with the Advanced Spaceborne Thermal Emission and Reflection Radiometer (ASTER). *Remote Sensing of Environment*.

Giglio L, Descloitres J, Justice CO, Kaufman YJ (2003). An enhanced contextual fire detection algorithm for MODIS. *Remote Sensing of Environment* **87**, 273-282.

Giglio L, Loboda T, Roy DP, Quayle B, Justice CO (submitted). An active-fire based burned area mapping algorithm for the MODIS sensor.

Giglio L, van der Werf GR, Randerson JT, Collatz GJ, Kasibhatla P (2006b). Global estimation of burned area using MODIS active fire observations. *Atmospheric Chemistry and Physics* **6**, 957-974.

Girod CM, Hurtt GC, Frolking SE, Aber JD, King AW (2007). The tension between fire risk and carbon storage: evaluating U.S. carbon and fire mitigation strategies through ecosystem models. *Earth Interactions* **11**(2), 33.

GOFC-GOLD (2008). Reducing greenhouse gas emissions from deforestation and degradation in developing countires: a sourcebook of methods and procedures for monitoring, measuring, and reporting, GOFC-GOLD Report version COP13-2. Alberta, Canada, Natural Resources Canada.

Goldammer JG (1990). Fire in the tropical biota: ecosystem processes and global challenges. New York, Spginer-Verlag.

Goulden ML, Miller SD, Da Rocha HR, Menton M, De Freitas HC, Figueira AMS, de Sousa CAD (2004). Diel and seasonal patterns of tropical forest CO2 exchange. *Ecological Applications* **14**(4), S42-S54.

Govender N, Trollope WSW, van Wilgen BW (2006). The effect of fire season, fire frequency, rainfall and management on fire intensity in savanna vegetation in South Africa. *Journal of Applied Ecology* **43**, 748-758.

Guild LS, Kauffman JB, Cohen WB, Hlavka CA, Ward DE (2004). Modeling biomass burning emissions for Amazon forest and pastures in Rondônia, Brazil. *Ecological Applications* **14**(4), S232-S246.

Guild LS, Kauffman JB, Ellingson LJ, Cummings DL, Castro EA, Babbitt RE, Ward DE (1998). Dynamics associated with total aboveground biomass, C, nutrient

pools, and biomass burning of primary forest and pasture in Rondônia, Brazil during SCAR-B. *Journal of Geophysical Research* **103**(D24), 32091-32100.

Gullison RE, Frumhoff PC, Canadell JG, Field CB, Nepstad DC, Hayhoe K, Avissar R, Curran LM, Friedlingstein P, Jones C, Nobre CA (2007). Tropical forests and climate policy. *Science* **316**, 985-986.

Hansen MC, DeFries RS, Townshend J, Sohlberg R, Dimiceli C, Carroll M (2002). Towards an operational MODIS continuous field of percent tree cover algorithm: examples using AVHRR and MODIS data. *Remote Sensing of Environment* **83**, 303-319.

Hansen MC, Shimabukuro YE, Potapov PV, Pittman KW (in press). Comparing annual MODIS and PRODES forest cover change dta for advancing monitoring of Brazilian forest cover. *Remote Sensing of Environment*.

Hansen MC, Stehman SV, Potapov PV, Loveland TR, Townshend J, DeFries RS, Pittman KW, Arunarwati B, Stolle F, Steininger MK, Carroll M, DiMiceli C (2008). Humid tropical forest clearing from 2000 to 2005 quantified by using multitemporal and multiresolution remotely sensed data. *Proceedings of the National Academy of Sciences* **105**(27), 9439-9444.

Haugaasen T, Barlow J, Peres CA (2003). Surface wildfires in central Amazonia: short-term impact on forest structure and carbon loss. *Forest Ecology and Management* **179**, 321-331.

Hirsch AI, Little WS, Houghton RA, Scott NA, White JD (2004). The net carbon flux due to deforestation and forest re-growth in the Brazilian Amazon: analysis using a process-based model. *Global Change Biology* **10**, 908-924.

Hoffmann WA, Schroeder W, Jackson RB (2003). Regional feedbacks among fire, climate, and tropical deforestation. *Journal of Geophysical Research* **108**(D23), doi:10.1029/2003JD003494, 11.

Holdsworth AR, Uhl C (1997). Fire in Amazonian selectively logged rain forest and the potential for fire reduction. *Ecological Applications* **7**(2), 713-725.

Houghton RA (2003). Revised estimates of the annual net flux of carbon to the atmosphere from changes in land use and land management 1850-2000. *Tellus Series B-Chemical and Physical Meteorology* **55**, 378-390.

Houghton RA, Lawrence KT, Hackler JL, Brown S (2001). The spatial distribution of forest biomass in the Brazilian Amazon: a comparison of estimates. *Global Change Biology* **7**, 731-746.

Houghton RA, Skole DL, Nobre CA, Hackler JL, Lawrence KT, Chomentowski WH (2000). Annual Fluxes of carbon from deforestation and regrowth in the Brazilian Amazon. *Nature* **403**, 301-304.

Huete AR, Didan K, Miura T, Rodriguez EP, Gao X, Ferreira LG (2002). Overview of the radiometric and biophysical performance of the MODIS vegetation indices. *Remote Sensing of Environment* **83**, 195-213.

Huete AR, Didan K, Shimabukuro YE, Ratana P, Saleska SR, Hutyra LR, Yang W, Nemani RR, Myneni RB (2006). Amazon rainforests green-up with sunlight in dry season. *Geophysical Research Letters* **33**, doi:10.1029/2005GL025583.

Huffman GJ, Adler RF, Bolvin DT, Gu G, Nelkin EJ, Bowman KP, Hong Y, Stocker EF, Wolff DB (2007). The TRMM Multisatellite Precipitation Analysis (TMPA): Quasi-global, multiyear, combined-sensor precipitation estimates at fine scales. *Journal of Hydrometeorology* **8**(1), 38-55.

Hurtt GC, Dubayah RO, Drake JB, Moorcroft PR, Pacala SW, Blair JB, Fearon MG (2004). Beyond potential vegetation: combining lidar data and a height-structured model for carbon studies. *Ecological Applications* **14**(3), 873-883.

Hurtt GC, Moorcroft PR, Pacala SW, Levin SA (1998). Terrestrial models and global change: challenges for the future. *Global Change Biology* **4**, 581-590.

Hurtt GC, Pacala SW, Moorcroft PR, Caspersen J, Shevliakova E, Houghton RA, Moore III B (2002). Projecting the future of the US carbon sink. *Proceedings of the National Academy of Sciences* **99**(3), 1389-1394.

IBGE (2007). Produção Agrícola Municipal, Instituto Brasileiro de Geografia e Estatística.

Ichii K, Hashimoto H, White MA, Potter C, Hutyra LR, Huete AR, Myneni RB, Nemani RR (2007). Constraining rooting depth in tropical rainforests using satellite data and ecosystem modeling for accurate simulation of gross primary production seasonality. *Global Change Biology* **13**, 67-77.

INPE (2006). Sistema DETER: Detecção de Desmatamento em Tempo Real, Instituto Nacional de Pesquisas Espaciais.

INPE (2007). Projeto PRODES: Monitoramento da floresta Amazônica Brasileira por satélite, Instituto Nacional de Pesquisas Espaciais.

INPE (2008). Projeto PRODES: Monitoramento da floresta Amazônica Brasileira por satélite, Instituto Nacional de Pesquisas Espaciais.

Ivanauskas NM, Monteiro R, Rodrigues RR (2003). Alterations following a fire in a forest community of Alto Rio Xingu. *Forest Ecology and Management* **184**, 239-250.

Justice CO, Giglio L, Boschetti L, Roy DP, Csiszar I, Morrisette J, Kauffman Y. (2006, 6 October 2006). "Algorithm Technical Background Document:

MODIS Fire Products (Version 2.3, 1 October 2006)." Retrieved 15 August, 2007, from http://modis.gsfc.nasa.gov/data/atbd/atbd_mod14.pdf.

Kasischke ES, French N (1995). Locating and estimating the areal extent of wildfires in Alaskan boreal forests using multiple-season AVHRR NDVI composite data. *Remote Sensing of Environment* **51**, 263-275.

Kauffman JB (1991). Survival by sprouting following fire in tropical forests of the eastern Amazon. *Biotropica* **23**(3), 219-224.

Kauffman JB, Cummings DL, Ward DE, Babbitt RE (1995). Fire in the Brazilian Amazon: 1. Biomass, nutrient pools, and losses in slashed primary forests. *Oecologia* **104**, 397-408.

Kennedy RE, Cohen WB, Schroeder TA (2007). Trajectory-based change detection for automated characterization of forest disturbance dynamics. *Remote Sensing of Environment* **110**, 370-386.

Kirby KR, Laurance WF, Albernaz AK, Schroth G, Fearnside PM, Bergen S (2006). The future of deforestation in the Brazilian Amazon. *Futures* **38**, 432-453.

Koren I, Remer LA, Longo KM (2007). Reversal of trend in biomass burning in the Amazon. *Geophysical Research Letters* **34**(L20404), 10.1029/2007GL031530.

Lefsky MA, Harding DL, Keller M, Cohen WB, Carabajal CC, Espirito-Santo FdB, Hunter MO, de Oliveira Jr. R (2005). Estimates of forest canopy height and aboveground biomass unsing ICESat. *Geophysical Research Letters* **32**, LS22S02.

Lentile LB, Holden ZA, Smith AMS, Falkowski MJ, Hudak AT, Morgan P, Lewis SA, Gessler PE, Benson NC (2006). Remote sensing techniques to assess active fire characteristics and post-fire effects. *International Journal of Wildland Fire* **15**(3), 319-345.

Lopez Garcia MJ, Caselles V (1991). Mapping burns and natural reforestation using Thematic Mapper data. *Geocarto International* **1**, 31-37.

Malak DA, Pausas JG (2006). Fire regime and post-fire Normalized Difference Vegetation Index changes in the eastern Iberian peninsula (Mediterranean basin). *International Journal of Wildland Fire* **15**, 407-413.

Malhi Y, Roberts JT, Betts R, Killeen TJ, Li W, Nobre CA (2008). Climate change, deforestation, and the fate of the Amazon. *Science* **319**, 169-172.

Margulis S (2004). World Bank Working Paper No. 22: Causes of deforestation of the Brazilian Amazon. Washington, The World Bank.

Matricardi EAT, Skole DL, Cochrane M, Qi J, Chomentowski WH (2005). Monitoring selective logging in tropical evergreen forests using Landsat: mutlitemporal regional analyses in Mato Grosso, Brazil. *Earth Interactions* **9**(Paper No. 24), 1-24.

MCT (2004). Brazil's initial national communication to the United Nations Framework Convention on Climate Change. Brasilia, Ministry of Science and Technology.

Meehl G, Stocker T, Collins W, Friedlingstein P, Gaye A, Gregory J, Kitoh A, Knutti R, Murphy J, Noda A, Raper S, Watterson I, Weaver A, Zhao ZC (2007). Global Climate Projections. Climate Change 2007: The Physical Science Basis. Contribution of Working Group I to the Fourth Assessment Report of the Intergovernmental Panel on Climate Change. S. Solomon, D. Qin, D. Manning *et al.* . Cambridge, United Kingdom and New York, NY, USA, Cambridge University Press.

Meeson B, Corprew F, McManus J, Myers D, Closs J, Sun K, Sunday D, Sellers P (1995). ISLSCP Initiative I--global data sets for land-atmosphere models, 1987-1988. . Washington, DC, American Geophysical Union**:** [Available on CD-ROM].

Millennium Ecosystem Assessment (2005). Ecosystems and Human Well-being: Synthesis. Washington, DC, Island Press.

Mollicone D, Eva HD, Achard F (2006). Human role in Russian wildfires. *Nature* **440**, 436-437.

Monteiro A, Souza Jr. CM, Barreto PG, Pantoja FLS, Gerwing J (2004). Impactos da exploração madeireira e do fogo em florestas de transição da Amazônia Legal. *Scientia Florestalis* **65**, 11-21.

Moorcroft PR, Hurtt GC, Pacala SW (2001). A method for scaling vegetation dynamics: the Ecosystem Demography model (ED). *Ecological Monographs* **71**(4), 557-586.

Morton DC, DeFries RS, Randerson JT, Giglio L, Schroeder W, Van der Werf GR (2008). Agricultural intensification increases deforestation fire activity in Amazonia. *Global Change Biology* **14**, 2262-2275.

Morton DC, DeFries RS, Shimabukuro YE (in press). Cropland expansion in cerrado and transition forest ecosystems: Quantifying habitat loss from satellite-based vegetation phenology. Cerrado Land-use and Conservation: Assessing Trade-offs Between Human and Ecological Needs. C. Klink, R. S. DeFries and R. Cavalcanti. Washington, Conservation International.

Morton DC, DeFries RS, Shimabukuro YE, Anderson LO, Arai E, Espirito-Santo FdB, Freitas R, Morisette J (2006). Cropland expansion changes deforestation

dynamics in the southern Brazilian Amazon. *Proceedings of the National Academy of Sciences* **103**(39), 14637-14641.

Morton DC, DeFries RS, Shimabukuro YE, Anderson LO, del bon Espírito-Santo F, Hansen MC, Carroll M (2005). Rapid assessment of annual deforestation in the Brazilian Amazon using MODIS data. *Earth Interactions* **9**(8), 22.

Morton DC, Shimabukuro YE, Freitas R, Arai E, DeFries RS (2007a). Secondary forest dynamics and Cerradão loss in Mato Grosso during 2001-2005 from MODIS phenology time series. XIII Simpósio Brasileiro de Sensoriamento Remoto, Florianopolis, SC Brasil.

Morton DC, Shimabukuro YE, Rudorff BFT, Lima A, Freitas R, DeFries RS (2007b). Challenge for conservation at the agricultural frontier: deforestation, fire, and land use dynamics in Mato Grosso. *Agua & Ambiente* **2**(1), 5-20.

Naylor R, Steinfeld H, Falcon W, Galloway J, Smil V, Bradford E, Alder J, Mooney H (2005). Losing the links between livestock and land. *Science* **310**, 1621-1622.

Nepstad DC, Carvalho G, Barros AC, Alencar A, Capobianco JP, Bishop J, Moutinho P, Lefebvre P, Silva Jr. UL, Prins E (2001). Road paving, fire regime feedbacks, and the future of Amazon forests. *Forest Ecology and Management* **154**, 395-407.

Nepstad DC, Lefebre P, da Silva UL, Tomasella J, Schlesinger P, Solórzano LA, Moutinho P, Ray D, Benito JG (2004). Amazon drought and its implications for forest flammability and tree growth: a basin-wide analysis. *Global Change Biology* **10**, 704-717.

Nepstad DC, Moreira AG, Alencar AA (1999a). Flames in the rain forest: origins, impacts and alternatives to Amazonian fire. Brasilia, Brazil, The Pilot Program to Conserve the Brazilian Rain Forest.

Nepstad DC, Schwartzman S, Bamberger B, Santilli M, Ray D, Schlesinger P, Lefebre P, Alencar A, Prins E, Fiske G, Rolla A (2006a). Inhibition of Amazon deforestation and fire by parks and indigenous lands. *Conservation Biology* **20**(1), 65-73.

Nepstad DC, Stickler CM, Almeida OT (2006b). Globalization of the Amazon soy and beef industries: opportunities for conservation. *Conservation Biology* **20**(6), 1595-1603.

Nepstad DC, Tohver IM, Ray D, Moutinho P, Cardinot G (2007). Mortality of large trees and lianas following experimental drought in an Amazon forest. *Ecology* **88**(9), 2259-2269.

Nepstad DC, Veríssimo A, Alencar A, Nobre CA, Lima E, Lefebre P, Schlesinger P, Potter C, Moutinho P, Mendoza E, Cochrane M, Brooks V (1999b). Large-scale impoverishment of Amazonian forests by logging and fire. *Nature* **398**, 505-508.

Oliveira PJC, Asner GP, Knapp DE, Almeyda A, Galvan-Gildemeister R, Keene S, Raybin R, Smith RC (2007). Land-use allocation protects the Peruvian Amazon. *Science* **317**, 1233-1236.

Ottmar RD, Vihnanek RE, Miranda HS, Sata MN, Andrade SM (2001). Stereo photo series for quantifying Cerrado fuels in central Brazil, U.S. Department of Agriculture, Forest Service, Pacific Northwest Research Station **Vol. I:** 87.

Oyama MD, Nobre CA (2003). A new climate-vegetation equilibrium state for tropical South America. *Geophysical Research Letters* **30**(23), 2199.

Page SE, Siegert F, Rieley JO, Boehm H-DV, Jaya A, Limin S (2002). The amount of carbon released from peat and forest fires in Indonesia during 1997. *Nature* **420**, 61-65.

Pereira MC, Setzer AW (1993). Spectral characteristics of fire scars in Landsat-5 TM images of Amazonia. *International Journal of Remote Sensing* **14**(11), 2061-2078.

Peres CA, Barlow J, Laurance WF (2006). Detecting anthropogenic disturbance in tropical forests. *Trends in Ecology & Evolution* **21**(5), 227-229.

Phulpin T, Lavenu F, Bellan MF, Mougenot B, Blasco F (2002). Using SPOT-4 HRVIR and VEGETATION sensors to assess impact of tropical forest fires in Roraima, Brazil. *International Journal of Remote Sensing* **23**(10), 1943-1966.

Pinard M, Putz F, Licona J (1999). Tree mortality and vine proliferation following a wildfire in a subhumid tropical forest in eastern Bolivia. *Forest Ecology and Management* **116**, 247-252.

Prins E, Menzel W (1992). Geostationary satellite detection of biomass burning in South America. *International Journal of Remote Sensing* **13**, 2783-2799.

Ramankutty N, Gibbs HK, Achard F, DeFries RS, Foley JA, Houghton RA (2007). Challenges to estimating carbon emissions from tropical deforestation. *Global Change Biology* **13**, 51-66.

Randerson JT, van der Werf GR, Collatz GJ, Still CJ, Kasibhatla P, Miller JB, White JWC, DeFries RS, Kasischke ES (2005). Fire emissions from C3 and C4 vegetation and their influence on interannual variability of atmospheric C02 and d13 CO2. *Global Biogeochemical Cycles* **19**, GB2019, doi:10.1029/2004GB002366.

Ray D, Nepstad DC, Moutinho P (2005). Micrometeorological and canopy controls on fire susceptibility in a forested landscape. *Ecological Applications* **15**(5), 1664-1678.

Rothermel R (1972). A mathematical model for predicting fire spread in wildand fuels, Forest Service General Technical Report INT-115, Intermountain Forest and Range Experiment Station. Forest Service. U.S. Department of Agriculture.

Roy DP, Boschetti L, Justice CO, Ju J (2008). The collection 5 MODIS burned area product--Global evaluation by comparison with the MODIS active fire product. *Remote Sensing of Environment* **112**, 3690-3707.

Roy DP, Jin Y, Lewis P, Justice CO (2005). Prototyping a global algorithm for systematic fire-affected area mapping using MODIS time series data. *Remote Sensing of Environment* **97**, 137-162.

Roy DP, Lewis P, Justice CO (2002). Burned area mapping using multi-temporal moderate spatial resolution data--a bi-directional reflectance model-based expectation approach. *Remote Sensing of Environment* **83**, 263-286.

Saatchi SS, Houghton RA, Dos Santos Alvalá R, Soares JV, Yu Y (2007). Distribution of aboveground live biomass in the Amazon basin. *Global Change Biology* **13**, 816-837.

Saleska SR, Miller SD, Matross DM, Goulden ML, Wofsy SC, da Rocha HR, de Camargo PB, Crill P, Daube BC, de Freitas HC, Hutyra LR, Keller M, Kirchhoff V, Menton M, Munger JW, Pyle EH, Rice AH, Silva H (2003). Carbon in Amazon forests: Unexpected seasonal fluxes and disturbance-induced losses. *Science* **302**, 1554-1557.

Salomonson VV, Wolfe RE (2004). MODIS geolocation approach, results and the future. *IEEE Geoscience and Remote Sensing Letters*(2003 IEEE Workshop on Advances in Techniques for Analysis of Remote Sensing Data), 424-427.

Sanford RL, Saldarriaga J, Clark KE, Uhl C, Herrera R (1985). Amazon rain-forest fires. *Science* **277**, 53-55.

Santilli M, Moutinho P, Schwartzman S, Nepstad DC, Curran LM, Nobre CA (2005). Tropical deforestation and the Kyoto Protocol. *Climatic Change* **71**, 267-276.

Santos AJB, Silva GTDA, Miranda HS, Miranda AC, Lloyd J (2003). Effects of fire on surface carbon, energy and water vapour fluxes over *campo sujo* savanna in central Brazil. *Functional Ecology* **17**, 711-719.

Sawyer D (1984). Frontier expansion and retraction in Brazil. Frontier expansion in Amazônia. M. Schmink and C. Wood. Gainsville, University of Florida Press.

Schmink M, Wood C (1992). Contested frontiers in Amazonia. New York, Columbia University Press.

Schroeder W, Alencar A, Arima E, Setzer AW (in press). The spatial distribution and inter-annual variability of fire in Amazonia. Amazonia and Global Change. J. Gash, M. Keller and P. Silva Dias.

Schroeder W, Csiszar I, Morisette J (2008a). Quantifying the impact of cloud obscuration on remote sensing of active fires in the Brazilian Amazon. *Remote Sensing of Environment* **112**(2), 456-470.

Schroeder W, Morisette J, Csiszar I, Giglio L, Morton DC, Justice CO (2005). Characterizing vegetation fire dynamics in Brazil through multisatellite data: Common trends and practical issues. *Earth Interactions* **9**, Paper 09-013.

Schroeder W, Prins E, Giglio L, Csiszar I, Schmidt C, Morrisette J, Morton DC (2008b). Validation of GOES and MODIS active fire detection productions using ASTER and ETM+. *Remote Sensing of Environment*(112), 2711-2726.

Scott JH, Burgan RE (2005). Standard fire behavior fuel models: a comprehensive set for use with Rothermel's surface fire spread model, USDA-Forest Service, Rocky Mountain Research Station.

SEPLAN-MT (2004). Mapa: Zoneamento Sócio Econômico Ecológico do Estado de Mato Grosso - 2002. GIS data layers for social, economic, and ecological characteristics of Mato Grosso state, Brazil, available at: http://www.zsee.seplan.mt.gov.br/.

Setzer AW, Pereira MC (1991). Operational detection of fires in Brazil with NOAA/AVHRR. 24th International Symposium on Remote Sensing of the Environment, Rio de Janeiro, Brazil, ERIM.

Shimabukuro YE, Duarte V, Arai E, de Freitas RM, Valeriano DM, Brown IF, Maldonado MLR (2006). Fraction images derived from Terra MODIS data for mapping burned area in Acre State, Brazilian Amazonia. IEEE International Geoscience and Remote Sensing Symposium. Denver, Colorado.

Soares-Filho BS, Nepstad DC, Curran LM, Cerqueira GC, Garcia RA, Ramos CA, Voll E, McDonald A, Lefebre P, Schlesinger P (2006). Modeling conservation in the Amazon basin. *Nature* **440**, 520-523.

Souza Jr. CM, Roberts DA (2005). Mapping forest degradation in the Amazon region with Ikonos images. *International Journal of Remote Sensing* **26**(3), 425-429.

Souza Jr. CM, Roberts DA, Cochrane MA (2005a). Combining spectral and spatial information to map canopy damage from selective logging and forest fires. *Remote Sensing of Environment* **98**, 329-343.

Souza Jr. CM, Roberts DA, Monteiro A (2005b). Multitemporal analysis of degraded forests in the southern Brazilian Amazon. *Earth Interactions* **9**(Paper no. 19).

Stephens BB, Gurney KR, Tans PP, Sweeney C, Peters W, Bruhwiler L, Ciais P, Ramonet M, Bousquet P, Nakazawa T, Aoki S, Machida T, Inoue G, Vinnichenko N, Lloyd J, Jordan A, Heimann M, Shibistova O, Langenfelds RL, Steele LP, Francey RJ, Denning AS (2007). Weak northern and strong tropical land carbon uptake from vertical profiles of atmospheric CO_2. *Science* **216**, 1732-1725.

Thonicke K, Venevsky S, Sitch S, Cramer W (2001). The role of fire disturbance for global vegetation dynamics: coupling fire into a Dynamic Global Vegetation Model. *Global Ecology & Biogeography* **10**, 661-677.

Uhl C, Buschbacher R (1985). A disturbing synergism between cattle ranch burning practices and selective tree harvesting in the eastern Amazon. *Biotropica* **17**(4), 265-8.

Uhl C, Kauffman JB (1990). Deforestation, fire susceptibility, and potential tree responses to fire in the eastern Amazon. *Ecology* **71**(2), 437-449.

van der Werf GR, Dempewolf J, Trigg SN, Randerson JT, Kasibhatla P, Giglio L, Murdiyarso D, Peters W, Morton DC, Collatz GJ, DeFries RS, Dolman H (in press-a). Climate regulation of fire emissions and deforestation in equatorial Asia. *Proceedings of the National Academy of Sciences*.

van der Werf GR, Morton DC, DeFries RS, Giglio L, Randerson JT, Collatz GJ, Kasibhatla PS (in press-b). Estimates of deforestation-induced carbon fluxes in the southern Amazon based on satellite data and biogeochemical modeling. *Biogeosciences Discussion*.

van der Werf GR, Randerson JT, Collatz GJ, Giglio L, Kasibhatla P, Arellano Jr. AF, Olsen SC, Kasischke ES (2004). Continental-scale partitioning of fire emissions during the 1997 to 2001 El Niño/La Niña period. *Science* **303**, 73-76.

van der Werf GR, Randerson JT, Giglio L, Collatz GJ, Kasibhatla P, Arellano Jr. AF (2006). Interannual variability in global biomass burning emissions from 1997 to 2004. *Atmospheric Chemistry and Physics* **6**, 3423-3441.

Venevsky S, Thonicke K, Sitch S, Cramer W (2002). Simulating fire regimes in human-dominated ecosystems: Iberian Peninsual case study. *Global Change Biology* **8**, 984-998.

Vermote EF, El Saleous NZ, Justice CO (2002). Atmospheric correction of visible to middle infrared EOS-MODIS data over land surface: background, operational algorithm and validation. *Remote Sensing of Environment* **83**(1-2), 97-111.

Viedma O, Meliá J, Segarra D, García-Haro J (1997). Modeling rates of ecosystem recovery after fires by using Landsat TM data. *Remote Sensing of Environment* **61**, 383-398.

Vourlitis GL, Priante Filho N, Hayashi MMS, Nogueira JdS, Caseiro FT, Holanda Campelo J, J. (2001). Seasonal variations in the net ecosystem CO2 exchange of a mature Amazonian transitional tropical forest (cerradão). *Functional Ecology* **15**, 388-395.

Warnken P (1999). The development and growth of the soybean industry in Brazil. Ames, IA, Iowa State University.

Werth D, Avissar R (2002). The local and global effects of Amazon deforestation. *Journal of Geophysical Research* **107**(D20), doi:10.1029/2001JD000717.

Zarin DJ, Davidson EA, Brondizio E, Vieira IC, Sá T, Feldspausch T, Schuur EA, Mesquita R, Moran E, Delamonica P, Ducey MJ, Hurtt GC, Salimon C, Denich M (2005). Legacy of fire slows carbon accumulation in Amazonian forest regrowth. *Frontiers in Ecology & Environment* **3**(7), 365-369.

Zeng N, Dickinson RE, Zeng X (1996). Climatic impact of Amazon deforestation--a mechanistic model study. *Journal of Climate* **9**, 859-883.

Zeng N, Qian H, Munoz E, Iacono R (2004). How strong is carbon cycle-climate feedback under global warming? *Geophysical Research Letters* **31**(L20203), doi:10.1029/2004GL020904.

Zeng N, Yoon J-H, Marengo J, Subramaniam A, Nobre CA, Mariotti A, Neelin JD (2008). Causes and impacts of the 2005 Amazon drought. *Environmental Research Letters* **3**, 014002.